AD 726469

Office of Army Research

Contract DAHC04-68-C-0037

Duration of Contract: June 1970 - June 1971
Amount of Contract: $35,000

STIMULATED LIGHT SCATTERING IN BINARY GAS MIXTURES

Quarterly Technical Report

Period Ending June 27, 1971

Contractor: President and Fellows of Harvard College

Principal Investigator: N. Bloembergen, 617/495-8376

Project Scientist: H. Lowdermilk, 617/495-4466

Technical Report No. 2

This research was supported by the Advanced Research Projects Agency of the Department of Defense and was monitored by the U. S. Army Research Office-Durham, Box CM, Duke Station, Durham, North Carolina 27706 under Contract No. DAHC04-68-C-0037.

June 1971

Division of Engineering and Applied Physics
Harvard University · Cambridge, Massachusetts

Sponsored by
Advanced Research Projects Agency
ARPA Order No. 675 Am 7
Program Code No. 9E20

Unclassified

DOCUMENT CONTROL DATA - R & D

(Security classification of title, body of abstract and indexing annotation must be entered when the overall report is classified)

1. ORIGINATING ACTIVITY (Corporate author)
Division of Engineering and Applied Physics
Harvard University
Cambridge, Massachusetts

2a. REPORT SECURITY CLASSIFICATION
Unclassified

2b. GROUP

3. REPORT TITLE
STIMULATED LIGHT SCATTERING IN BINARY GAS MIXTURES

4. DESCRIPTIVE NOTES (Type of report and inclusive dates)
Quarterly Technical Report - Period Ending June 27, 1971

5. AUTHOR(S) (First name, middle initial, last name)
N. Bloembergen and H. Lowdermilk

6. REPORT DATE	7a. TOTAL NO. OF PAGES	7b. NO. OF REFS
June 1971	178	67

8a. CONTRACT OR GRANT NO.	9a. ORIGINATOR'S REPORT NUMBER(S)
DAHC04-68-C-0037	Technical Report No. 2
b. PROJECT NO.	
c.	9b. OTHER REPORT NO(S) (Any other numbers that may be assigned this report)
d.	

10. DISTRIBUTION STATEMENT
This document has been approved for public release and sale; its distribution is unlimited. Reproduction in whole or in part is permitted by the U. S. Government.

11. SUPPLEMENTARY NOTES	12. SPONSORING MILITARY ACTIVITY
	Advanced Research Projects Agency of the Department of Defense and the U.S. Army Research Office-Durham

13. ABSTRACT

The theory of stimulated light scattering from a binary gas mixture has been developed. It considers the coupling of a laser wave and a scattered light wave with the collective modes of the mixture. It has been found that in a binary gas mixture in which the different types of molecules have a large difference in mass and polarizibility, it is possible to generate stimulated scattering from local fluctuations in the concentration.

The shift in frequency between the laser and backward scattered wave has been observed systematically as a function of helium concentration from 0 to 90% in mixtures of He and SF_6 in which the partial pressure of SF_6 was 5 atm., and in mixtures of He and Xe in which the partial pressure of Xe was 8 atm. In both cases, for helium concentration less than 60% the frequency shift of the backscattered light is characteristic of stimulated Brillouin scattering in the mixture. As the helium concentration increases above 60%, the frequency shift decreases and rapidly approaches the small values which are characteristic of stimulated concentration scattering. The experimental observations are in good agreement with theoretical predictions.

DD FORM 1 NOV 65 1473 (PAGE 1)

S/N 0101-807-6801

Unclassified
Security Classification

14 KEY WORDS	LINK A		LINK B		LINK C	
	ROLE	WT	ROLE	WT	ROLE	WT
Stimulated Brillouin Scattering						
Stimulated Concentration Rayleigh Scattering						
Binary Gas Mixture						

Office of Army Research

Contract DAHC04-68-C-0037

Duration of Contract: June 1970 - June 1971
Amount of Contract: $35,000

STIMULATED LIGHT SCATTERING IN BINARY GAS MIXTURES

Quarterly Technical Report

Period Ending June 27, 1971

Contractor: President and Fellows of Harvard College

Principal Investigator: N. Bloembergen, 617/495-8376

Project Scientist: H. Lowdermilk, 617/495-4466

Technical Report No. 2

This research was supported by the Advanced Research Projects Agency of the Department of Defense and was monitored by the U. S. Army Research Office-Durham, Box CM, Duke Station, Durham, North Carolina 27706 under Contract No. DAHC04-68-C-0037.

June 1971

Division of Engineering and Applied Physics
Harvard University · Cambridge, Massachusetts

Sponsored by
Advanced Research Projects Agency
ARPA Order No. 675 Am 7
Program Code No. 9E20

ABSTRACT

The theory of stimulated light scattering from a binary gas mixture has been developed. It considers the coupling of a laser wave and a scattered light wave with the collective modes of the mixture. It has been found that in a binary gas mixture in which the different types of molecules have a large difference in mass and polarizibility, it is possible to generate stimulated scattering from local fluctuations in the concentration.

The shift in frequency between the laser and backward scattered wave has been observed systematically as a function of helium concentration from 0 to 90% in mixtures of He and SF_6 in which the partial pressure of SF_6 was 5 atm., and in mixtures of He and Xe in which the partial pressure of Xe was 8 atm. In both cases, for helium concentration less than 60% the frequency shift of the backscattered light is characteristic of stimulated Brillouin scattering in the mixture. As the helium concentration increases above 60%, the frequency shift decreases and rapidly approaches the small values which are characteristic of stimulated concentration scattering. The experimental observations are in good agreement with theoretical predictions.

TABLE OF CONTENTS

Page

Page

Page

LIST OF FIGURES

LIST OF TABLES

BLANK PAGE

CHAPTER I

INTRODUCTION

A. Spectrum of the Scattered Light

1. Introduction

It is a well known phenomenon that when a beam of light passes through a transparent medium, some of the light is scattered. This scattering, specifically excluding Raman scattering, is due to the fact that the density of the medium is not uniform[1]. For a macroscopic system in thermodynamic equilibrium, small amplitude fluctuations in the density, and all other thermodynamic parameters which characterize the system, occur. These zero point or thermal fluctuations produce a space and time dependent index of refraction in the medium and thereby cause the scattering of light. The scattered light has a frequency spectrum which is characteristic of the time dependence of the fluctuations[2].

The basic theory of light scattering from dense media was introduced by Einstein[3]. He recognized the importance of the coherence between waves scattered by neighboring molecules, and derived what are essentially the Laue equations for the scattering of light. These equations show that light is scattered by fluctuations whose wave vector conserves momentum between the incident and scattered photons.

Einstein did not, however, compute the spectrum of the scattered light, since the time dependence of the thermal fluctuations

was not known. The earliest information on the time dependence was Debye's theory of specific heat[4], which showed that the thermal content of the medium could be regarded as sound waves.

Following this work, Brillouin[5] calculated the spectrum of light scattered from these thermally excited sound waves. This frequency spectrum is determined by energy and momentum conservation. Momentum conservation requires that the scattering of light with incident wave vector $\vec{k}_L$ through an angle θ to a final wave vector $\vec{k}_S$ couples only to spatial fluctuations with wave vector $\vec{k} = \vec{k}_L - \vec{k}_S$. Energy conservation requires that the frequency of the scattered light is shifted from the incident frequency by an amount $\Delta\omega = k v_S$ where v_S is the sound velocity in the medium. The frequency spectrum of the scattered light consists of two lines shifted symmetrically about the laser frequency by an amount $\Delta\omega$. The down-shifted "Stokes" line is the result of the creation of a phonon by the incident photon, while the up-shifted "anti-Stokes" line is due to the absorption of a phonon by the incident photon. The shifted lines may be viewed as arising from the modulation of the incident light by the time dependence ($e^{\pm ikv_S t}$) of the propagating fluctuations or as a Doppler shift of the incident light by periodic density fluctuations moving with velocity v_S in the direction $\vec{k}$. The lines are broadened due to dissipative processes which damp the sound waves[6].

The first observation of the existence of the Brillouin doublets was made by E. Gross[7]. Gross, and subsequent workers, found that in addition to the Brillouin doublets, the spectrum of the scattered light

contained a component at the same frequency as the incident light. This feature was explained by Landau and Placzek[8] who pointed out that the thermal content of the body consists of non-propagating density fluctuations in addition to the sound waves. These thermal excitations, which are governed by the heat diffusion equation, lead to light scattering which is not shifted in frequency but is broadened by the thermal dissipative processes which damp out these fluctuations. The resulting central peak in the spectrum is known as the Rayleigh line.

In the binary fluid mixture, fluctuations in the local concentration of one component also occur. If the two, component molecules have a different polarizibility, the concentration fluctuation produces a fluctuation in the index of refraction. Thus the concentration fluctuations also contribute to the scattered light spectrum. Since the concentration fluctuations are non-propagating, the central Rayleigh component in this case will contain the combined effects of temperature and concentration fluctuations.

In general, the effects of heat conduction and diffusion on the width of the Rayleigh component cannot be separated in a simple way[9]. The cross effects between energy transport and diffusion which are present in a binary fluid result in a more complicated structure for the Rayleigh line. These cross effects are known in nonequilibrium thermodynamics as the Dufour effect (a concentration gradient inducing heat flow) and the Soret effect (a temperature gradient inducing diffusion flux).

The spectrum of the scattered light thus contains detailed information on the processes of the transfer of mass, energy, momentum, temperature gradients etc., over distances which are on the order of a wavelength of light. However due to the small frequency shifts and cross sections involved, the use of spontaneous light scattering to study density fluctuations was limited until 1964[10,11] when the laser, an ideal source for such experiments due to its intensity, monochromaticity and collimation, was introduced, making possible accurate measurements of spectra[2,12].

B. Light Scattering Formalism

Information about the correlations in the medium are obtained directly from the spontaneous scattering spectrum. Komarov and Fisher[13] have shown, by adapting Van Hove's[14] neutron scattering results to light scattering, that the intensity of the scattered light is given by

$$I(\vec{R}, \vec{k}, \omega) = \left(\frac{\omega_S}{c_0}\right)^4 \frac{I_0}{(4\pi R)^2} \sin^2 \Phi \, S(\vec{k}, \omega) \quad . \qquad (1.1)$$

The light scattered at the origin is observed at $\vec{R}$. The frequency of the scattered light is ω_S, ω is the shift in frequency and $\vec{k}$ is the change in wave vector of the light upon scattering, and Φ is the angle between the electric vector of the incident intensity I_0 and $\vec{R}$ $S(\vec{k}, \omega)$ is the dynamical structure factor given by

$$S(\vec{k}, \omega) = 2 \, \mathrm{Re} \, < \delta\epsilon \, (\vec{k}, i\omega) \, \delta\epsilon \, (-\vec{k}) >$$

where

$$\delta\epsilon(\vec{k}, i\omega) = \int_0^\infty dt \int d^3r\, \delta\epsilon(r,t)\, e^{-ikr - i\omega t}.$$

The Fourier-Laplace transform of the correlation function of the dielectric constant can be expressed in terms of similar correlation functions of any complete set of dynamical variables Q_i which describe the system

$$\langle \epsilon(\vec{k}, i\omega)\, \epsilon(-\vec{k}) \rangle = \sum_{ij} \frac{\partial\epsilon}{\partial Q_i} \frac{\partial\epsilon}{\partial Q_j} \langle Q_i(\vec{k}, i\omega)\, Q_j(-\vec{k}) \rangle$$

The choice of the thermodynamic variables is not important in the sence that the final result will be the same regardless of which variables are used in the formulation. However, the form of the equations and comparison with experimental results is simplified by a choice of the "proper" set of variables. In this work, the state variables were chosen to be pressure P, temperature T, and concentration of the lighter molecule c.

The calculation of the correlation functions $\langle Q(\vec{k}, i\omega)\, Q(-\vec{k}) \rangle$ can be approached from a macroscopic or microscopic point of view. The macroscopic approach can be applied if the system remains in thermodynamic equilibrium. This approach, suggested by Landau and Placzek[8], is as follows. The space-time response of the system to a deviation from the equilibrium state is calculated using the linearized hydrodynamic equations to determine the modes by which the system returns to equilibrium as well as the relative amplitudes for each mode. Thermodynamic fluctuation theory provides the initial

values for the correlation functions.

The resulting "hydrodynamic" spectrum is characteristic of the dominant collective modes of the system and has been described in the preceding section. This spectrum is related to many of the thermodynamic derivatives and transport coefficients and thus leads to a measurement of them. The hydrodynamic equations are valid only in the regime in which local thermodynamic equilibrium is maintained by interparticle collisions. This is the long wavelength, low frequency limit in which the particle undergoes many collisions over the characteristic length $\frac{1}{k}$ and time $\frac{1}{\omega}$ which the thermodynamic fluctuations are probed. The conditions which must be satisfied are $\bar{\ell} \ll \frac{1}{k}$ and $\tau_c \ll \frac{1}{\omega}$ where $\bar{\ell}$ is the particle mean free path and τ_c is the time between collisions. If these conditions are not satisfied, as in a dilute gas, a more generalized, microscopic approach must be taken. The basis for this microscopic approach is the Boltzmann equation with the appropriate boundary conditions. In the low frequency, long wavelength limit, the macroscopic conservation laws (hydrodynamic equations) may be obtained from the Boltzmann equation by the Chapman-Enskog[15] procedure and the transport coefficients are obtained in terms of molecular parameters.

The macroscopic approach has been discussed in greater detail in the study of spontaneous scattering from the binary mixture by Mountain and Deutch[9] and recent experimental results on a binary gas mixture by Gornall et. al.[16] are in excellent agreement with theoretical calculations.

The important point is that the thermal fluctuations in the medium cause scattering of light by modulating the index of refraction through the various coupling terms $\frac{\partial \epsilon}{\partial Q}$. The spectrum of the spontaneous light scattering is shown in Fig. (1.1). The central Rayleigh peak consists of the contribution from thermal fluctuations which results in light scattering through the coupling constant $(\frac{\partial \epsilon}{\partial T})$ where ϵ is the local dielectric constant of the medium, and the contribution from concentration fluctuations through the coupling constant $(\frac{\partial \epsilon}{\partial c})$. The shifted Brillouin peaks are due to the pressure fluctuations with coupling constant $(\frac{\partial \epsilon}{\partial P})$.

In addition to the low-lying excitations of the medium which give rise to the Rayleigh-Brillouin triplet (thermal and concentration diffusion and the acoustic phonon mode) there are many other types of excitations which contribute to the spectrum of the scattered light. Examples are rotational motions or librations of anisotropic molecules (inelastic Rayleigh wing scattering) and vibrational excitations or optical phonon modes (Raman scattering). All of these effects have been studied with renewed interest and much greater precision during the past decade[12].

C. Stimulated Light Scattering

If the incident light wave has a very large amplitude and the coupling between the light and the scattering medium is strong, the amplitude of the scattered wave will also become large. In this regime it is no longer only the zero point or thermal fluctuations of the medium which are involved in the scattering process. Instead the

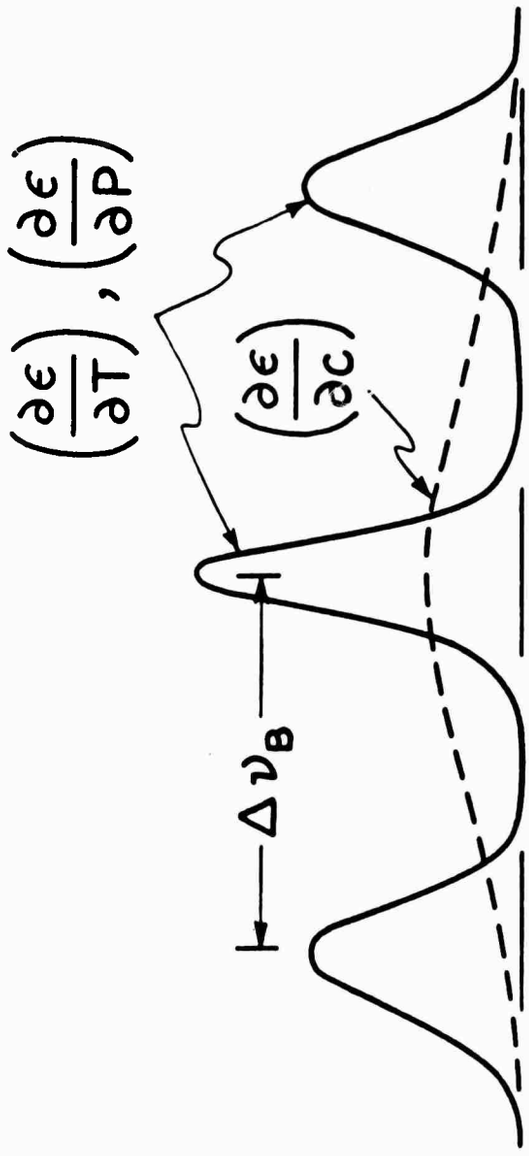

Fig. 1.1 Components of the Spontaneous Light Scattering Spectrum

scattered wave interferes with the incident wave and produces a force on the medium through the dependence of the dielectric constant on the material coordinate. This force drives a coherent oscillation of the material coordinate. The enhanced motion of Q then causes enhanced scattering through the dependence of the dielectric constant on the material coordinate. The enhanced scattering reacts back even more strongly on the coordinate Q. This mutual reinforcement of scattering and oscillation of the material coordinate leads to an exponential growth of the waves proportional to the square of the coupling constant $(\frac{\partial \epsilon}{\partial Q})$. This process is called "stimulated" scattering.

In this picture of stimulated scattering, it is necessary to describe the amplification and attenuation of the fields through their mutual coupling. This description requires knowledge of the relative phases among the waves and thus the problem may most conveniently be treated by a classical, coupled wave approach.

In principle there are stimulated scattering processes associated with each spontaneous process[17]. The first stimulated light scattering process to be observed was stimulated Raman scattering[18], and since then many other stimulated processes have been observed, and studied in great detail[17,19].

The coupled wave appraoch in nonlinear optics was introduced by Armstrong et. al.[20] and has since been used by many authors[17,19,21] to describe various types of stimulated scattering. This is the approach which will be taken in this work to describe stimulated scattering from

local fluctuations in concentration in a binary gas mixture.

In the study of stimulated scattering, the important point is to determine how the electromagnetic fields couple to the medium in such a way that they can drive coherent fluctuations of the coordinates Q. Obviously the way to do this is to find the interaction energy between the medium and the fields in terms of Q. Then, differentiation with respect to Q gives the "force" (i.e. the form of the coupling term) on the coordinate due to the presence of the electromagnetic fields. This force acts on the medium in a manner which reduces the dielectric energy.

In the coupled wave approach, the coupling of the electromagnetic fields with the medium is given by an interaction Hamiltonian of the general form[22]

$$H_{int} = (\frac{\partial \epsilon}{\partial Q}) Q^* E_L E_S^* \qquad (1.2)$$

where $(\frac{\partial \epsilon}{\partial Q})$ is the coupling constant, Q is the amplitude of a normal mode coordinate of the material excitation, and E_L and E_S are field amplitudes of the incident and scattered electromagnetic waves. This form of the interaction energy determines the complete solution of the problem.

The solution for the scattered wave amplitude is indicated below. This discussion is presented in order to introduce the terminology used in treating stimulated scattering processes and to demonstrate the general structure of the solution. A more physical interpretation will then be given in order to make clear how the fields

and the medium interact.

The equation of motion for the material coordinate Q may be obtained in general from the classical Lagrangian density. The exact form of the equation of motion depends on the response of the particular material coordinate Q. However there will always be a coupling term of the form

$$\frac{\partial H_{int}}{\partial Q} \sim \left(\frac{\partial \epsilon}{\partial Q}\right) E_L E_S^* \tag{1.3}$$

in the equation of motion for the coordinate Q. Thus the dependence of Q on the fields, which is obtained by taking a Fourier transform and equating all terms at the same frequency, is given by

$$Q \sim \left(\frac{\partial \epsilon}{\partial Q}\right) E_L E_S^* \tag{1.4}$$

The dynamical equation for the scattered wave amplitude (Maxwell's equation) can be obtained rigorously from the Lagrangian density. However, the same result is obtained by observing that the form of the interaction energy implies the existence of a nonlinear polarization of the medium at the Stokes frequency which is given by

$$P^{NLS}(\omega_S) = \left(\frac{\partial \epsilon}{\partial Q}\right) Q^* E_L \tag{1.5}$$

With this polarization, direct use can be made of Maxwell's equation to obtain the behavior of the Stokes wave amplitude. The result is given by

$$\nabla^2 E_S - \frac{\epsilon_0}{c_0^2}\frac{\partial^2}{\partial t^2} E_S = -\frac{4\pi}{c_0^2}\frac{\partial^2}{\partial t^2} P^{NLS}$$

$$= -\frac{4\pi}{c_0^2}\left(\frac{\partial \epsilon}{\partial Q}\right)\frac{\partial^2}{\partial t^2} Q^* E_L \qquad (1.6)$$

where ϵ_0 is the linear dielectric constant. If the relaxation times for the normal modes of the medium are short compared to the laser pulse duration, a steady state solution for the scattered wave may be found of the form

$$E_S(z\,t) = E_S(z)\, e^{-ik_S z - i\omega_S t} .$$

Substituting this solution into Equation (1.6) and using the dependence of the coordinate Q on the fields given by Equation (1.4) gives the result

$$\frac{\partial E_S}{\partial z} \sim \left(\frac{\partial \epsilon}{\partial Q}\right)^2 |E_L|^2 E_S \qquad (1.7)$$

The Stokes wave thus grows exponentially in space as

$$E_S(z) = E_{S0}\, e^{g|E_L|^2 z} .$$

The stimulated wave builds up from the noise input at the Stokes frequency E_{S0}. The gain coefficient g depends on the square of the coupling constant $\left(\frac{\partial \epsilon}{\partial Q}\right)$ for the coordinate Q, and on the incident laser intensity $|E_L|^2$. The stimulated scattering process depends only on the existence of a coordinate dependent susceptibility of the medium.

This approach is applied in Chapter II to determine the gain coefficients for scattering from the normal modes of the fluid mixture. One would like to understand now, on a simplified basis, how the electromagnetic fields interact with the binary gas mixture.

If a static electromagnetic field with some spatial variation in intensity is applied to the mixture, the density will increase in the regions of greater field intensity. This behavior is due simply to the reduction of dielectric potential energy which is achieved by an increase in the density. The dielectric energy is given by

$$W = -\frac{1}{2} N\alpha |E|^2$$

where N is the number of molecules per unit volume and α is the molecular polarizibility. This result is the well known electrostrictive effect. In a gas mixture, the dielectric potential energy is also decreased by an increase in the concentration of the more polarizible molecules in the regions of greater field intensity.

This response of the medium leads to stimulated Brillouin and concentration scattering when the static field is replaced by the sum of the incident light wave with frequency ω_L and scattered wave with frequency ω_S. These stimulated processes are very different because, although the responses of the density and concentration to a static field are the same, the characteristics of the dynamic response are quite different.

The time required for the density to change in response to the influence of the fields is on order of the inverse sound wave frequency

($\sim 10^{-9}$ sec). The concentration can change in a time on the order of the diffusion relaxation time which, for the gas mixtures under investigation, is also about 10^{-9} sec. These response times are very long compared to the period of the light wave ($\sim 10^{-15}$ sec). Thus when the incident and scattered wave propagate through the medium, it responds only to slow variations of the total field intensity. The slow variation of the total intensity, which is produced by the interference between the incident and scattered waves, oscillates with frequency $\omega = \omega_L - \omega_S$. Thus this field is referred to as the difference frequency field.

When the incident and scattered waves propagate through the medium, the density and concentration are modulated by the difference frequency field for the same reason as in the static case, that is to reduce the dielectric energy. Thus the slow variation of the total field drives coherent periodic variations in the density and concentration which have the same period in space and time, but not the same phase, as the difference frequency field.

The driven density variation, given by Equation (1.4) with Q replaced by ρ, is a sound wave which propagates with the sound velocity v_S through the medium. The sound wave modulates the index of refraction through the coupling term $(\frac{\partial \epsilon}{\partial \rho})$ which leads to scattering with a Doppler shift in frequency given by kv_S, where k is the wave vector of the sound wave. The damping of the sound wave causes the material polarization wave Equation (1.5) to lag in phase behind the Stokes wave. The part of the polarization which is out of phase with

the Stokes field by $\pi/2$ does work on the field. The work done on the field leads to an increase in energy or gain, in the Stokes wave[23]. The result is stimulated Brillouin scattering.

Stimulated concentration scattering is analogous to the situation described above. The slow variation of the total field drives the variation in concentration. This variation modulates the index of refraction through the coupling term $(\frac{\partial \epsilon}{\partial c})$ which causes scattering. The concentration fluctuations however do not propagate, but instead relax through diffusion. In this case, it is the diffusive response which causes the polarization to lag behind the Stokes field. The diffusion relaxation time is $\frac{1}{Dk^2}$ where D is the diffusion constant and k is the inverse wavelength of the time average field. It is to be expected that the gain for the Stokes wave will be maximum for a frequency shift of $\omega = Dk^2$. This is reasonable, since for $\omega = 0$ the polarization is in phase with the Stokes field so the gain is zero and since the concentration fluctuation cannot respond to frequencies much larger than Dk^2 the gain is also zero for $\omega \gg Dk^2$.

Stimulated light scattering from temperature variations in the mixture may be described in exactly the same language as the concentration scattering. In this case the coupling term is $(\frac{\partial \epsilon}{\partial T})$ and the temperature variation is induced by the electrocaloric effect[24]. In analogy with the concentration scattering, the frequency shift of the scattered wave should be χk^2 where χ is the thermal conductivity of the medium.

One of the main features of stimulated scattering is that generally the scattering from only one mode of the system will be

stimulated. The reason for this is that the first stimulated wave grows so rapidly that it quickly depletes the laser. In a system with several modes one would calculate the gain for scattering from each mode independently. Stimulated scattering would then be observed from whichever mode presented the largest gain.

In nearly all types of binary fluid mixtures the Brillouin gain dominates the concentration gain. The object then of calculating the gain coefficients for the various modes is to determine the dependence of the gain on the physical parameters so that a mixture can be found in which it is possible to observe concentration scattering.

In a complicated system, such as the binary gas mixture, where there may be strong interaction between the various modes, one must determine the gain as a function of frequency shift for the complete coupled system in order to obtain good agreement with experiment results. The frequency shift of the stimulated wave is given by the value of the shift at which the gain is largest.

D. Summary

The object of this work was to attempt to observe stimulated light scattering from concentration fluctuations in the binary gas mixture. The theory of the response of the binary mixture and the way in which it couples to electromagnetic fields was considered in detail. The purpose of this investigation was to determine the dependence of the gain coefficient on various physical parameters so that an appropriate mixture could be chosen to investigate experimentally. The results of the theoretical study are presented in Chapter II. It

was found that a mixture of gases at relatively low pressure in which the two component molecules have a large difference in mass and in polarizibility is favorable for the observation of concentration scattering.

The main experimental difficulties were to produce a laser pulse of sufficiently large intensity that the threshold for stimulated scattering could be reached ($\sim 150 \frac{MW}{cm^2}$) and yet maintain a narrow linewidth ($\sim .005\ cm^{-1}$) so that the small frequency shift of the stimulated wave could be observed. The experimental techniques are discussed in Chapter III.

The frequency shift of the stimulated wave has been observed as a function of concentration in two gas mixtures He-SF_6 and He-Xe. In order to compare the experimental results with the predictions of the theory, it was necessary to calculate the gain coefficient as a function of frequency shift. This calculation required use of a computer. The gas transport coefficients were calculated from molecular parameters and the effects of the non ideal behavior of the gases were included. The results, presented in Chapter IV, show good agreement between theory and experiment.

References: Chapter I

1. von Smoluchowski, Ann. Physik 25, 205 (1908).

2. I. L. Fabelinskii, Adv. Phys. Sci. 63, 474 (1967).

3. A. Einstein, Ann. Physik 38, 1275 (1910).

4. P. J. W. Debye, Ann. Physik 39, 789 (1912).

5. L. Brillouin, Compt. Rend. 158, 1331 (1914); Ann. Physik 17, 88 (1922).

6. M. Leontovitch, Z. Physik 72, 247 (1931).

7. E. Gross, Nature 126, 201, 400, 603 (1930); Ann. Physik (Paris) 17, 88 (1922).

8. L. Landau and G. Placzek, Physik Z. Sowejetunion 5, 172 (1932).

9. R. D. Mountain and J. M. Deutch, J. Chem. Phys. 50, 1103 (1969).

10. G. B. Benedik, J. B. Lastkova, K. Fritsch, and T. J. Greytak, J. Opt. Soc. Am. 54, 1284 (1964).

11. R. Y. Chaio and B. P. Stoicheff, J. Opt. Soc. Am. 54, 1286 (1964).

12. I. L. Fabelinskii, Molecular Scattering of Light (Plenum N.Y. 1968) and references quoted therein. G. B. Benedik, in Statistical Phase Transition and Superfluidity, edited by M. Chietien, E. P. Gross, and S. Deser (Gordon and Breach, N.Y. 1968).

13. L. I. Komarov and I. Z. Fisher, Soviet Physics J.E.T.P. 16, 1358 (1963).

14. L. Van Hove, Phys. Rev. 95, 249 (1954).

15. S. Chapman and T. G. Cowling, The Mathematical Theory of Non Uniform Gases, (Cambridge University Press, Cambridge, England 1970), Chapt. 15.

16. W. S. Gornall, C. S. Wang, C. C. Young and N. Bloembergen, Phys. Rev. Letters 26, 1094, (1971).

17. N. Bloembergen, Am. J. Phys. 989 (1967) and references quoted therein.

References continued

18. E. J. Woodbury and W. K. Ng, Proc. IRE 50, 2347 (1962).

19. See Chapter II, ref. 5-9.

20. J. A. Armstrong, N. Bloembergen, J. Duccuing and P. S. Pershan, Phys. Rev., 127, 1918 (1962).

21. Y. R. Shen and N. Bloembergen, Phys. Rev. 137, 1787 (1965).

22. C. S. Wang, Phys. Rev. 182, 482 (1969).

23. N. Bloembergen, Nonlinear Optics (W. A. Benjamin Inc., N.Y. 1965), Chapt. 1.

24. L. D. Landau and E. M. Lifshitz, Electrodynamics of Continuous Media, (Addison Wesley Publ. Co., Reading, Mass., 1960) p. 56 f. f.

CHAPTER II

THEORY OF STIMULATED CONCENTRATION SCATTERING

A. Introduction

In this chapter the analysis of stimulated light scattering in a binary gas mixture is developed following, in general, the analysis given by Bloembergen et. al.[1] The dynamical equations which characterize the mixture are presented. The collective modes of the mixture and their mutual coupling which are described by the hydrodynamic equations are discussed in detail. The manner in which the electromagnetic field couples to the gas mixture is described. Finally, the gains for the various stimulated scattering processes are calculated and it is shown that gas mixtures at relatively low pressures with a large difference in mass and polarizibility of the two component molecules are favorable for the observation of stimulated concentration scattering.

B. Fundamental Equations of Fluid Dynamics

1. Ideal Fluid

The mathematical description of the state of a homogeneous, moving fluid is determined by means of functions which give the distribution of the fluid velocity $\vec{v} = \vec{v}(x, y, z, t)$ and any of two thermodynamic quantities which characterize the fluid, such as the pressure $P(x, y, z, t)$ and density $\rho(x, y, z, t)$. It is well known that all of the thermodynamic quantities are determined by the values of any two of them and the equation of state. Thus the state of the fluid is completely

determined by five quantities; the three components of velocity and the density and pressure.

All of these quantities are in general functions of the coordinates x, y, z and the time t. These coordinates refer to a point fixed in space and not to the particles in the fluid. The fundamental equations which describe the fluid behavior arise from simple expressions of basic conservation laws. These equations are well known[2] and will only be briefly reviewed.

The first of the fundamental equations of hydrodynamics expresses conservation of matter and is

$$\frac{\partial \rho}{\partial t} + \operatorname{div}(\rho \vec{v}) = 0 \qquad (2.1)$$

where ρ is the fluid density and $\vec{v}$ the velocity. This result is the well known equation of continuity. The second fundamental equation of fluid dynamics is Newton's Second Law applied to a volume element of the fluid. The result is

$$\frac{\partial \vec{v}}{\partial t} + (\vec{v} \cdot \operatorname{grad})\vec{v} = -\frac{1}{\rho} \operatorname{grad} P \qquad (2.2)$$

where P is the pressure. This result is Euler's equation. In deriving this equation, all processes of energy dissipation which may occur in a moving fluid due to internal friction (viscosity) in the fluid or heat exchange between different parts of the fluid are ignored. This equation then is valid only for an ideal fluid in which viscosity and thermal conductivity are not important. Since there is no heat exchange in an ideal fluid, its motion is adiabatic. This result leads

to the final (adiabatic) equation

$$\frac{ds}{dt} = \frac{\partial s}{\partial t} + \vec{v} \cdot \text{grad}\, s = 0 \qquad (2.3)$$

where s is the entropy per unit mass.

A complete set of equations which describe the dynamics of an ideal fluid then are Euler's equations, the equation of continuity, and the adiabatic equation. In order to describe the fluid dynamics for the experimental situation, the effects of viscosity, thermal conductivity and diffusion must be included. Before proceeding with this program it is useful to consider an expression for the energy flux in an ideal fluid. The energy of the fluid per unit volume is

$$\frac{1}{2}\rho v^2 + \rho \epsilon \qquad (2.4)$$

where ϵ is the internal energy per unit mass. Using the equation of continuity and Euler's equation it can be easily shown that

$$\frac{\partial}{\partial t}\left(\frac{1}{2}\rho v^2 + \rho \epsilon\right) = -\,\text{div}\left[\rho \vec{v}\left(\frac{1}{2}v^2 + w\right)\right] \qquad (2.5)$$

where w is the enthalpy per unit mass ($w = \epsilon + P/\rho$). This equation is a simple statement of energy conservation.

2. Fluids with Viscosity and Thermal Conductivity

The energy dissipation which occurs during the motion of a non-ideal fluid is a result of the thermodynamic irreversibility of the motion. This irreversibility always occurs to some extent and is due to internal friction (viscosity) and thermal conduction. Euler's

equation can be written in the form

$$\frac{\partial}{\partial t}(\rho \vec{v}_i) = -\frac{\partial \pi_{ik}}{\partial x_k} \qquad (2.6)$$

$$\pi_{ik} = P\delta_{ik} + \rho v_i v_k$$

where π_{ik} is the momentum flux density tensor; i.e. π_{ik} is the i^{th} component of the momentum density flowing per unit time through a unit area perpendicular to the x_k axis. This momentum flux represents a completely reversible transfer of momentum, due simply to the mechanical transport of fluid particles and to the pressure forces acting in the fluid. The viscosity is due to another, irreversible transfer of momentum from points where the velocity is large to those where it is small. The equation of motion for a viscous fluid may be obtained by adding to the "ideal" momentum flux a term $-\sigma_{ik}$ which gives the irreversible "viscous" transfer of momentum in the fluid.

$$\pi_{ik} = P\delta_{ik} + \rho v_i v_k - \sigma'_{ik} \quad . \qquad (2.7)$$

The fact that internal friction can occur only when there is relative motion between various parts of the fluid requires that σ'_{ik} have the general form

$$\sigma'_{ik} = \eta\left(\frac{\partial v_i}{\partial x_k} + \frac{\partial v_k}{\partial x_i} - \frac{2}{3}\delta_{ik}\frac{\partial v_\ell}{\partial x_\ell}\right) + \zeta\,\delta_{ik}\frac{\partial v_\ell}{\partial x_\ell} \qquad (2.8)$$

where the constants η, ζ are the coefficients of shear and bulk viscosity, respectively, and are functions of pressure and temperature. In most

cases however the coefficients of viscosity do not change appreciably in the fluid and may be regarded as constants. The equation of motion in a viscous fluid then becomes

$$\rho \left[\frac{\partial \vec{v}}{\partial t} + (\vec{v} \cdot \text{grad}) \vec{v} \right] = - \text{grad } P + \eta \nabla^2 v + \left(\zeta + \frac{1}{3} \eta \right) \text{grad div } \frac{1}{v} \tag{2.9}$$

This result is called the Navier-Stokes equation, and it replaces Euler's equation in a viscous fluid.

In a viscous fluid the equation of conservation of entropy is not valid since irreversible processes of energy dissipation occur. This equation must therefore be replaced by a more general result. In the ideal fluid the law of conservation of energy is given by equation (2.5)

$$\frac{\partial}{\partial t} \left(\frac{1}{2} \rho v^2 + \rho \epsilon \right) = - \text{div} \left[\rho \vec{v} \left(\frac{1}{2} v^2 + w \right) \right] \tag{2.10}$$

In a viscous fluid, energy conservation still holds, of course: the change per unit time in the total energy of the fluid in any volume must still be equal to the total flux of energy through the surface bounding that volume. However, the energy flux density now has a different form. In addition to the flux $\rho \vec{v} \left(\frac{1}{2} v^2 + w \right)$ due to the simple transfer of mass by motion of the fluid, there is a flux due to the process of internal friction. This flux is given by the vector $\vec{v} \cdot \underset{\approx}{\sigma}'$. Also if the temperature of the fluid is not uniform there will be a transfer of energy by thermal conduction. This process is a direct molecular transfer of energy from points where the temperature is high to those where it is low. It does not involve a macroscopic motion, and occurs even in a fluid at rest.

The heat flux density $\vec{q}$ is then related to temperature variations throughout the fluid. If the temperature variations are small, $\vec{q}$ may be expanded as power series in the temperature gradient and only the first term in the expansion retained.

$$\vec{q} = -\lambda \text{ grad } T$$

The thermal conductivity λ is in general a function of temperature and pressure.

The law of energy conservation in a fluid which has viscosity and thermal conduction is then given by

$$\frac{\partial}{\partial t}\left(\frac{1}{2}\rho v^2 + \rho\epsilon\right) = -\text{div}\left[\rho\vec{v}\left(\frac{1}{2}v^2 + w\right) - \vec{v}\cdot\underline{\sigma}' - \lambda \text{ grad } T\right] \quad (2.11)$$

This equation along with the equation of continuity and the Navier-Stokes equation form a complete set of equations for the viscous, homogeneous fluid.

3. Binary Fluid Mixture

Up to this point in the discussion, it has been assumed that the fluid is completely homogeneous. In this work however, the physical system is a mixture of two gases. To describe this system the equations of fluid dynamics must be modified.

Consider a mixture of two fluids containing N_1 molecules of mass m_1 and N_2 molecules of mass m_2 per unit volume. The chemical potentials of the two species are μ_1 and μ_2. The differential free energy may then be expressed as

$$dF = - sdT - PdV + \mu_1 dN_1 + \mu_2 dN_2 \quad . \tag{2.12}$$

The mass density is

$$\rho = N_1 m_1 + N_2 m_2 = N[(1-c')\, m_1 + c' m_2] \tag{2.13}$$

where N is the total number of particles per unit volume and c' is the relative number concentration of the second species, i.e.

$$c' = \frac{N_2}{N} \tag{2.14}$$

It is related to the relative mass concentration c by

$$c = \frac{N_2 m_2}{N_1 m_1 + N_2 m_2} = c'[c' + (1 - c')\, \frac{m_1}{m_2}]^{-1}$$

$$c' = c[c + (1 - c)\, \frac{m_2}{m_1}]^{-1} \tag{2.15}$$

and

$$\frac{\partial c}{\partial c'} = (\frac{\partial c'}{\partial c})^{-1} = \frac{m_1 m_2}{[m_2 c' + m_1(1 - c')]^2} \tag{2.16}$$

$$= \frac{[m_1 c + (1 - c) m_2]^2}{m_1 m_2}$$

The distribution of concentration changes in time in two ways. First, when there is macroscopic motion of the fluid, any small portion of it moves as a whole without changing composition. This results in a purely mechanical mixing of the fluid. If thermal conduction and internal friction are ignored, this change in concentration

is a thermodynamically reversible process and does not result in energy dissipation. Second, a change in composition can occur by the molecular transfer of the components from one region in the fluid to another. This process is diffusion which is irreversible and, like viscosity and thermal conduction, is one of the sources of energy dissipation in a fluid mixture.

In a fluid mixture, the equation of continuity still holds

$$\frac{\partial \rho}{\partial t} + \text{div}\,(\rho \vec{v}) = 0 \qquad (2.17)$$

Strictly speaking the concept of velocity must be redefined for a mixture. As written in Equation (2.17), the velocity is defined as the total momentum per unit mass of the fluid. The Navier-Stokes equation (2.9) is also unchanged for a fluid mixture.

It was shown earlier that a complete set of equations for the fluid dynamics of a single component fluid are the continuity equation, the Navier-Stokes equation and the energy conservation equation. For the binary fluid mixture, one additional equation is required. This equation is obtained from the fact that, in addition to conservation of total mass, the number (or mass) of molecules of the individual species must also be conserved. In the absence of diffusion

$$\frac{dc}{dt} = 0$$

or

$$\frac{\partial c}{\partial t} + (v \cdot \text{grad})\, c = 0 \qquad (2.18)$$

Combining with Equation (2.17) gives the result

$$\frac{\partial}{\partial t}(\rho c) + \operatorname{div}(\rho c v) = 0 \qquad (2.19)$$

When diffusion occurs, there is another contribution to the flux. Let $\vec{i}$ be the density of the diffusion flux, i.e. the amount of one component transported by diffusion through a unit area in unit time. This leads to the equation of continuity for one component

$$\rho\left(\frac{\partial c}{\partial t} + \vec{v}\cdot \operatorname{grad} c\right) = -\operatorname{div} i \qquad (2.20)$$

The final equation for a fluid mixture is again the equation of conservation of energy Equation (2.11)

$$\frac{\partial}{\partial t}\left(\tfrac{1}{2}\rho v^2 + \rho\epsilon\right) = -\operatorname{div}\left[\rho v\left(\tfrac{1}{2}v^2 + w\right) - \vec{v}\cdot\underline{\sigma}' + \vec{q}\right]$$

It is convenient to put this equation in another form.
Direct evaluation of the left hand side of Equation (2.11) gives

$$\frac{\partial}{\partial t}\left(\tfrac{1}{2}\rho v^2 + \rho\epsilon\right) = \tfrac{1}{2}v^2\frac{\partial\rho}{\partial t} + \rho\vec{v}\cdot\frac{d\vec{v}}{dt} + \rho\frac{\partial\epsilon}{\partial t} + \epsilon\frac{\partial\rho}{\partial t}$$

Using the equation of continuity for $\frac{\partial\rho}{\partial t}$ and the Navier-Stokes equation for $\frac{\partial\vec{v}}{\partial t}$ gives the result

$$\frac{\partial}{\partial t}\left(\tfrac{1}{2}\rho v^2 + \epsilon\right) = -\tfrac{1}{2}v^2\operatorname{div}(\rho\vec{v}) - \rho\vec{v}\cdot\operatorname{grad}\tfrac{1}{2}v^2 - \vec{v}\cdot\operatorname{grad} P$$

$$+ v_i\frac{\partial\sigma'_{ik}}{\partial x_k} + \rho\frac{\partial\epsilon}{\partial t} - \epsilon\operatorname{div}(\rho\vec{v}) \quad . \qquad (2.21)$$

For a mixture of two fluids, the internal energy is given by

$$d\epsilon = Tds - PdV + \mu_1 dn_1 + \mu_2 dn_2$$

where n_1, n_2 are the numbers of particles of the two species per unit mass of the mixture. The numbers n_1, n_2 satisfy the relation $n_1 m_1 + n_2 m_2 = 1$. Using the concentration $c = n_2 m_2$ gives

$$d\epsilon = Tds - PdV + \left(\frac{\mu_2}{m_2} - \frac{\mu_1}{m_1}\right) dc$$

which can also be written as

$$d\epsilon = Tds + P/\rho^2 \, d\rho + \mu \, dc$$

where $\mu = \frac{\mu_2}{m_2} - \frac{\mu_1}{m_1}$ is the chemical potential per unit mass of the mixture. This relation may be used to calculate $\frac{\partial \epsilon}{\partial t}$ and further, grad P may be obtained from the differential enthalpy per unit mass

$$dw = Tds + \frac{1}{\rho} dP + \mu \, dc$$

Also

$$v_i \frac{\partial \sigma'_{ik}}{\partial x_k} = \text{div } \vec{v} \cdot \underset{\approx}{\sigma'} - \sigma'_{ik} \frac{\partial v_i}{\partial x_k}$$

After adding and subtracting div $\vec{q}$, the result is obtained

$$\frac{\partial}{\partial t}\left(\frac{1}{2}\rho v^2 + \rho\epsilon\right) = -\operatorname{div}\left[\rho\vec{v}\left(\frac{1}{2}v^2 + w\right) - \vec{v}\cdot\underline{\sigma}' + \vec{q}\right]$$

$$+ \rho T\left(\frac{\partial s}{\partial t} + v\cdot\operatorname{grad} s\right) - \sigma'_{ik}\frac{\partial v_i}{\partial x_k} + \operatorname{div} q - \mu \operatorname{div} i \qquad (2.22)$$

Comparing this result with the equation of energy conservation in (2.21) gives the result:

$$\rho T\left(\frac{\partial s}{\partial t} + v\cdot\operatorname{grad} s\right) = \sigma'_{ik}\frac{\partial v_i}{\partial x_k} - \operatorname{div}\left(\vec{q} - \mu\vec{i}\right) - i\operatorname{grad}\mu \qquad (2.23)$$

This is the general equation of heat transfer for a binary fluid mixture. The left hand side is simply $\rho T\frac{ds}{dt}$ which is the quantity of heat gained per unit volume per unit time. The first term on the right hand side is the energy dissipated into heat by viscosity. The remaining terms are the heat conducted into the volume concerned.

The complete set of equations of fluid mechanics for a mixture has now been determined and consists of the equation of continuity (2.17), and continuity for one component (2.20), the Navier-Stokes equation (2.9) and the general heat transfer equation (2.23). These equations, however, are not determinate until the fluxes $\vec{i}$ and $\vec{q}$ are replaced by expressions in terms of the gradients of concentration and temperature. If the gradients are small, $\vec{i}$ and $\vec{q}$ can be written in the form

$$\vec{i} = -\alpha \text{ grad } \mu - \beta \text{ grad } T$$
$$\vec{c_i} - \mu\vec{i} = \delta \text{ grad } \mu - \gamma \text{ grad } T \qquad (2.24)$$

The symmetry principle for kinetic coefficients requires

$$\delta = \beta T,$$

and, if grad $\vec{\mu}$ is eliminated from the expression for the heat flux, the result is obtained that

$$i = -\alpha \text{ grad } \mu - \beta \text{ grad } T$$
$$q = (\mu + \frac{\beta T}{\alpha})\vec{i} - \lambda \text{ grad } T$$

where

$$\lambda = \gamma - \frac{\beta^2 T}{\alpha}$$

is the thermal conductivity.

The chemical potential μ may be expanded as a function of P, T, c

$$\text{grad } \mu = (\frac{\partial \mu}{\partial c})_{P,T} \text{ grad } c + (\frac{\partial \mu}{\partial T})_{c,P} \text{ grad } T + (\frac{\partial \mu}{\partial P})_{c,T} \text{ grad } P \ .$$

The Gibbs free energy per unit mass is given by

$$d\Phi = -s\,dT + V\,dP + \mu\,dc \qquad (2.25)$$

from which it can easily be shown that

$$(\frac{\partial \mu}{\partial P})_{c,T} = \frac{\partial^2 \Phi}{\partial P \partial c} = (\frac{\partial V}{\partial c})_{P,T}$$

The coefficients of diffusion, thermal diffusion and barodiffusion are

introduced by the following relations

$$D = \frac{a}{\rho}\left(\frac{\partial \mu}{\partial c}\right)_{T,P}$$

$$\rho k_T \frac{D}{T} = a\left(\frac{\partial \mu}{\partial T}\right)_{c,P} + \beta \qquad (2.26)$$

$$k_P = P\left(\frac{\partial V}{\partial c}\right)_{P,T} \Big/ \left(\frac{\partial \mu}{\partial c}\right)_{P,T} = -P\left(\frac{\partial \rho}{\partial c}\right)_{P,T} \Big/ \rho^2 \left(\frac{\partial \mu}{\partial c}\right)_{P,T} .$$

Using these definitions gives the result

$$i = -\rho D\left[\text{grad } c + \frac{k_T}{T}\ \text{grad } T + \frac{k_P}{P}\ \text{grad } P\right] \qquad (2.27)$$

$$q = \left[k_T\left(\frac{\partial \mu}{\partial c}\right)_{P,T} - T\left(\frac{\partial \mu}{\partial T}\right)_{P,c} + \mu\right]\vec{i} - \lambda\ \text{grad } T.$$

The discussion which follows will apply only to fluid mixtures which satisfy the conditions: 1) The concentration and temperature vary slowly so that the coefficients in Equation (2.27) may be considered as constant; although they are in general functions of c, T. 2) There is no macroscopic motion of the fluid except that which may be caused by temperature or concentration gradients. The velocity of this motion is proportional to the gradients so the terms in (2.20) and (2.23) which contain the velocity are of second order and may be ignored. The term $-i\ \text{grad}\ \mu$ in (2.23) is also of second order. In this case the equation of continuity for one component and the heat transfer equation become

$$\rho \frac{\partial c}{\partial t} + \text{div}\, \vec{i} = 0$$

$$\rho T \frac{\partial s}{\partial t} + \text{div}\, (\vec{q} - \mu \vec{i}) = 0.$$

Substituting for $\vec{i}$ and $\vec{q}$ from Equation (2.27) and transforming the derivative $\frac{\partial s}{\partial t}$ as follows

$$\frac{\partial s}{\partial t} = \left(\frac{\partial s}{\partial T}\right)_{c_P} \frac{\partial T}{\partial t} + \left(\frac{\partial s}{\partial c}\right)_{T,P} \frac{\partial c}{\partial t} + \left(\frac{\partial s}{\partial P}\right)_{T,c} \frac{\partial P}{\partial t}$$

$$= \frac{c_P}{T} \frac{\partial T}{\partial t} - \left(\frac{\partial \mu}{\partial T}\right)_{P,c} \frac{\partial c}{\partial t} + \left(\frac{\partial s}{\partial P}\right)_{T,c} \frac{\partial P}{\partial t}$$

gives the result

$$\frac{\partial T}{\partial t} - \frac{k_T}{c_P} \left(\frac{\partial \mu}{\partial c}\right)_{P,T} \frac{\partial c}{\partial t} + \frac{T}{c_P} \left(\frac{\partial s}{\partial P}\right)_{T,c} \frac{\partial P}{\partial t} = \chi \nabla^2 T \qquad (2.28)$$

where

$$\chi = \frac{\lambda}{\rho c_P}$$

and

$$\frac{\partial c}{\partial t} = D \left[\nabla^2 c + \frac{k_T}{T} \nabla^2 T + \frac{k_P}{P} \nabla^2 P\right] \qquad (2.29)$$

The complete set of equations for a binary fluid mixture have now been obtained in their final form from the basic laws of conservation of mass, momentum, energy and mass of one component. These results are summarized here:

(i) Continuity equation (conservation of mass)

$$\frac{\partial \rho}{\partial t} + \text{div}\,(\rho \vec{v}) = 0 \qquad (2.17)$$

(ii) Navier-Stokes equation (conservation of momentum)

$$\frac{\partial \vec{v}}{\partial t} + (\vec{v} \cdot \text{grad})\,\vec{v} = -\frac{1}{\rho}\,\text{grad}\,P + \frac{\eta}{\rho}\nabla^2 \vec{v} + \frac{1}{\rho}\left(\frac{1}{3}\eta + \zeta\right)\text{grad div}\,\vec{v} \qquad (2.9)$$

(iii) Thermal diffusion equation (conservation of energy)

$$\frac{\partial T}{\partial t} - \frac{k_T}{c_P}\left(\frac{\partial \mu}{\partial c}\right)_{P,T}\frac{\partial c}{\partial t} + \frac{T}{c_P}\left(\frac{\partial s}{\partial P}\right)_{T,c}\frac{\partial P}{\partial t} = \chi \nabla^2 T \qquad (2.28)$$

(iv) Concentration diffusion equation (conservation of particle number of individual species)

$$\frac{\partial c}{\partial t} = D\left[\nabla^2 c + \frac{k_T}{T}\nabla^2 T + \frac{k_P}{P}\nabla^2 P\right] \qquad (2.29)$$

In this macroscopic thermodynamic approach the transport coefficients are regarded as constants, to be obtained experimentally, which describe the properties of a continuous medium. In a microscopic approach, the macroscopic conservation laws are derived from the Boltzman equation according to the Chapman-Enskog procedure. The transport coefficients are then obtained in terms of the molecular parameters. This procedure will be discussed in greater detail in Chapter IV.

For very dilute gases, the hydrodynamic equations are no longer valid because the change in the dynamical variables over the mean free

path length becomes large. The dimensionless constant which is characteristic of the transition from the hydrodynamic to the kinetic regime may be written in the form

$$y = (8\pi)^{\frac{1}{2}} N \frac{\sigma^2}{k} = \frac{\lambda}{\pi^{3/2}\bar{\ell}} \qquad (2.30)$$

where λ is the wavelength of periodic variations and $\bar{\ell} = \frac{1}{\sqrt{2}\pi N\sigma^2}$ is the mean free path. For $y > 3$ the hydrodynamic equations are valid. The values of the parameter y for the various gases used are given in Chapter IV.

C. Collective Modes in a Binary Mixture - Their Damping and Mutual Coupling.

1. Introduction

Before proceeding to include the effects of the electromagnetic fields into the basic hydrodynamic equations for the binary fluid mixture, let us examine the collective modes (sound wave, concentration and thermal diffusion) described by these equations and the coupling between them. Of course the collective modes and all the effects of coupling may be immediately obtained from the general dispersion relation, and this is done later in connection with the gain calculation. However, this dispersion relation is quite complicated so a better physical understanding of the system may be obtained by considering the collective modes and their coupling individually.

2. Concentration and Thermal Diffusion Modes and Their Coupling

The concentration diffusion mode is defined by the equation

$$\frac{\partial c}{\partial t} = D \nabla^2 c \quad , \tag{2.31}$$

which represents a non-propagating wave with a damping constant $\Gamma = i\omega = Dk^2$. The thermal diffusion mode is given by an equation which is identical in form to the concentration equation.

$$\frac{\partial T}{\partial t} = \chi \nabla^2 T \quad . \tag{2.32}$$

This equation again represents a non-propagating mode with damping constant $i\omega = \chi k^2$.

The coupling between the concentration and thermal diffusion modes is described by the equations

$$\begin{aligned} &\frac{\partial T}{\partial t} - \frac{k_T}{c_P} \left(\frac{\partial \mu}{\partial c}\right)_{P,T} \frac{\partial c}{\partial t} = \chi \nabla^2 T \\ &\frac{\partial c}{\partial t} = D \left[\nabla^2 c + \frac{k_T}{T_0} \nabla^2 T\right] \end{aligned} \tag{2.33}$$

Taking the Fourier transform of these equations leads to the dispersion relation

$$(i\omega)^2 - (\mathcal{D}k^2 + \chi k^2)\, i\omega + \chi D k^4 = 0$$

where

$$\mathcal{D} = D \left[1 + \frac{k_T^2}{T_0 c_P} \left(\frac{\partial \mu}{\partial c}\right)_{P,T}\right] \quad .$$

The roots of the dispersion equation are

$$i\omega = \frac{1}{2}(\mathcal{D}k^2 + \chi k^2) \pm \frac{1}{2}[(\mathcal{D}k^2 + \chi k^2)^2 - 4\chi D k^4]^{\frac{1}{2}} \qquad (2.34)$$

These roots give the damping constants for the coupled concentration and thermal diffusion modes. Of course, in the limit of $k_T = 0$ when there is no coupling, these results reduce to the original results for the uncoupled modes

$$i\omega = Dk^2, \quad \chi k^2 \qquad \text{for} \qquad k_T \to 0$$

A simple expression for the effect of the thermal diffusion mode on the concentration mode can be obtained in the limit of $\chi \ll D$. Then the concentration damping constant is given by

$$i\omega = Dk^2 \left[1 + \frac{k_T^2}{T_0 c_P} \left(\frac{\partial \mu}{\partial c}\right)_{P,T} \right] \qquad (2.35)$$

The term $\frac{k_T^2}{T_0 c_P} \left(\frac{\partial \mu}{\partial c}\right)$ is of the order of 10^{-2} for the gas mixtures used in this experiment and thus is negligible. In liquids, c_P becomes larger and $\left(\frac{\partial \mu}{\partial c}\right)_{P,T}$ smaller so the additional term is even smaller. The result is that, in this limit, coupling between the thermal and concentration modes is negligible. In the linear response to an external field, each mode will exhibit a separate Lorentzian line shape. This result could also have been easily obtained from the coupled equations (2.33) for then, since χ is small,

$$\frac{\partial T}{\partial t} \simeq \frac{k_T}{c_P} \left(\frac{\partial \mu}{\partial t}\right)_{P,T} \frac{\partial c}{\partial t}$$

which, after taking the Fourier transform, leads directly to the result given in Equation (2.35).

The effect of the concentration mode on the thermal diffusion in the limit $D \ll \chi$ can be obtained in an analogous fashion. The thermal damping constant is then given by

$$i\omega = \chi k^2 + \frac{Dk^2 k_T^2}{T_0 c_P} \left(\frac{\partial \mu}{\partial c}\right)_{P,T} \tag{2.36}$$

The additional damping introduced by the coupling is again negligible due to the small value of k_T.

In general, for the gas mixtures used in this experiment, in the region of concentrations in which the concentration and thermal diffusion modes are important, the diffusion coefficient and the thermal diffusion coefficient are approximately equal so the effects of the coupling must be determined from the complete dispersion relation Equation (2.34).

3. The Sound Wave Mode

If the sound wave amplitude is small, the pressure and density may be written in the form

$$P = P_0 + P_1$$

$$\rho = \rho_0 + \rho_1$$

where P_0 and ρ_0 are the constant equilibrium pressure and density and P_1 and ρ_1 are the variations in the sound wave ($P_1 \ll P_0$, $\rho_1 \ll \rho_0$).

The equation of continuity (2.17) and the Navier-Stokes equation (2.9) may be linearized and combined to give a small amplitude sound wave equation

$$\frac{\partial^2 \rho_1}{\partial t^2} = \nabla^2 P_1 + \frac{1}{\rho_0} \left(\frac{4}{3}\eta + \zeta\right) \nabla^2 \frac{\partial \rho_1}{\partial t} \quad . \tag{2.37}$$

The set of thermodynamic variables which will be used are P, T, c. The density variation may be written in terms of these variables as

$$\rho_1 = \left(\frac{\partial \rho}{\partial P}\right)_{T,c} P_1 + \left(\frac{\partial \rho}{\partial T}\right)_{P,c} T_1 + \left(\frac{\partial \rho}{\partial c}\right)_{P,T} c_1$$

and let

$$\left(\frac{\partial P}{\partial \rho}\right)_T = v_T^2 = \frac{1}{\gamma}\left(\frac{\partial P}{\partial \rho}\right)_s = \frac{v_s^2}{\gamma}$$

where v_T and v_s are the isothermal and adiabatic sound velocities respectively. The subscript 1 on the non equilibrium part of the thermodynamic variables will now be dropped. Equation (2.37) becomes

$$\left(\frac{\partial \rho}{\partial c}\right)_{P,T} \frac{\partial^2 c}{\partial t^2} + \left(\frac{\partial \rho}{\partial t}\right)_{P,c} \frac{\partial^2 T}{\partial t^2} + \frac{1}{v_T^2} \frac{\partial^2 P}{\partial t^2} = \nabla^2 P + \frac{1}{\rho_0}\left(\frac{4}{3}\eta + \zeta\right) \tag{2.38}$$

$$\times \left[\frac{1}{v_T^2} \nabla^2 \frac{\partial P}{\partial t} + \left(\frac{\partial \rho}{\partial c}\right)_{T,P} \nabla^2 \frac{\partial c}{\partial t} + \left(\frac{\partial \rho}{\partial T}\right)_{P,c} \nabla^2 \frac{\partial T}{\partial t}\right]$$

When the concentration and temperature fluctuations are small, Equation (2.38) reduces to

$$\frac{\partial^2 P}{\partial t^2} = v_T^2 \nabla^2 P + \frac{\eta'}{\rho_0} \nabla^2 \frac{\partial P}{\partial t}$$

where

$$\eta' = \frac{4}{3}\eta + \zeta$$

which gives the dispersion relation

$$(i\omega)^2 - \frac{\eta' k^2}{\rho_0} i\omega + v_T^2 k^2 = 0 \quad . \tag{2.39}$$

For long wavelength $k \ll \frac{v_T \rho_0}{\eta'}$, the dispersion relation is given by

$$i\omega \simeq \frac{\eta' k^2}{2\rho_0} \pm i k v_T \left[1 - \frac{\eta'^2 k^2}{8\rho_0^2 v_T^2} \right]$$

which represents the damped propagating sound wave mode $P = P_0 e^{ik\cdot z - (i\omega + \Gamma_v)t}$ with velocity $\simeq v_T$ and viscous damping constant

$$\Gamma_v = \frac{k^2}{2\rho_0} \left(\frac{4}{3}\eta + \zeta\right) \quad .$$

4. Coupling of Sound Wave and Thermal Diffusion Mode

In examining the coupling between the sound wave and the thermal diffusion mode, the concentration fluctuations and viscous damping may be ignored. In this case, the equations which describe the physical system are

$$\left(\frac{\partial \rho}{\partial T}\right)_{P,c} \frac{\partial^2 T}{\partial t^2} + \frac{1}{v_T} \frac{\partial^2 P}{\partial t^2} = \nabla^2 P$$

$$\frac{\partial T}{\partial t} + \frac{T}{c_P} \left(\frac{\partial s}{\partial P}\right)_{T,c} \frac{\partial P}{\partial t} = \chi \nabla^2 T \qquad (2.40)$$

Taking a Fourier transform of these equations leads to a secular determinant of the form

$$\begin{vmatrix} \omega^2 \left(\frac{\partial \rho}{\partial T}\right)_P & \frac{\omega^2}{v_T^2} - k^2 \\ i\omega - \chi k^2 & i\omega \left(\frac{\partial s}{\partial P}\right)_T \frac{T}{c_P} \end{vmatrix} = 0$$

This dispersion relation can be put in the form

$$k^4 - k^2 \left(\frac{\omega^2}{v_T^2} + \frac{i\omega}{\chi}\right) + \frac{i\omega^3}{\chi v_s^2} = 0 \qquad (2.41)$$

The solution to this equation can be obtained for two limiting cases.

1) Adiabatic (low frequency or long wavelength)

$$\omega \ll \frac{v^2}{\chi} \quad ; \quad k \ll \frac{v_T}{\chi}$$

In this case, Equation (2.41) gives

$$k \simeq \frac{\omega}{v_s} + \frac{i\omega^2 \chi}{2 v_s} \left(\frac{1}{v_T^2} - \frac{1}{v_s^2}\right) \qquad (2.42)$$

or

$$\omega = kv_s \quad ; \quad \Gamma_T = \frac{k^2\chi}{2}\left(\frac{c_P}{c_v} - 1\right) = \frac{k^2\lambda}{2\rho}\left(\frac{1}{c_v} - \frac{1}{c_P}\right)$$

which corresponds to the propagation of sound with the adiabatic velocity and on absorption coefficient Γ_T. This result is correct $\omega \ll v^2/\chi$ means that during one period the distance which heat can be transmitted $\sim \sqrt{\frac{\lambda}{\omega}}$ is small compared with the wavelength $\frac{v_s}{\omega}$

2) Isothermal (high frequency)

$$\omega \gg \frac{v^2}{\chi} \; ; \quad k \gg \frac{v}{\chi}$$

In this case

$$k \simeq \frac{\omega}{v_T} + i\,\frac{v_T}{2\chi v_s^2}\,(v_s^2 - v_T^2) \qquad (2.43)$$

or

$$\omega = k v_T \quad ;$$

$$\Gamma_T = \frac{v_T^2}{2\chi}\left(1 - \frac{c_v}{c_P}\right) = \frac{v_T^2\rho}{2k}\,(c_P - c_v)$$

In this case, the sound is propagated with the isothermal velocity. The interest in this experiment is with light scattered in the backward direction from a gas. In this case $k = 2k_L$ where k_L is the wave vector of the laser light wave. Putting in numerical values, one finds that for all liquids, and gases with pressure greater than a few atmospheres, the adiabatic limit condition is satisfied. Typical results for some common gases are given in Table (2.1).

Gas	$\frac{k_L \chi}{v_T}$
He	3.811/P
χe	.786/P
SF_6	.443/P

Table (2.1) - Values of the parameter $\frac{k\chi}{v_T}$ for gases of interest

The dispersion relation Equation (2.41) for the coupled pressure and temperature equations is third order in $i\omega$. Two of the roots are the ones discussed above $\omega = \pm k v_s$ which correspond to sound waves traveling in opposite directions. The remaining root corresponds to the thermal diffusion mode including the effects of the sound wave coupling. For this mode $\omega \to 0$ so the dispersion relation becomes approximately

$$i\omega = \chi k^2 + \frac{(i\omega)^2 \chi}{v_T^2} \qquad (2.44)$$

In the low frequency, long wave length limit

$$\omega \ll \frac{v_T^2}{\chi} , \quad k \ll \frac{v_T}{\chi} , \quad \omega \ll k v_T ,$$

This result gives the normal thermal diffusion damping constant

$$i\omega = \chi k^2 + O(0)$$

Thus the coupling of the sound wave and the thermal diffusion mode introduces negligible change in the thermal damping constant.

5. Coupling of Sound Wave and Concentration Diffusion Mode

In the adiabatic regime the coupling between the sound wave and the concentration diffusion mode is given by the equations

$$\left(\frac{\partial \rho}{\partial c}\right)_{T,P} \frac{\partial^2 c}{\partial t^2} + \frac{1}{v_s^2} \frac{\partial^2 P}{\partial t^2} = \nabla^2 P + \frac{1}{\rho_0 v_s^2} \left[\frac{4}{3}\eta + \zeta\right] \nabla^2 \frac{\partial P}{\partial t}$$

$$\frac{\partial c}{\partial t} = D\left[\nabla^2 c + \frac{k_P}{P_0} \nabla^2 P\right] \qquad (2.44)$$

For high frequency $\omega \gg Dk^2$, which is valid for the sound wave mode, the concentration and pressure fluctuations are related by

$$\frac{\partial c}{\partial t} = \frac{Dk_P}{P_0} \nabla^2 P \ .$$

The sound wave equation then becomes

$$\frac{1}{v_s^2} \frac{\partial^2 P}{\partial t^2} = \nabla^2 P + \frac{1}{\rho_0 v_s^2} \left(\frac{4}{3}\eta + \zeta\right) \nabla^2 \frac{\partial P}{\partial t} - \frac{Dk_P}{P_0} \left(\frac{\partial \rho}{\partial c}\right)_{T,P} \nabla^2 \frac{\partial P}{\partial c} \ .$$

Thus the coupling with the concentration diffusion mode causes additional damping of the sound wave by an amount

$$\Gamma_c = \frac{Dv_s^2 k^2}{2\rho^2 \left(\frac{\partial \mu}{dc}\right)_{P,T}} \left(\frac{\partial \rho}{\partial c}\right)^2_{P,T} = \frac{Dv_s^2 k^2 \left(\frac{\partial \rho}{\partial c'}\right)_{P,T} \left(\frac{\partial c'}{\partial c}\right)}{2\rho^2 \left(\frac{\partial \mu}{\partial c'}\right)_{P,T}} \qquad (2.45)$$

For a dilute gas obeying the ideal gas law, the chemical potentials of the individual species have the form

$$\mu_1 = k_B T \ell n (1 - c') + \psi_1(T) \quad ; \quad \mu_2 = k_B T \ell n\, c' + \psi_2(T)$$

where k_B is the Boltzman constant and ψ_1, ψ_2 are functions of temperature only. Using these relationships, it can be shown that

$$(\frac{\partial \mu}{\partial c}) = \frac{k_B T}{c(1-c)[m_1 c+(1-c)m_2]} \tag{2.45}$$

and

$$k_P (\frac{\partial c'}{\partial c}) = N(m_1 - m_2)c'(1 - c')/\rho$$

which gives the result

$$\Gamma_c = \frac{D v_s^2 k^2 N(m_1 - m_2)^2 c'(1 - c')}{2\rho k_B T}$$

Thus, for a mixture of two gases, the concentration diffusion contribution to the sound wave damping becomes largest for a large difference in the mass of the two component molecules. This damping occurs for the following reason: diffusion currents of each species are driven by density gradients, i.e. the density gradients produce non-zero average particle velocities $\vec{v}_i$ for each species. The gradient in the overall pressure in a mixture of disparate masses produced by the sound wave causes a relative particle flux in the mixture, that is a non-zero relative velocity $\vec{v}_1 - \vec{v}_2$. The relative velocity is reduced in a dissipative way by intercomponent collisions and this dissipation contributes to the acoustic attenuation.

The total sound wave damping coefficient in a viscous thermal conductive fluid mixture is given by

$$\Gamma = \Gamma_v + \Gamma_T + \Gamma_D$$

$$= \frac{k^2}{2\rho_0}\left[\frac{4}{3}\eta + \xi + \lambda\left(\frac{1}{c_V} - \frac{1}{c_P}\right) + \frac{Dv_s^2}{\rho_0\left(\frac{\partial\mu}{\partial c}\right)_{P,T}}\left(\frac{\partial\rho}{\partial c}\right)^2_{P,T}\right] \tag{2.46}$$

The effect of the sound wave on the concentration diffusion mode is obtained in manner analogous to the effect of the sound wave on the thermal diffusion mode. We consider again small frequencies $\omega \ll kv_s$. Then the concentration and pressure are related by

$$\left(\frac{\partial\rho}{\partial c}\right)_{P,T}\left(\frac{\partial^2 c}{\partial t^2}\right) = \nabla^2 P$$

The concentration equation then becomes

$$\frac{\partial c}{\partial t} = D\left[\nabla^2 c + \frac{k_P}{P_0}\left(\frac{\partial\rho}{\partial c}\right)_{P,T}\frac{\partial^2 c}{\partial t^2}\right]$$

which leads to the low frequency limit of the dispersion relation

$$i\omega = Dk^2 - \frac{Dk_P}{P_0}\left(\frac{\partial\rho}{\partial c}\right)(i\omega)^2 \tag{2.47}$$

For the gas mixtures under investigation,

$$D^2k^2\,\frac{k_P}{P_0}\left(\frac{\partial\rho}{\partial c}\right) \sim 10^{-8}$$

so the dispersion relation reduces to the uncoupled concentration damping constant.

$$i\omega = Dk^2 + O(0)$$

To summarize, we have seen that the basic collective modes described by the hydrodynamic equations are the sound wave, thermal diffusion and concentration diffusion. The primary effect of the coupling between these modes is to increase the damping constants for each mode.

D. Coupling with the Electromagnetic Field

In the presence of an electromagnetic field, the differential free energy per unit mass must be augmented by terms due to variations in the electric field and the dielectric constant and takes the form

$$dF = -s_0 dT + \mu_0 dc + \frac{P_0}{\rho^2} d\rho - \frac{\epsilon \vec{E} \cdot d\vec{E}}{4\pi\rho} - \frac{E^2 d\epsilon}{8\pi\rho} \qquad (2.48)$$

where s_0, μ_0, and P_0 are the entropy, chemical potential and pressure respectively when the electric field is absent. Here ϵ must be regarded as a function of the variables T, c, ρ. It can be shown that the force per unit volume on an uncharged dielectric is increased in the presence of an electric field by an amount[4]

$$\frac{\rho}{8\pi} \text{ grad } [E^2 (\frac{\partial \epsilon}{\partial \rho})_{T,c}] - \frac{E^2}{8\pi} (\frac{\partial \epsilon}{\partial T})_{\rho,c} \text{ grad } T - \frac{E^2}{8\pi} (\frac{\partial \epsilon}{\partial c})_{T,\rho} \text{ grad } c \ .$$

The last two terms are usually negligible compared to the first term.

The effect of electrostriction is therefore to add a term

$$\frac{1}{8\pi} \left[E^2 \left(\frac{\partial \epsilon}{\partial \rho}\right)_{T,c}\right]$$

to the right hand side of the Navier-Stokes equation (2.9). For an isotropic fluid without macroscopic flow so that the nonlinear hydrodynamic term $(\vec{V} \cdot \text{grad})\vec{V}$ may be ignored, combination of the linearized equation of continuity (2.17) and Navier-Stokes equation leads to a small amplitude sound wave equation

$$\frac{\partial^2 \rho}{\partial t^2} = \nabla^2 P - \frac{\rho_0}{8\pi} \nabla^2 \left[\left(\frac{\partial \epsilon}{\partial \rho}\right)_{T,c} E^2\right] + \frac{1}{\rho_0} \left(\frac{4}{3}\eta + \zeta\right) \nabla^2 \left(\frac{\partial \rho}{\partial t}\right) . \tag{2.49}$$

In this equation, ρ may be expressed in terms of the independent variables P, T, c by means of the equation of state.

The coupling between the electric field and the thermal and concentration diffusion modes arises from the change in entropy and chemical potential when the electric field is added. Integration of Equation (2.48) gives the result

$$F(T, \rho, c, E) = F_0(T, \rho, c) - \frac{\epsilon E^2}{8\pi\rho}$$

where F, F_0 are respectively the values of the free energy with and without the electric field. The changes in entropy and chemical potential when the electric field is added are given by

$$s = -\left(\frac{\partial F}{\partial T}\right)_{\rho, c, E} = -\left(\frac{\partial F_0}{\partial T}\right)_{\rho, c} + \frac{E^2}{8\pi\rho}\left(\frac{\partial \epsilon}{\partial T}\right)_{\rho, c}$$

$$= s_0 + \frac{E^2}{8\pi\rho}\left(\frac{\partial \epsilon}{\partial T}\right)_{\rho, c}$$

$$\mu = -\left(\frac{\partial F}{\partial c}\right)_{\rho, T, E} = \mu_0 - \frac{E^2}{8\pi\rho}\left(\frac{\partial \epsilon}{\partial c}\right)_{\rho, T}$$

The coupling between the entropy (or temperature) and the electric field manifests itself in the electrocaloric effect and is the coupling term which produces Stokes-shifted stimulated thermal Rayleigh scattering[5]. The coupling between the chemical potential and the electric field drives the concentration diffusion current which produces the stimulated concentration Rayleigh scattering. In the presence of an optical absorption constant α an additional term must be added to the thermal diffusion equation which finally becomes

$$\frac{\partial T}{\partial t} + \frac{T_0}{c_P}\left(\frac{\partial s}{\partial P}\right)_{T, c}\frac{\partial P}{\partial t} - \left[\frac{k_T}{c_P}\left(\frac{\partial \mu}{\partial c}\right)_{P, T} + \frac{E^2}{8\pi\rho c_P}\left(\frac{\partial \epsilon}{\partial c}\right)_{P, T}\right]\frac{\partial c}{\partial t} =$$

$$\chi\nabla^2 T - \frac{T_0}{8\pi\rho c_P}\left(\frac{\partial \epsilon}{\partial T}\right)_{P, c}\frac{\partial E^2}{\partial t} + \frac{\alpha c_0 n E^2}{8\pi\rho c_P} \qquad (2.50)$$

The coupling between the temperature and electric field provided by the optical absorption produces the anti-Stokes shifted stimulated thermal Rayleigh scattering[6]. The concentration diffusion equation becomes

$$\frac{\partial c}{\partial t} = D\left\{ \nabla^2 c + \frac{k_T}{T_0}\nabla^2 T + \frac{k_P}{P_0}\nabla^2 P - \frac{1}{8\pi\rho\left(\frac{\partial \mu}{\partial c}\right)_{T,P}} \nabla^2 \left[\left(\frac{\partial \epsilon}{\partial c}\right)_{T,P} E^2\right] \right\} \tag{2.51}$$

To these three equations the wave equation for the electromagnetic field in the isotropic medium must be added

$$\nabla^2 E - \frac{\epsilon}{c_0^2}\frac{\partial^2 E}{\partial t^2} = \frac{1}{c_0^2}\frac{\partial^2}{\partial t^2} E\left[\left(\frac{\partial \epsilon}{\partial P}\right)_{T,c} P + \left(\frac{\partial \epsilon}{\partial T}\right)_{P,c} T + \left(\frac{\partial \epsilon}{\partial c}\right)_{P,T} c\right] \tag{2.52}$$

Since the characteristic relaxation times for thermal diffusion, mass diffusion, and acoustic damping are short compared to the duration of the laser pulse, solutions to the set of four simultaneous second order differential equations may be found in the parametric linearized approximation, in which the laser field

$$E_L(\vec{r}, t) = \frac{1}{2} E_L e^{ik_L z - i\omega_L t} + cc$$

is considered as a constant parameter. The scattered light is represented as a backscattered wave with amplitude E_s, frequency ω_s and wave number k_s

$$E_s(\vec{r}, t) = \frac{1}{2} E_s e^{-ik_s z - i\omega_s t} + cc$$

The pressure, concentration and temperature variations are assumed to have solutions of the form

$$P(\vec{r},t) = \frac{1}{2} P_1 e^{ikz-i\omega t} + cc$$

$$c(\vec{r},t) = \frac{1}{2} c_1 e^{ikz-i\omega t} + cc \qquad (2.53)$$

$$T(\vec{r},t) = \frac{1}{2} T_1 e^{ikz-i\omega t} + cc$$

with k and ω satisfying the phase and frequency matching conditions

$$k = k_L + k_s$$

$$\omega = \omega_L - \omega_s \quad .$$

When these expressions are substituted into equations (2.49) - (2.52) and all terms of higher order than linear in the four small amplitudes are ignored, a secular determinant is obtained which gives a general dispersion relation. For the special case $E_L = E_s = 0$, absence of the electromagnetic field, the relation must reduce to the description of sound waves in a fluid mixture[2]. Numerous papers have been devoted to the description of stimulated thermal and Brillouin scattering of light in a single component fluid where $c' = 0$, $\frac{\partial \epsilon}{\partial c} = 0$.[5-9]

The interest in this work is directed toward concentration scattering in a nonabsorbing gaseous mixture. Solutions for this case will be presented in the next section after explicit expressions for the coupling coefficients $\frac{\partial \epsilon}{\partial P}$, $\frac{\partial \epsilon}{\partial c}$ and $\frac{\partial \epsilon}{\partial T}$ have been given.

For a substance which obeys the Clausius-Mosotti relation,

$$\frac{\epsilon-1}{\epsilon+2} = \frac{4\pi}{3} N [c' a_1 + (1 - c') a_2]$$

where α_1 and α_2 are the polarizibilities of the two molecular species, one readily obtains with the aid of Equations (2.13) - (2.16)

$$P_0\left(\frac{\partial \epsilon}{\partial P}\right)_{c,T} = \rho_0\left(\frac{\partial \epsilon}{\partial \rho}\right)_{c,T} = \rho_0\left(\frac{\partial \epsilon}{\partial \rho}\right)_{c',T} = \frac{1}{3}(\epsilon - 1)(\epsilon + 2) \tag{2.54}$$

$$\left(\frac{\partial \epsilon}{\partial c}\right)_{P,T} = \left(\frac{\partial \epsilon}{\partial c'}\right)_{N,T} \frac{\partial c'}{\partial c} = \frac{4\pi}{9} \frac{(\epsilon+2)^2 m_1 m_2 N}{[m_1 c + (1-c)m_2]^2} (\alpha_1 - \alpha_2)$$

and

$$T_0\left(\frac{\partial \epsilon}{\partial T}\right)_{T,c} = -\frac{1}{3}(\epsilon - 1)(\epsilon + 2)$$

For a gas with a small optical density one may put $\frac{(\epsilon+2)}{3} \simeq 1$.

It should be noted that the coupling of the electric field to the concentration can become comparable to the density coupling only for $\alpha_1 \gg \alpha_2$.

E. Stimulated Brillouin and Concentration Scattering

1. Introduction

In previous sections, the equations which describe the dynamics of the binary gas mixture have been developed. We have also seen how the fluctuations in the thermodynamic parameters which characterize the system are coupled to the electromagnetic fields, and have observed that through these coupling mechanisms the electromagnetic fields can drive coherent fluctuations in the pressure, concentration and temperature. The final step in the analysis is to then discover how the electromagnetic fields interact with these coherent fluctuations. We have seen that if the gain factor for the

stimulated wave is sufficiently large the amplitude of this wave will increase, in the steady state approximation, exponentially with the distance traveled through the medium. The frequency of the stimulated scattered wave is the frequency at which the gain is maximum. The calculation of the scattered wave gain as a function of frequency is the subject of this section.

Since the collective modes of the binary mixture are strongly coupled, the gain must be determined by a simultaneous solution of the hydrodynamic equations and Maxwell's equation for the Stokes wave. This solution has been found and is in good agreement with experimental results. However, the expression for the gain which is obtained when the coupling between the normal modes of the system is included is quite complicated, so the dependence of the gain on the various parameters is difficult to observe. For this reason, it is desirable to investigate the gain which is obtained when the coupling between the collective modes is ignored. In this approach, we calculate separately the gain for scattering from the sound wave, concentration diffusion mode and thermal diffusion mode. As a first approximation then, the frequency shift of the scattered wave should be the shift which is characteristic of scattering from whichever mode produces the highest gain.

2. The Coupled Equations

The sound wave equation, including the effects of the coupling with the electromagnetic field Equation (2.49), may be written in the form

$$\frac{1}{v_T^2}\frac{\partial^2 P}{\partial t^2} + \left(\frac{\partial \rho}{\partial c}\right)_{P,c}\frac{\partial^2 T}{\partial t^2} + \left(\frac{\partial \rho}{\partial c}\right)\frac{\partial^2 c}{\partial t^2} = \nabla^2 P$$

$$+ \frac{1}{\rho_0}\left(\frac{4}{3}\eta + \zeta\right)\left[\frac{1}{v_T^2}\nabla^2\frac{\partial P}{\partial t} + \left(\frac{\partial \rho}{\partial c}\right)_{P,T}\nabla^2\frac{\partial c}{\partial t} + \left(\frac{\partial \rho}{\partial T}\right)_{P,c}\frac{\partial T}{\partial t}\right]$$

$$- \frac{\rho_0}{8\pi}\left(\frac{\partial \epsilon}{\partial \rho}\right)_{T,c}\nabla^2 E^2 \qquad (2.55)$$

$$- \frac{\rho_0 E^2\left(\frac{\partial \epsilon}{\partial \rho}\right)^2_{c,T}}{4\pi(\epsilon+2)}\left[\frac{1}{v_T^2}\nabla^2 P + \left(\frac{\partial \rho}{\partial c}\right)_{P,T}\nabla^2 c + \left(\frac{\partial \rho}{\partial T}\right)_{P,c}\nabla^2 T\right]$$

The last term, which arises from $\nabla^2\left(\frac{\partial \epsilon}{\partial \rho}\right)$ in Equation (2.49) results in an intensity dependent contribution to the Brillouin shift in addition to the contribution which was pointed out by Wang[10]. The intensity dependent effects for the gases used in this experiment are negligible and are not included in further discussion. The concentration diffusion Equation (2.51) takes the form

$$\frac{\partial c}{\partial t} = D\left[\nabla^2 c + \frac{k_P}{P_0}\nabla^2 P + \frac{k_T}{T_0}\nabla^2 T\right] \qquad (2.56)$$

$$- \frac{D\left(\frac{\partial \epsilon}{\partial c}\right)\nabla^2 E}{8\pi\rho_0\left(\frac{\partial \mu}{\partial c}\right)_{P,T}} - \frac{D E^2\nabla^2\left(\frac{\partial \epsilon}{\partial c}\right)}{8\pi\rho_0\left(\frac{\partial \mu}{\partial c}\right)_{P,T}}$$

The last term may be evaluated by means of Equation (2.54) in terms of $\nabla^2 P_1$, $\nabla^2 c_1$, $\nabla^2 T_1$. This term produces an intensity dependent

shift of the stimulated concentration scattering analogous to the similar term in Equation (2.55). The contribution of this term is also small and will not be included in further calculations.

The thermal diffusion equation (2.50) may be given in the form

$$\frac{\partial T}{\partial t} - \frac{T_0 \alpha_T}{\rho_0 c_P} \frac{\partial P}{\partial t} - \frac{k_T}{c_P} \left(\frac{\partial \mu}{\partial c}\right)_{P,T} \frac{\partial c}{\partial t} = \chi \nabla^2 T - \frac{T_0}{8\pi \rho_0 c_P} \left(\frac{\partial \epsilon}{\partial T}\right)_{P,c} \frac{\partial E^2}{\partial t} \tag{2.57}$$

where Maxwells' relations have been used to show

$$\left(\frac{\partial s}{\partial P}\right)_{T,c} = - \frac{\alpha_T}{\rho_0} \quad ,$$

where α_T is isothermal expansion coefficient.

3. Gain for Scattering from Uncoupled Modes

a. Brillouin Gain

In the decoupled mode approximation, the Brillouin gain G_B is obtained from the sound wave equation and the Stokes wave equation ignoring the dependence upon temperature and concentration.

$$\frac{\partial^2 P}{\partial t^2} = v_s^2 \nabla^2 P + \frac{\eta_T}{\rho_0} \frac{\partial}{\partial t} \nabla^2 P - \frac{\rho_0}{8\pi} \left(\frac{\partial \epsilon}{\partial \rho}\right)_{T,c} v_s^2 \nabla^2 E^2$$

$$\nabla^2 E_s - \frac{\epsilon(\omega_s)}{c_0^2} \frac{\partial^2}{\partial t^2} E_s = \frac{1}{c_0^2} \frac{\partial^2}{\partial t^2} \left(\frac{\partial \epsilon}{\partial P}\right)_{T,c} P E_L \tag{2.58}$$

where

$$\eta_T = \frac{2\rho_0 \Gamma}{k^2}$$

Substituting the steady state expressions (2.53) one finds the dispersion relation

$$(\omega^2 - k^2 v_s^2 + i\omega k^2 \eta_T)\left(\frac{\epsilon}{c_0^2}\omega_s^2 - k_s^2\right) + \frac{\rho_0}{8\pi}\left(\frac{\partial \epsilon}{\partial \rho}\right)^2 \frac{k^2 v_s^2 \omega_s^2}{c_0^2 v_T^2} |E_L|^2 = 0 \tag{2.59}$$

The spatial gain of the Stokes wave amplitude is given by the imaginary part of the Stokes wave vector. We make the following separation

$$\begin{aligned} k_s &= k_{sr} + i G_B & G_B &\ll k_{sr} \\ k &= k_r + i G_B & \frac{\epsilon}{c_0^2}\omega_s^2 &= k_{sr}^2 \\ k_{sr} &= k_L \\ k &= 2k_{sr} \end{aligned} \tag{2.60}$$

The Brillouin gain coefficient $G_B(\omega)$ is then given by

$$G_B(\omega) = \mathrm{Re}\ \frac{i\omega_s^2 k_r \gamma \rho_0 \left(\frac{\partial \epsilon}{\partial \rho}\right)^2_{T,c} |E_L|^2}{8\pi c_0^2 \left(\omega^2 - k_r^2 v_s^2 - i\omega k_r^2 \frac{\eta_T}{\rho_0} - \left[\frac{\rho_0}{8\pi c_0^2}\left(\frac{\partial \epsilon}{\partial \rho}\right)^2_{T,c} \gamma \omega_s^2 |E_L|^2\right]\right)}$$

The term in square brackets in the denominator gives the intensity dependent pulling of the Brillouin frequency which was discussed by Wang[10]. For the system under investigation here, this term is a small correction and will be ignored. Then the Brillouin gain becomes

$$G_B(\omega) = \frac{\omega_s^2 k_r^3 \gamma \eta_T \left(\frac{\partial \epsilon}{\partial \rho}\right)^2_{T,c} |E_L|^2_\omega}{8\pi c_0^2 \left[(\omega^2 - k_r^2 v_s^2)^2 + (k_r^2 \omega \frac{\eta_T}{\rho_0})^2\right]} \qquad (2.61)$$

In the approximation that the inverse damping time for the sound wave Γ is much smaller than the sound wave frequency kv_s ($\Gamma \ll kv_s$), the Brillouin gain is maximum at

$$\omega^2 = k_r^2 v_s^2 - \Gamma^2 \simeq k_r^2 v_s^2$$

The maximum value of the Brillouin gain is then given by

$$G_{B\,max} \simeq G_B(\omega = \omega_B = kv_s) = \frac{\omega_s |E_L|^2 \rho_0 \left(\frac{\partial \epsilon}{\partial \rho}\right)^2_{T,c} \omega_B}{32\pi c_0 n v_s^2 \Gamma}$$

$$= g_B I_L$$

where

$$I_L = \frac{c_0 n |E_L|^2}{8\pi} \quad \text{is the laser intensity}$$

and

$$g_B = \frac{\gamma \rho_0^2 \left(\frac{\partial \epsilon}{\partial \rho}\right)^2}{4 c_0 n^3 v_s \eta_T} \qquad (2.62)$$

It should be noted that the Brillouin gain increases proportionally to the square of the density.

b. Concentration Rayleigh Gain

The gain due to scattering from the concentration diffusion mode

is obtained in the decoupled mode approximation from the equations

$$\frac{\partial c}{\partial t} = D\nabla^2 c - \frac{D\left(\frac{\partial \epsilon}{\partial c}\right)_{P,T} \nabla^2 E}{8\pi\rho_0 \left(\frac{\partial \mu}{\partial c}\right)_{P,T}} \tag{2.63}$$

$$\nabla^2 E_s = -\frac{\epsilon(\omega_s)}{c_0^2} \frac{\partial^2}{\partial t^2} E_s = \frac{1}{c_0^2} \frac{\partial^2}{\partial t^2} \left(\frac{\partial \epsilon}{\partial c}\right)_{P,T} c E_L$$

Following the procedure used in the previous section, one finds the concentration gain $G_c(\omega)$ is given by

$$G_c = \mathrm{Re} \frac{i D \omega_s^2 \left(\frac{\partial \epsilon}{\partial c}\right)^2_{P,T} k_r |E_L|^2}{8\pi c_0^2 \rho_0 \left(\frac{\partial \mu}{\partial c}\right)_{T,P} \left(i\omega + Dk^2 + \left[\frac{D\omega_s^2 \left(\frac{\partial \epsilon}{\partial c}\right)^2_{P,T} |E_L|^2}{8\pi\rho_0 c_0^2 \left(\frac{\partial \mu}{\partial c}\right)_{P,T}} \right] \right)}$$

The term in the square bracket in the denominator gives the frequency dependent pulling of the stimulated concentration frequency. Again, this term is negligible. Thus the concentration gain is given by

$$G_c = \frac{Dk^2 \omega_s \left(\frac{\partial \epsilon}{\partial c}\right)^2_{P,T} |E_L|^2}{16\pi c_0 n \rho_0 \left(\frac{\partial \mu}{\partial c}\right)_{P,T}} \times \frac{\omega}{\omega^2 + D^2 k^4} \tag{2.64}$$

This gain assumes a maximum value for a small Stokes shift $\omega = Dk^2$

$$\frac{G_{c\,max}}{I_L} = g_c = \frac{k_s \left(\frac{\partial \epsilon}{\partial c}\right)^2_{P,T}}{4 c_0 n^3 \rho_0 \left(\frac{\partial \mu}{\partial c}\right)_{P,T}} \tag{2.65}$$

Since the coupling constant $(\frac{\partial \epsilon}{\partial c})$ is proportional to the density, the concentration gain is proportional to the density.

Numerical values for the gain constants g_B and g_c are given in Chapter IV.

The ratio of the gain constants for stimulated Brillouin and concentration scattering is

$$\frac{g_c}{g_B} = \frac{k v_s \Gamma (\frac{\partial \epsilon}{\partial c})^2_{P,T}}{\rho_0^2 (\frac{\partial \epsilon}{\partial \rho})^2_{c,T} (\frac{\partial \mu}{\partial c})_{P,T}} \quad . \tag{2.66}$$

In this decoupled mode approximation, one would expect to observe stimulated concentration scattering when this ratio is greater than 1. From Equations (2.46) and (2.54), it follows that a large difference in polarizibility and a large difference in mass of the two components is favorable to make this ratio large. Furthermore, the total density or pressure should be kept low since the ratio is inversely proportional to the density[12]. For a gaseous mixture, Equation (2.66) can be simplified with the aid of Equations (2.45) and (2.54) to

$$\frac{g_c}{g_B} = \frac{k v_s \Gamma \rho_0}{N k_B T} \frac{c'(1-c')(a_1 - a_2)^2}{[a_1 c' + (1-c')a_2]^2} \tag{2.67}$$

c. Thermal Rayleigh Gain

The thermal Rayleigh gain due to the stimulated scattering from the thermal diffusion mode is obtained from the equations

$$\frac{\partial T}{\partial t} = \chi \nabla^2 T - \frac{T_0}{8\pi \rho_0 c_P} \left(\frac{\partial \epsilon}{\partial T}\right)_{P,c} \frac{\partial E^2}{\partial t}$$

$$\nabla^2 E_s - \frac{\epsilon(\omega_s)}{c_0^2} \frac{\partial^2}{\partial t^2} E_s = \frac{1}{c_0^2} \frac{\partial^2}{\partial t^2} \left(\frac{\partial \epsilon}{\partial T}\right)_{P,c} T E_L$$

The thermal Rayleigh gain is given by

$$G_T(\omega) = \frac{\chi k^2 \omega_s T_0 \left(\frac{\partial \epsilon}{\partial T}\right)^2_{P,c} |E_L|^2}{16\pi c_0 n \rho_0 c_P} \times \frac{\omega}{\omega^2 + \chi^2 k^4} \qquad (2.68)$$

One may observe that the form of the driving term due to the electromagnetic fields in the temperature equation is different from that in the concentration and sound wave equations; and, as a result, there is no intensity dependent pulling of the frequency of the stimulated thermal Rayleigh line.

The maximum of the gain $G_T(\omega)$ occurs at $\omega = \chi k^2$ and is given by

$$\frac{G_{T\,max}}{I_L} = g_T = \frac{k_s T_0 \left(\frac{\partial \epsilon}{\partial T}\right)^2}{4\rho_0 c_0 n^3 c_P} \qquad (2.69)$$

The ratio of the gain constants for stimulated scattering from the concentration and thermal diffusion modes is

$$\frac{g_c}{g_T} = \frac{c_P \left(\frac{\partial \epsilon}{\partial c}\right)^2_{P,T}}{T_0 \left(\frac{\partial \epsilon}{\partial T}\right)^2_{P,c} \left(\frac{\partial \mu}{\partial c}\right)_{P,T}} \qquad (2.70)$$

which, for a gas mixture, becomes

$$\frac{g_c}{g_T} = \frac{c_P(a_1 - a_2)\,[m_2 c' + m_1 (1 - c')]}{k_B[c' a_2 + (1 - c')\, a_2]^2} \qquad (2.71)$$

Numerical values for the gain constant g_T are presented in Chapter IV.

4. Complete Solution to the Coupled Equations

The behavior of the stimulated light scattering from the gas mixture is well described by this uncoupled mode approximation when the helium concentration is low. As the helium concentration increases, the mode coupling becomes stronger, and the sound wave damping becomes comparable to the frequency shift. In this case an adequate description of the frequency dependence of the gain can be obtained only by solving simultaneously the set of hydrodynamic equations (2.55) - (2.57) and the Stokes wave equation (2.52).

The gain of the Stokes wave due to scattering from the coupled mode of the gas mixture $G_{BcT}(\omega)$ can of course be obtained in the same manner in which G_B, G_c, and G_T were obtained. That is, substituting the steady state expressions (2.53) into the coupled hydrodynamic equations and the Stokes wave equation leads to a 4×4 secular determinant which gives the general dispersion relation. The spatial gain of the Stokes wave amplitude is then given by the imaginary part of the Stokes wave vector.

For computational purposes, it is easier to solve the three hydrodynamic equations for the amplitudes of the pressure, concentration, and temperature fluctuations and substitute the results into the Stokes wave equation to obtain the gain. The manner in which this solution is accomplished is as follows. The Stokes wave is given by

$$E_s(z\,t) = \tfrac{1}{2} E_s(z)\, e^{-ik_{sr}z - i\omega_s t} + cc\ .$$

where

$$E_s(z) = E_{s0}\, e^{zG_{BcT}} \quad \text{and} \quad E_{s0} \quad \text{is a constant.}$$

Again assuming that the variation of the amplitude over one wavelength is small, $\left| \frac{\partial^2 E_s(z)}{\partial z^2} \right| \ll k_{sr} \left| \frac{\partial E_s(z)}{\partial z} \right|$,

or $G_{BcT} \ll k_{sr}$, the Stokes wave equation becomes

$$\frac{\partial E_s(z)}{\partial z} = \frac{\omega_s^2}{2ik_{sr}c_0^2} \frac{E_L}{2} \left[\left(\frac{\partial \epsilon}{\partial P}\right)_{T,c} P_1^* + \left(\frac{\partial \epsilon}{\partial T}\right)_{P,c} T_1^* + \left(\frac{\partial \epsilon}{\partial c}\right)_{T,P} C_1^* \right] \tag{2.72}$$

Since the three complex amplitudes P_1^*, T_1^*, c_1^* are each proportional to $E_L^* E_s(z)$ (again neglecting the intensity dependent terms), this result may be written as

$$G_{BcT} = \frac{1}{E_s(z)} \frac{\partial E_s(z)}{\partial z} = \frac{2\pi\omega_s^2}{ik_{sr}c_0^2} \chi^{NLS} = \frac{2\pi\omega_s}{c_0 n} I_m \chi^{NLS} \tag{2.73}$$

which defines χ^{NLS} as

$$\chi^{NLS} = \frac{E_L}{8\pi E_s(z)} \left[\left(\frac{\partial \epsilon}{\partial P}\right) P_1^* + \left(\frac{\partial \epsilon}{\partial T}\right) T_1^* + \left(\frac{\partial \epsilon}{\partial c}\right) c_1^* \right] \qquad (2.74)$$

After substitution of the expressions (2.53), the coupled hydrodynamic equations can be written in matrix form

$$W \cdot A = Y \qquad (2.75)$$

where A is the column vector $\begin{pmatrix} P_1^* \\ c_1^* \\ T_1^* \end{pmatrix}$

The matrix W has the form

$$W = \begin{bmatrix} \frac{i\omega}{v_T^2}(i\omega + bk^2) + k^2 & i\omega\left(\frac{\partial \rho}{\partial c}\right)_{P,T}(i\omega + bk^2) & i\omega\left(\frac{\partial \rho}{\partial T}\right)_{P,c}(i\omega + bk^2) \\ Dk^2 \frac{k_P}{P_0} & Dk^2 + i\omega & Dk^2 \frac{k_T}{T_0} \\ -i\omega \frac{T_0}{c_P} \frac{a_T}{\rho_0} & -i\omega \frac{k_T}{c_P}\left(\frac{\partial \mu}{\partial c}\right)_{P,T} & i\omega + \chi k^2 \end{bmatrix} \qquad (2.76)$$

where

$$b = \left(\frac{4}{3}\eta + \zeta\right) \frac{1}{\rho_0}$$

and

$$\chi = \frac{\lambda}{\rho_0 c_P}$$

And Y is the column vector

$$Y = \begin{bmatrix} \frac{\rho_0}{8\pi}\left(\frac{\partial \epsilon}{\partial \rho}\right)_{T,c} k^2 E_L^* E_s \\ \\ \frac{Dk^2\left(\frac{\partial \epsilon}{\partial c}\right)_{P,T}}{8\pi\rho_0\left(\frac{\partial \mu}{\partial c}\right)_{P,T}} E_L^* E_s \\ \\ -\frac{T_0\left(\frac{\partial \epsilon}{\partial T}\right)_{P,c}}{8\pi\rho_0 c_P} i\omega E_L^* E_s \end{bmatrix}$$

The solution for the Stokes wave gain due to the coupled Brillouin, concentration and thermal diffusion modes of the gas mixture G_{BcT} may now be obtained in a straightforward manner. The matrix equation (2.75) is solved for the amplitudes P_1^*, c_1^*, T_1^*, which gives in turn the nonlinear susceptibility χ^{NLS}. The gain G_{BcT} then follows directly from Equation (2.73). For the purposes of calculation, we write

$$G_{BcT} = g_{BcT} I_L$$

where $I_L = \frac{c_0 n |E_L|^2}{8\pi}$ is the laser intensity.

The complete solution for g_{BcT} is too lengthy to write out fully here. A numerical solution has been made by use of a computer and will be presented in Chapter IV. It is of interest however to determine

the roots of det(W) since those are the points at which the gain has a resonance, and therefore the points at which stimulated scattering may occur. The approximate roots of det(W)are found considering the dimensionless parameters $(\frac{\chi k}{v_s})$, $(\frac{bk}{v_s})$ and $(\frac{Dk}{v_s})$ as small. For the gas mixtures under consideration, all three of these parameters are $\simeq 0.1$. To lowest order (i.e. $\Gamma = 0$), the roots of $\det(\omega) = 0$ are $\omega = 0, \pm v_s k$. In the next approximation ($0 < \Gamma \ll kv_s$) when linear terms in the small quantities are retained, the roots should correspond to the values of the frequency shift which were obtained from the decoupled mode approximation. One obtains

$$\det(\omega) = -v_s^2(\omega - z_1)(\omega - z_2)(\omega - v_s k - i\Gamma)(\omega + v_s k - i\Gamma) \qquad (2.77)$$

The two roots

$$\omega = \pm v_s k + i\Gamma k^2$$

are the propagating sound wave modes with the damping coefficient Γ given by

$$\Gamma = \frac{k^2}{2\rho_0}\left\{(\frac{4}{3}\eta + \zeta) + \frac{\lambda}{c_P}(\gamma - 1) + \frac{Dv_s^2}{\rho_0(\frac{\partial\mu}{\partial c})_{P,T}}\left[(\frac{\partial\rho}{\partial c})_{P,T} + \frac{k_T}{c_P}(\frac{\partial\rho}{\partial T})_{P,c}(\frac{\partial\mu}{\partial c})_{P,T}\right]\right\} \qquad (2.78)$$

The positive root corresponds to the Stokes shifted stimulated Brillouin which has positive gain, while the negative root corresponds to the anti-Stokes wave which has negative gain.

It is important to note that in a binary mixture the sound wave has an extra damping term due to the coupling with the concentration

fluctuations[11]. This extra damping depends on $(\frac{\partial \rho}{\partial c})^2_{P,T}$ and consequently the sound wave is heavily damped in a mixture with a large difference of component masses. Thus the threshold of stimulated Brillouin scattering is increased by mixing. This factor is of primary importance in making possible the observation of stimulated concentration scattering. The roots which are related to the nonpropagating modes are

$$\omega_{1,2} = +ik^2 \left\{ \tfrac{1}{2}(\chi + \mathcal{D}) \pm \tfrac{1}{2} \left[(\chi + \mathcal{D})^2 - 4\chi D\right]^{\frac{1}{2}} \right\} \qquad (2.79)$$

where

$$\mathcal{D} = D\left[1 + \frac{k_T^2}{T_0 c_P} \left(\frac{\partial \mu}{\partial c}\right)_{P,T}\right]$$

when

$$k_T = 0, \quad \omega_{1,2} = iDk^2, \quad i\chi k^2$$

The root ω_1 corresponds to the concentration diffusion mode and gives stimulated concentration scattering while the root ω_2 corresponds to the thermal diffusion mode which gives stimulated thermal Rayleigh scattering. These roots have previously been obtained by Martin[13], and by Mountain and Deutch[14]. Thus the resonances in the coupled gain expression, in the limit of small coupling between the modes, do reduce to the values predicted by the decoupled mode approximation.

References: Chapter II

1. N. Bloembergen, W. H. Lowdermilk, M. Matsuoka, and C. S. Wang, Phys. Rev. 3, 404, (1971).

2. L. D. Landau and E. M. Lifshitz, Fluid Mechanics (Addison-Wesley, Reading, Mass., 1958).

3. S. Yip and M. Nelkin, Phys. Rev. 135, A1241 (1964); N. Clark, Ph.D. Thesis, M.I.T., 1970 (unpublished).
The parameter y characterizes the transition of the kinetic to the hydrodynamic regime of a single component fluid: the transition between these regimes in a mixture has yet to be investigated. However, one can expect that if one component is in the hydrodynamic regime with its partial pressure, the mixture should also be in the hydrodynamic regime.

4. C. D. Landau and E. M. Lifshitz, Electrodynamics of Continuous Media (Addison-Wesley, Reading, Mass., 1960).

5. V. S. Starunov, Physics Letters, 26A, 428 (1968); Yu. P. Kyzylasov, V. S. Starunov, I. L. Fabelinskii, Z.E.T.P. Lett. 11, 66 (1970).

6. R. M. Herman and M. A. Gray, Phys. Rev. Lett. 19, 824 (1967); W. Rother, D. Pohl, W. Kaiser, Phys. Rev. Lett. 18, 915 (1969).

7. K. A. Brueckner and S. Jorna, Phys. Rev. Lett. 17, 78 (1966); Phys. Rev. 164, 182 (1967); N. M. Kroll and P. L. Kelly (unpublished).

8. D. H. Rank, C. W. Cho, N. D. Foltz and T. A. Wiggins, Phys. Rev. Lett. L9, 828 (1967); D. Pohl, I. Reinhold and W. Kaiser, ibid 20, 1141 (1968).

9. D. I. Mash, V. V. Morozov, V. S. Starunov and I. L. Fabelinskii, Soviet Phys. Z.E.T.P. 28, 1085 (1969).

10. C. S. Wang, Phys. Rev. Letters 24, 1394 (1970).

11. M. Kohler, Ann. Physik 39, 209 (1941).

12. E. E. Hagenlocker, R. W. Minck and W. G. Rado, Phys. Rev. 154, 226 (1967).

13. P. C. Martin in Statistical Mechanics of Equilibrium and Non-Equilibrium, J. Meixner, Ed. (North Holland Publ. Co., Amsterdam, 1965), p. 124.

14. R.D. Mountain and J.M. Deutch, Journal of Chemical Physics 50, 1103 (1969).

CHAPTER III

EXPERIMENTAL APPARATUS AND TECHNIQUES

A. Introduction

In this chapter the experimental apparatus and techniques developed to generate stimulated light scattering in the gas mixtures under investigation and to measure the difference in frequency between the laser and the stimulated light wave are discussed in detail. The basic problem was to produce laser pulses with high intensity and sharp frequency spectrum, focus this beam into the gas mixture and analyze the spectrum of the backward scattered light with a suitably high resolution Fabry-Perot interferometer.

The necessary sharp frequency spectrum of the laser output was achieved by careful axial mode selection of an existing ruby oscillator. The high intensity of the laser output was attained by constructing a ruby amplifier system.

Successful completion of the experiment was also due to the development of a new technique for reaching stimulated oscillation in the gas mixture with limited laser power. This technique is applicable to facilitate the observation of any low gain stimulated scattering process, as it lowers the required threshold power.

We now proceed to discuss the various parts of the experimental apparatus in detail.

B. The Laser

1. Ruby Oscillator

The ruby oscillator used in this experiment was a Maser Optics Model 868. This laser has a double ellipse head. Optical pumping of the ruby is done with two water-cooled Xenon flashlamps (E. G. and G. FX47C-6.5). The ruby rod used was a Verneuil grown rod, 6 inches long by 1/2 inch diameter with a doping of 0.04% CrO^{+3}. This rod has the end faces perpendicular to the rod axis and the optical axis of the ruby at 60 degrees to the rod axis. The rod was water cooled by a Model K-2 Landau Circulator which maintained the water temperature constant to within $\pm$ 0.1 degree centigrade. The ruby rod was of very poor optical quality, containing many small bubbles and crystal dislocations, which was a primary contributing factor in making single transverse mode operation of this laser virtually impossible. The laser cavity was defined by front and rear reflectors separated by 150 centimeters. The rear reflector was a quartz flat (1 inch diameter by 3/8 inch thick) with a surface figure of 1/20 λ. This flat was supplied by Perkin Elmer Corporation with a high field damage dielectric coating with reflectivity of 99 + % at 6943 Å. The flat was mounted in a Model 10.203 Angular Orientation Device (A.O.D.) supplied by Lansing Research Corporation. The front reflector was a Model RR223-4 Resonant Reflector from Laser Systems Corporation. The resonant reflector consisted of four optically aligned quartz plates (i.e. an eight surface Fabry-Perot interferometer) which provided excellent axial mode discrimination.

This point will be discussed in greater detail later. The front reflector was mounted in a Lansing Model 10.253 A.O.D. On this mounting, the mirror alignment is controlled by a differential screw micrometer with an angular resolution of 0.1 arc second. The Lansing mounts permit precise alignment of the laser reflectors to be made easily and they are sufficiently stable that, with care, adjustments in alignment needed to be made only about once every two weeks.

The laser is Q-switched with a solution of cryptocyanine dye dissolved in methanol. The dye cell was located between the ruby rod and the rear reflector. The dye concentration was adjusted so that the laser operates just slightly above threshold. This condition was found to give the best reproducibility in laser power output and the narrowest linewidth.

The rod holder supplied with the Maser Optics head had two serious problems which required modifications to correct. This holder was very unstable to mechanical vibrations making it impossible to hold exact alignment of the rod with the cavity mirrors for more than a few hours. Also in the original design, the rod cooling water flowed past both faces of the rod with the rod holder sealed at both ends by 1/8 inch thick quartz windows. These windows were of poor optical quality and it was not possible to align them parallel to the cavity mirrors. The windows and water in the beam path introduced off-axis reflections and scattering in the beam which increased beam divergence. A new rod holder was designed in which the rod faces were exposed to air, thus eliminating the unnecessary

quartz windows. This holder was also attached securely to the laser base plate which greatly improved stability against mechanical vibration.

After mechanical stability of the laser head and cavity mirrors had been achieved, the problem of mode selection was undertaken. It was necessary to produce consistent, single axial mode output of the laser in order to perform the high resolution spectroscopy required to observe the stimulated Brillouin and concentration scattering from the gas mixture.

2. Mode Selection

a. Modes in an Optical Resonator

The general problem of the interaction of an excited atomic system with the optical cavity is of primary importance in understanding laser behavior. The earliest proposal for using open resonators, consisting of a pair of opposing plane or curved reflectors was that of Dicke[1]. Schawlow and Townes[2] suggested that such a resonator will discriminate heavily against modes whose energy propagates along directions other than normal to the reflectors. In order to support high Q (low loss) field modes, the dimensions of the reflectors must satisfy the condition

$$\frac{a^2}{\lambda D} \gtrsim 1 \qquad (3.1)$$

where a is the radius of the reflector, λ the radiation wavelength and D the reflector separation. Also there must be a family of rays which upon sequential specular reflection do not miss either reflector before

making a reasonable number ($\sim$ 20-100) of passes. An open resonator which satisfies these two conditions is referred to as a stable resonator. Theoretical studies of the modes in a stable, open resonator have been made by Fox and Li[3], Boyd and Gordon[4], and Boyd and Kogelnik[5]. The result of this analysis has been to show that, for any stable resonator, there exists a set of steady state, discrete standing wave modes specified by three indices ($TEM_{m, n, q}$). These modes take the form of almost plane wave beams which propagate back and forth between the reflectors. The field intensity distribution of the modes depends upon the parameters of the optical cavity: shape, dimension and curvature of the mirrors and their separation. The q index specifies the number of half wavelengths which are contained in the distance of the mirror separation D. This index is the longitudinal mode index. The values of the indices m, n for the observable modes of an optical resonator are small and they specify the transverse mode pattern $TEM_{m, n}$.

The electric field distribution of the transverse modes is calculated by use of the scalar formulation of Huygen's principle to compute the field at one of the mirrors in terms of an integral of the field at the other. The steady state transverse modes are then specified by the requirement that the field pattern at one reflector be reproduced after one round trip of the cavity multiplied by some complex number which gives the total phase shift and loss. The resulting integral equation is solved by use of a computer.

Ordinarily within the active volume of the laser crystal many

longitudinal and transverse modes are excited, each transverse mode having a cross-sectional area much smaller than the total cross-sectional area of the active volume. This behavior is characteristic of a laser medium which is optically inhomogeneous, has inhomogeneous distribution of excited ions (resulting from non-uniform pumping) and long spatial cross relaxation time ($\sim 10^{-6}$ second for ruby).

For a plane parallel resonator, the mode separation is approximately given by

$$\Delta\left(\frac{1}{\lambda}\right) \simeq \frac{1}{2D} \left[\Delta q + \frac{1}{16} \left(\frac{\lambda D}{a^2}\right) (2m\,\Delta m + (\Delta m)^2 + 2n\,\Delta n + (\Delta n)^2) \right] \quad (3.2)$$

where a is the radius of the mirror. This approximation improves rapidly with increasing Fresnel number $\frac{a^2}{\lambda D}$. The longitudinal mode separation given by $\Delta q = 1$ is easily resolvable and is given by $\Delta\left(\frac{1}{\lambda}\right) = \Delta\gamma = \frac{1}{2D}$. The mode separation corresponding to Δm or $\Delta n = 1$ is much smaller and usually not resolvable at optical frequencies due to large Fresnel numbers and low reflectivity of practical laser resonators. For the laser used in this experiment:

$$\begin{aligned} \frac{1}{2D} &= .003\ \text{cm}^{-1} \\ \frac{a^2}{\lambda D} &\simeq 100 \end{aligned} \quad (3.3)$$

so the spread in frequency of the first few lowest order transverse modes is $\sim 3 \times 10^{-5}$ cm^{-1} (1 MHz).

To do high resolution spectroscopy of stimulated light scattering

which requires focusing of the laser beam into the scattering medium to produce sufficient intensity to reach threshold for stimulation, it is desirable to limit the laser output to a single longitudinal and single transverse mode. The techniques used to effect mode selection are discussed in the following sections.

b. Longitudinal Mode Control

For ruby at room temperature, the natural fluorescent linewidth of the R lines is approximately 10 cm^{-1}. The longitudinal mode spacing for a cavity 150 cm long is $\sim .003\ cm^{-1}$. So in general, many longitudinal modes will be close to the maximum of the gain profile and will oscillate. The number of longitudinal modes may be limited by reducing the cavity length and operating the laser at low temperatures so that the fluorescent linewidth becomes narrow enough to allow oscillation in only one axial mode. It is, however, more desirable to obtain mode control at room temperature. This may be done, as was first suggested by Kleinman and Kisliuk[6], by introducing additional reflecting surfaces inside the resonator. In particular, if the front reflector is replaced by an etalon and the laser operated just above threshold, only those modes which are reflected in phase from both sides of the etalon will oscillate. The selected modes are then modes of the etalon itself. The etalon thickness may be adjusted so that only a few of its fundamental modes will be near the maximum of the laser gain profile. If additional reflecting surfaces are added the conditions on the possible oscillating modes become more stringent. With the ruby oscillator power output of $\sim 10 - 20\ \frac{MW}{cm^2}$

it was found by trial that the resonant reflector consisting of four optically aligned quartz plates provided sufficient axial mode discrimination that a single axial mode output was consistently obtained. This resonant reflector was constructed so that the optical path length was the same in the air gaps between the plates as in the plates themselves. A computer calculation of reflectivity of the resonant reflector as a function of wavelength was made[7] by extending the analysis given by Born and Wolf[8] of the two surface problem. The results of this calculation are shown on Figure (3.1). The reflectivity peaks are separated by about 1Å (2 cm^{-1}) and the width of the peak is about 0.1Å (0.2 cm^{-1}). The maximum reflectivity is $\sim 64\%$. The reflectivity peaks were sufficiently sharp and well separated that only a single axial mode reached oscillation threshold.

The spectrum of the laser output was examined with a 6 cm Fabry Perot interferometer. A typical result is shown in Figure (3.2a). It is clearly evident that only a single mode is oscillating and its linewidth is $< .005\ cm^{-1}$. The primary factors contributing to the laser linewidth are optical inhomogenieties of the ruby crystal and dye cell, reflector imperfections and mechanical vibrations of the cavity reflectors.

The temporal behavior of the laser Q-switched pulse is monitored by a TRG 105B planar photodiode. This photodiode has a rise time of < 0.3 nanosecond. The photodiode output is displayed on a Tektronix 519 oscilloscope with a rise time of ~ 0.3 nanosecond. Any temporal modulation of the laser output can easily be detected.

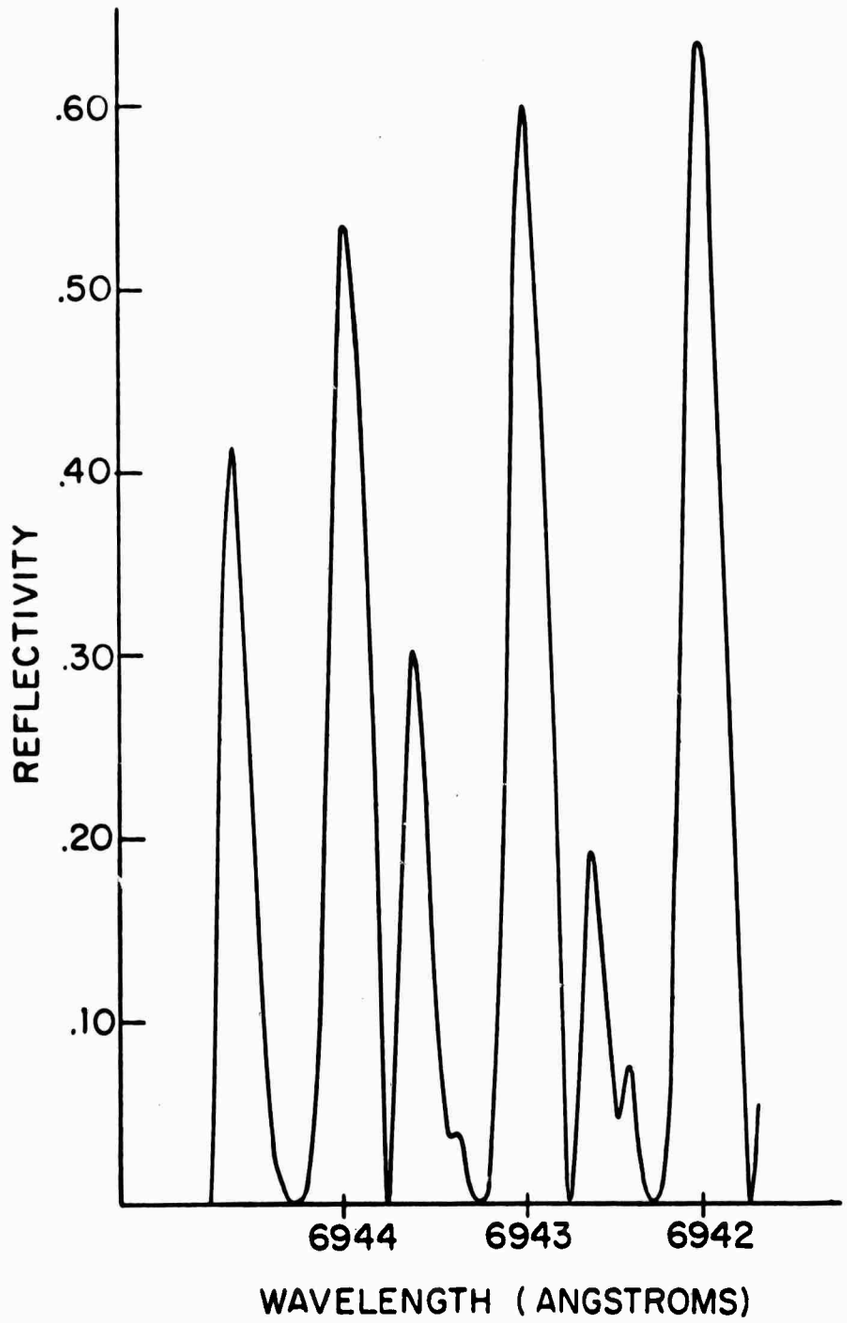

Fig. 3.1 Reflectivity versus Wavelength for the Resonant Reflector Consisting of Four Parallel Quartz Flats

(a)

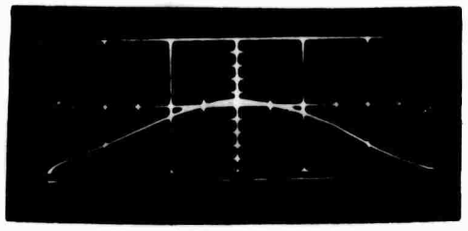

(b)

Fig. 3.2 (a) Frequency Content of the Laser Pulse Analyzed by 6 cm Fabry-Perot Etalon

(b) Oscilloscope Trace of the Laser Pulse. The Scale is 20 ns/division

If the oscillator is carefully aligned and operated slightly above threshold the temporal behavior of the laser pulse is as shown in Figure (3.2b). There is no visible modulation which confirms the oscillation of only a single axial mode. If the laser is operated considerably above threshold, the time trace shows modulation due to the beating of two or more axial modes. The relatively long time duration of the laser pulse indicated by Figure (3.2b) ($\sim$ 50 nanoseconds) for a laser of this type is due to the high reflectivity of the resonant reflector. This leads to high cavity Q. As the oscillator power output is increased from $\sim$ 5 MW/cm^2 to $\sim$ 20 MW/cm^2 with the dye concentration also increased so that laser threshold is only slightly exceeded, the pulse duration drops from $\sim$ 50 nanoseconds to $\sim$ 20 nanoseconds.

There has been some recent consideration of the frequency drift of a Q-switched ruby laser during the pulse. Pohl[9] has suggested that the drift is due to changes in the refractive index of the ruby and/or the saturable dye due to a time varying population inversion. He observed a drift of 350 MHz ($\sim$ 0.12 cm^{-1}). It appears, however, that this effect is not the same for all lasers since the total linewidth of this laser including any frequency drift is less than 150 MHz.

c. Transverse Mode Control

The reason why it is desirable to suppress oscillation of all but the lowest order transverse mode TEM$_{\infty}$ is that all higher order modes have a larger divergence. The very high values of electric

field intensity ($\sim 10^{11}$ W/cm^2) which are required to observe the stimulated concentration scattering are reached by focusing the laser beam. A beam with divergence angle θ will be focused by a lens of focal length f to a spot of diameter

$$d = f\theta . \tag{3.4}$$

Thus to obtain a particular threshold intensity at the focus of a lens, the total power output of the laser is minimized if the beam has the minimum divergence.

A laser beam which has only TEM_{oo} oscillating is commonly referred to as a diffraction limited beam and has divergence angle approximately given by

$$\theta_{D.L.} = \frac{n\lambda}{d} \tag{3.5}$$

where n is the index of refraction of the crystal and d is the diameter of the active area. When several transverse modes are oscillating, the beam divergence angle is given by the square root of the number of modes which are oscillating multiplied by the diffraction limited divergence angle $\theta_{D.L.}$ (under the assumption that if a particular mode $TEM_{m,n}$ is oscillating all the lower order modes are also oscillating).

The usual technique for transverse mode selection makes use of the fact that the diffraction losses for the TEM_{oo} mode are less than for any other mode. An aperture may be introduced into the cavity with diameter chosen so that the loss of higher order modes is increased sufficiently that they will not oscillate. Various

combinations of lenses may be used in addition to the aperture, but the principle is the same. In attempts to transverse mode select the laser used in this experiment, apertures of various sizes were tried, with and without lens combinations, both with flat rear reflector and a spherical rear reflector with 10 m radius of curvature. None of these methods gave TEM_{oo} operation of the laser. The observed beam divergence $\theta_{exp.} \sim 10\ \theta_{D.L.}$ indicates that approximately 100 transverse modes were oscillating. It is now clear that the reason for this behavior is the poor optical quality and the non-uniform pumping of the rod inherent in the double ellipse head design. In this case the laser oscillates in several areas with local conditions determining the mode properties. The areas may oscillate independently. This behavior is enhanced with high power Q-switched operation where the transient effects of gain saturation may lead to severe mode distortion[10].

d. Near and Far Field Patterns

The spatial and angular distribution of the field in the laser beam are given by the near (Fresnel zone) and far (Fraunhofer zone) patterns respectively.

The near field is the region close to the laser compared to $\frac{a^2}{2\lambda}$ ($\sim$ 5 m for this laser) where a is the beam radius. The near field pattern may be observed by exposing film to the laser beam (with suitable attenuation) close to the laser. A lens may also be used to magnify the beam so the detail of the spatial distribution is more easily observed. The near field pattern of this oscillator with

magnification of four is shown in Figure (3. 3). This photograph shows that the beam consists of many small diameter ($\sim$ 250μ) filaments, which are due to the interference of many transverse modes. It is exactly this type of output which one tries to avoid by transverse mode selection because these "hot spots" easily produce damage in the amplifier stage.

The far field is the region far from the laser compared to $\frac{a^2}{2\lambda}$. In this region, all of the light traveling in a particular direction arrives at some point, i.e. the spatial distribution of energy in the far field is directly related to angular distribution of energy in the beam. The far field pattern is also produced in the focal plane of a simple lens. If then the beam is focused onto a film plate, the beam divergence angle θ can be measured from the relation

$$\theta = \frac{d}{f} \qquad (3.7)$$

where d is the spot diameter and f the focal length of the lens. For this laser the beam divergence measured in this manner is $\sim$2 mr.

3. Amplifier

In order to produce the laser power required to reach threshold for stimulated concentration scattering it was necessary to build a ruby amplifier. The advantage of the oscillator-amplifier system over a very high power oscillator is that the high power can be reached while maintaining a single axial mode and consequently a narrow line-width. The well controlled beam from the low power oscillator is amplified on a single pass through the optically excited ruby amplifier

Fig. 3.3 Near Field Pattern of the Ruby Oscillator with Magnification of 4

rod. Since the amplifier gain is maximum at the center of the output spectrum from the oscillator, there should be some gain narrowing of the spectral profile. The amplifier system used in this experiment was built by the author. The necessary design considerations are briefly reviewed in the next section.

a. Design Considerations

The amplifier head was built to make use of a Vernuil ruby rod 7 inches long by 5/8 inch diameter with Brewster angle cut at each end. The maximum gain from ruby is approximately two for each 2 inches of length. The maximum gain for this rod is therefore ~ 11. The rod was water cooled at room temperature and mounted in a double ellipse cavity. The optical pumping was achieved with two water cooled E.G.G. Incorporated FX67-7 Xenon flashlamps. Energy storage for the amplifier consisted of two 375μF and one 480μF capacitors rated at 4 kilovolts. The necessary capacitance was calculated from the maximum safe energy loading for the quartz flashtubes. An old, laboratory built power supply was modified for use with the amplifier. The circuit diagram is shown in Figure (3.4). The circuit which was used to trigger the amplifier flashlamps is shown in Figure (3.5). To obtain maximum gain from the amplifier, it is necessary to trigger it at a short time ($\sim$200-400 seconds) after the oscillator has been triggered. Circuitry which performed this operation was designed and built[11]. It consists primarily of sequentially triggered monostable multivibrators. The operation of the timing circuit is indicated schematically in Figure (3.6) and the

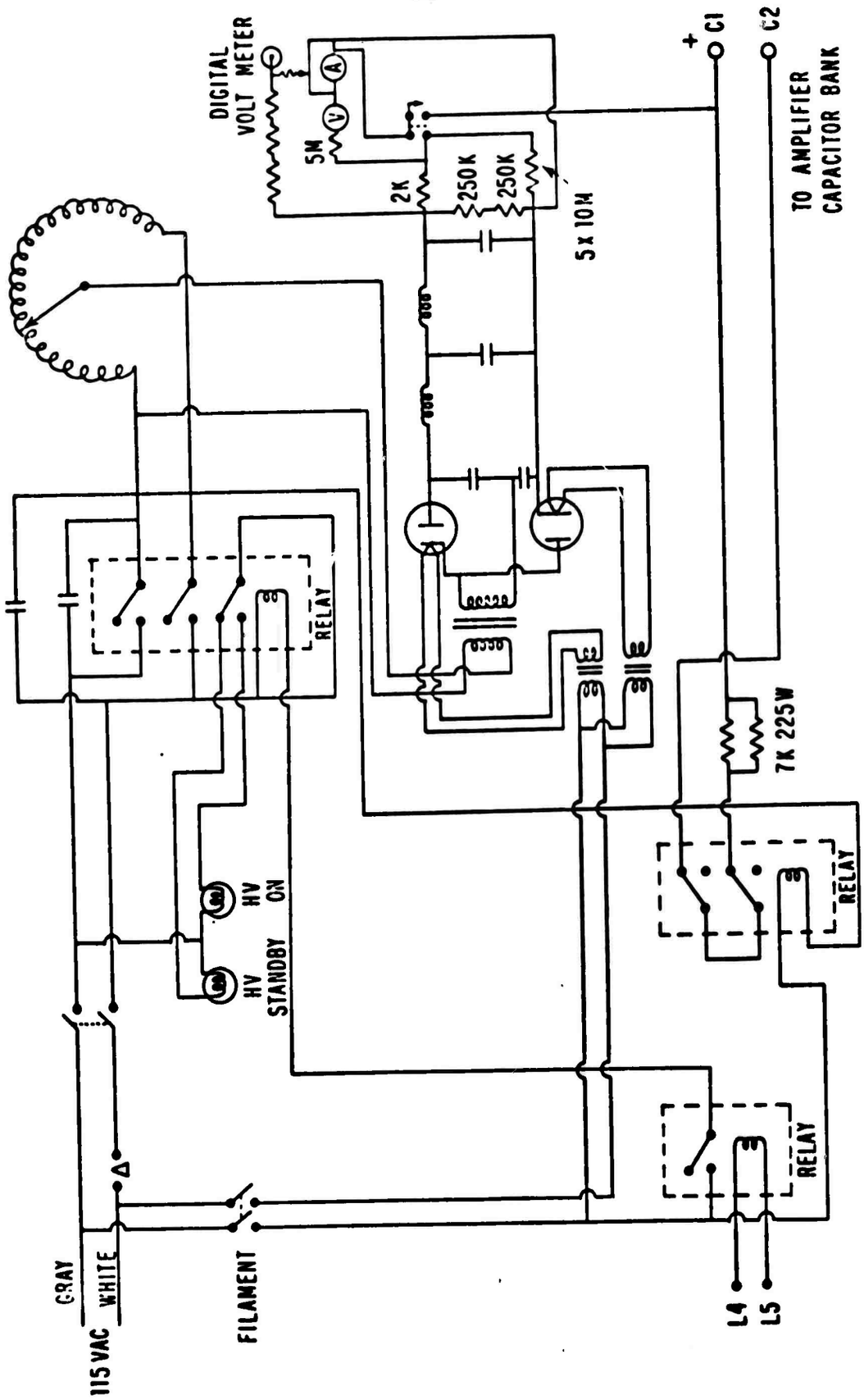

Fig. 3.4 Circuit Diagram of the Amplifier Power Supply

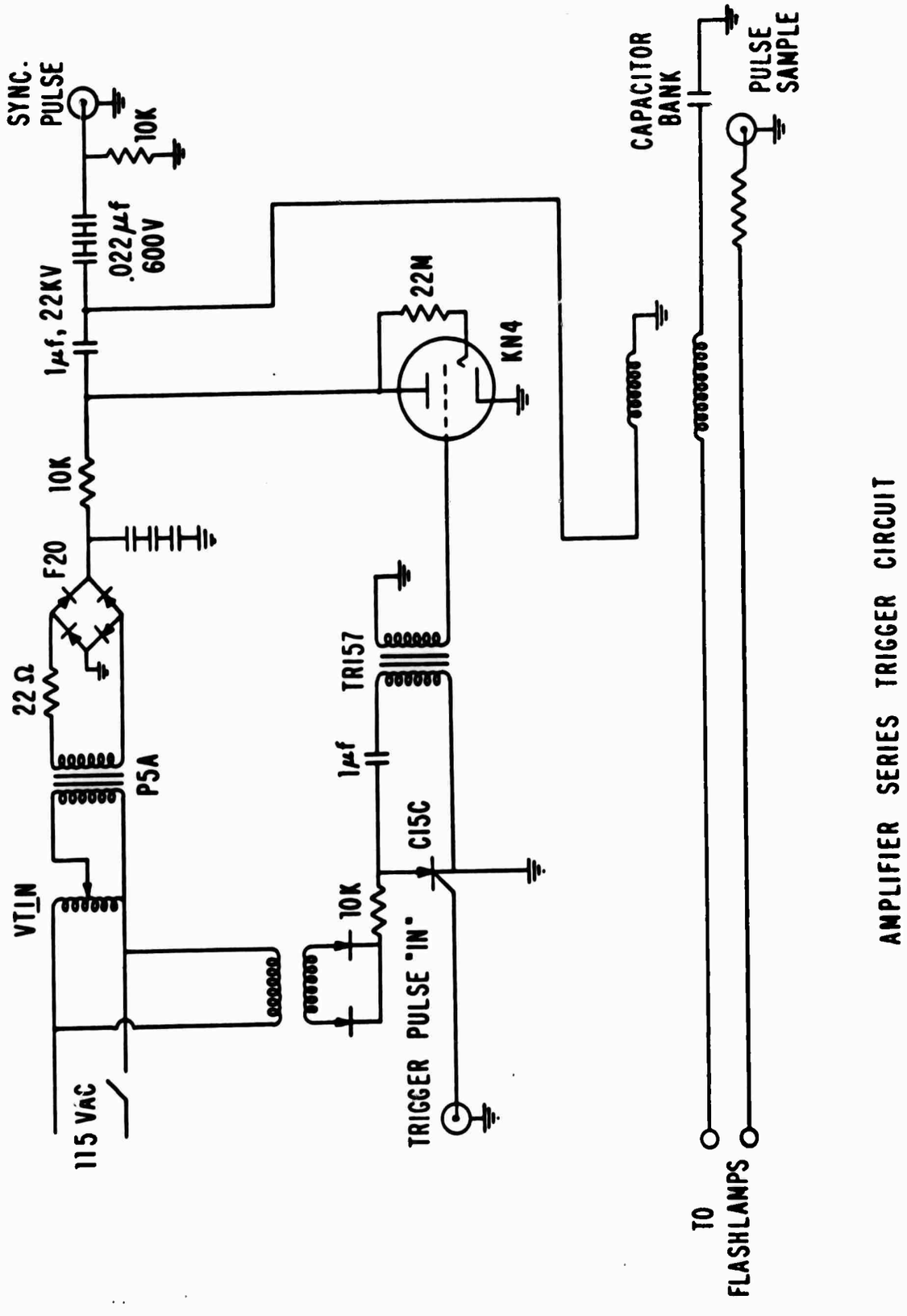

Fig. 3.5 Circuit Diagram of the Amplifier Trigger Circuit

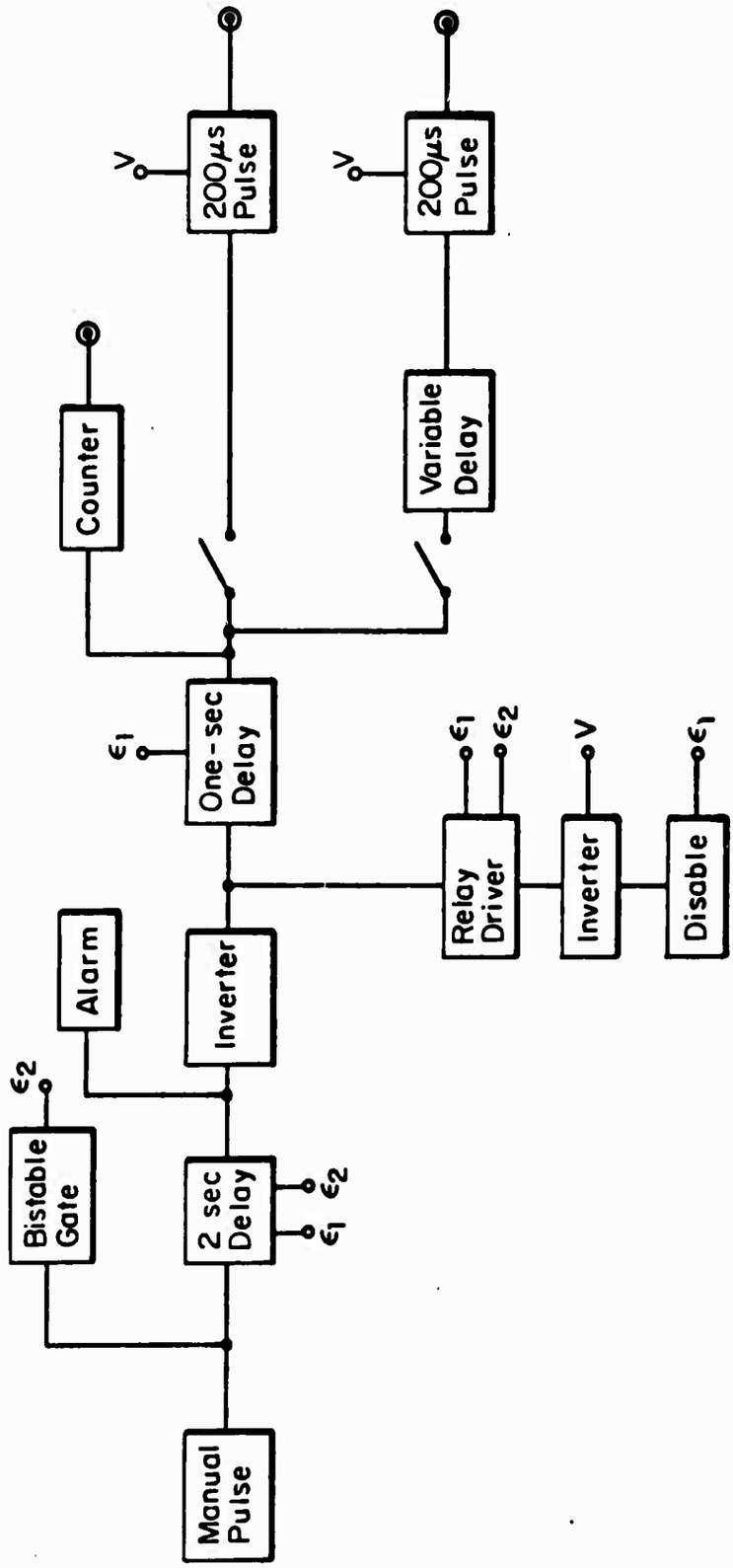

Fig. 3.6 Schematic Diagram of the Timing Circuit

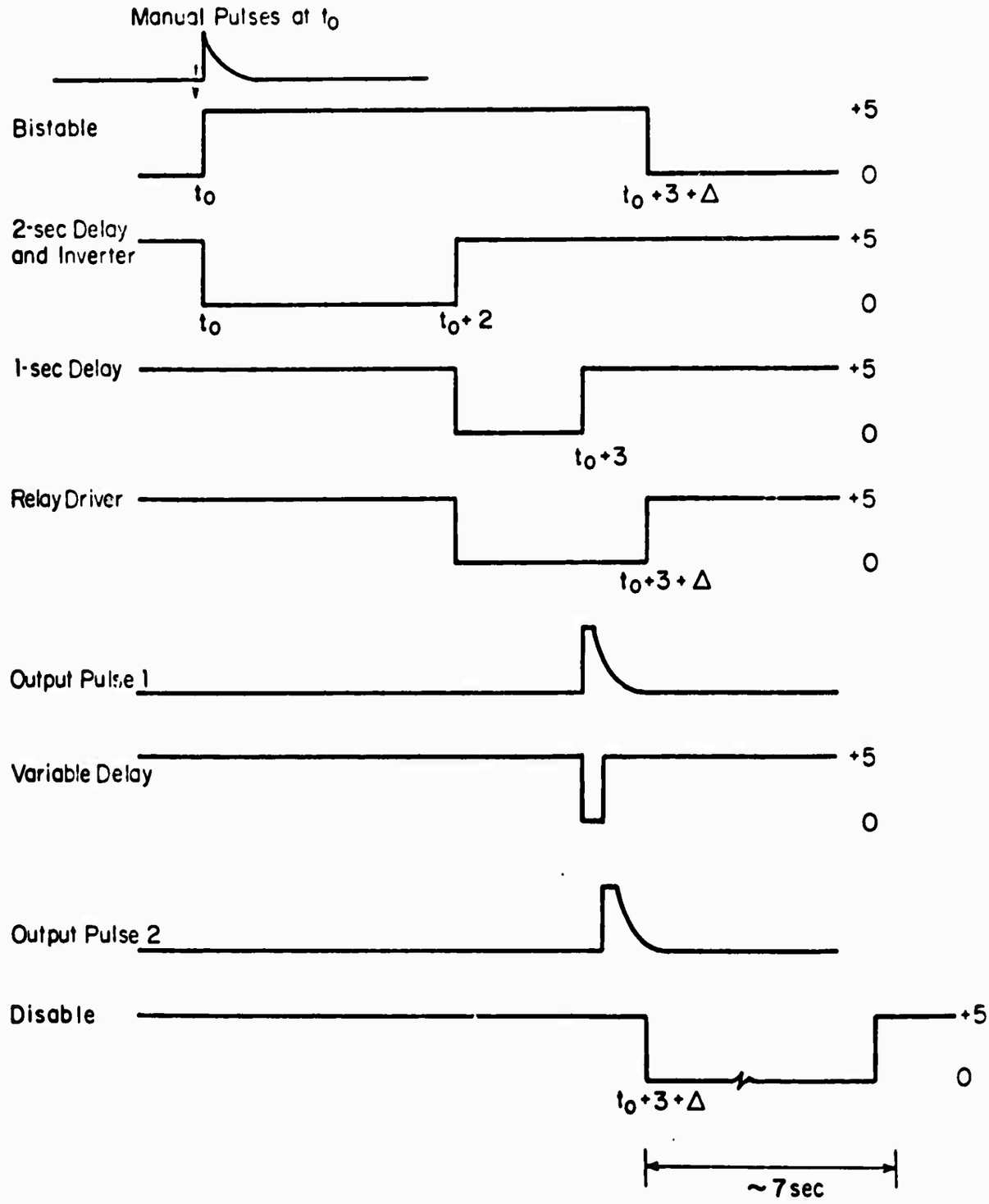

Fig. 3.7 Sequence of the Timing Circuit Operations

timing of the various stages is shown in Figure (3.7). Several features which improved the safety of the laser operation were included. The timing circuit operation basically is as follows: Initially all of the circuits are disabled by the "off" state of the bistable gate. Thus, no random noise or line voltage fluctuation can fire the laser. The firing sequence is initiated by making a ground connection with the trigger switch. This causes the manual pulse circuit to put out a pulse which turns the bistable gate to the "on" state and starts the two second delay. During the two second delay an audible buzzer signal is given to warn anyone in the area that the laser is about to fire. During these two seconds, the output pulse circuits are still disabled, so that no premature firing will occur. At the end of the two second delay, the one second delay is begun and the relay driver is turned "on" which enables the output pulse circuits. At the end of the one second delay, the oscillator is triggered by output pulse 1 and the variable delay is started. The duration of the variable delay can be set for 0-2 milliseconds with a 2μ second resolution. At the end of the variable delay, the amplifier is triggered by output pulse 2. About 0.5 second later the relay driver turns off which initiates the disable circuit. This disables all the circuits for 7 seconds, after which the laser may be fired again.

The relay logic panel shown in Figure (3.8) is a further safety precaution. The logic panel performs the following functions: In the event of an emergency, the oscillator and amplifier power supplies,

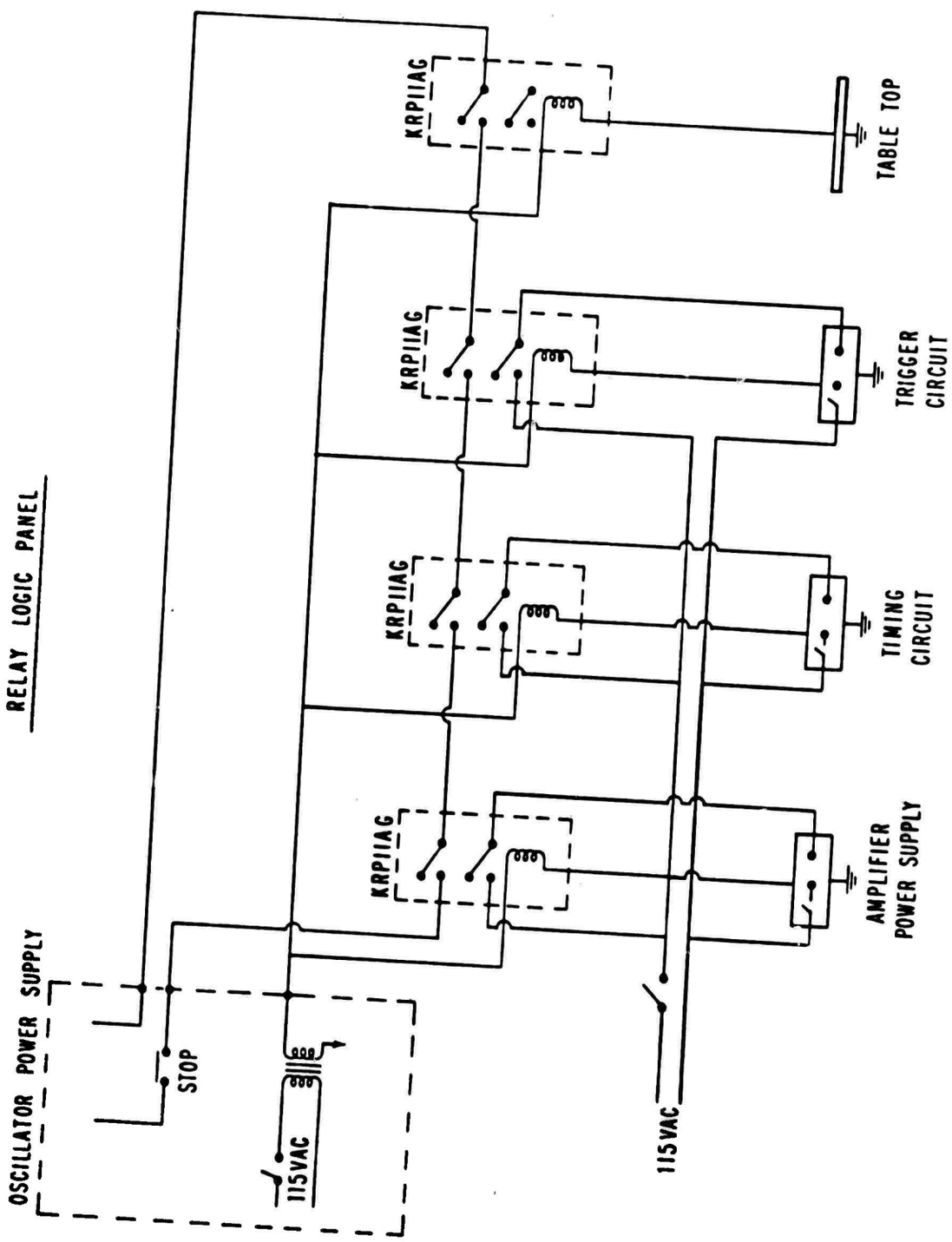

Fig. 3.8 Circuit Diagram of the Relay Logic Panel

timing and trigger circuits may all be turned off by a single switch. Also, if the amplifier power supply, timing or trigger circuit or the aluminum table top should become ungrounded, power to the offending unit is shut off and the capacitor banks are discharged.

b. Operation

The amplifier performance is determined by measuring the input and output energy of the beam. The ratio $\epsilon_{out}/\epsilon_{in}$ is the amplifier gain. The experimental arrangement used to make this measurement is shown in Figure (3.9). The capacitors serve to integrate the photodiode current so that the height of the pulse displayed on the oscilloscope is proportional to beam energy per unit area.

Using this arrangement, the amplifier gain was measured as a function of the voltage applied to the flashlamps and also as a function of the delay between triggering the oscillator and amplifier. It was found that the delay time which produced maximum gain increased as the amplifier pumping energy increased. This result is due to the fact that maximum inversion in the amplifier rod is reached more quickly as the pumping energy is increased. Thus the oscillator pulse must arrive sooner after the amplifier flashlamps have been triggered in order to see the maximum inversion in the amplifier rod. The delay which gives maximum gain varies from $\sim 200\ \mu$ seconds for pumping voltage of 2.6 kilovolts to $\sim 400\ \mu$ seconds for pumping voltage of 3.0 kilovolts. The amplifier gain as a function of the square of the pumping voltage is shown in Figure

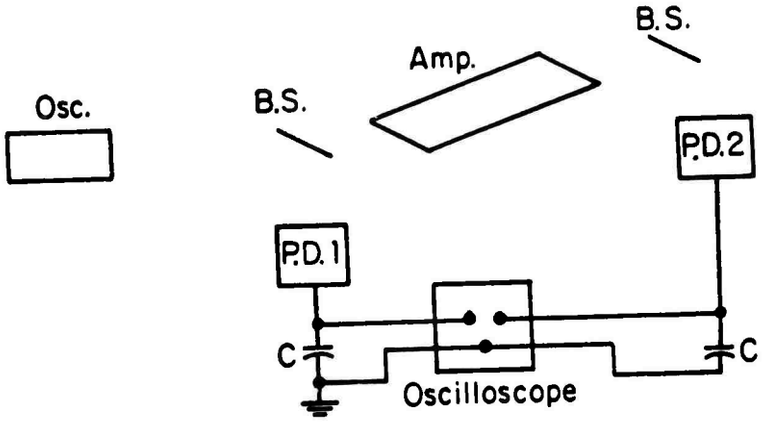

Fig. 3.9 Experimental Arrangement Used to Measure Amplifier Gain

(3.10). The value of gain given in each case is that obtained with the optimum delay. Saturation of the gain is evident when the pumping voltage exceeds 2.8 kilovolts. At 3.0 kilovolts the maximum gain of 11 has been reached.

The maximum intensity achieved with the amplifier was approximately 200 MW/cm^2. This power level however produced damage in the amplifier rod in the form of a small chip at the center of the exit face of the rod and a bubble about 1/2 cm in from that surface. Good quality rubies produced by the Czochralski technique are capable of withstanding intensities in excess of 1 GW/cm^2. The reason that this rod damaged at much lower power was that it has a definite core i.e. large optical inhomogeniety down the center of the rod, which greatly reduces the damage threshold. Also the oscillator beam has many small diameter hot spots as shown by the near field pattern Figure (3.3) which gives local regions of much higher intensity than the average beam intensity. To avoid further damage to the amplifier rod, a 2:1 inverted telescope was inserted between the oscillator and the amplifier. Also a small area was ground on the beam splitter which is before the amplifier. This ground spot scattered the center of the oscillator beam and so prevented light from traveling down the core of the amplifier rod. An aperture with diameter slightly smaller than the amplifier rod diameter was also inserted before the amplifier. The purpose of this aperture was to prevent light from the oscillator from falling on the beveled edge of the amplifier rod and thus avoid any chance focusing of the beam in

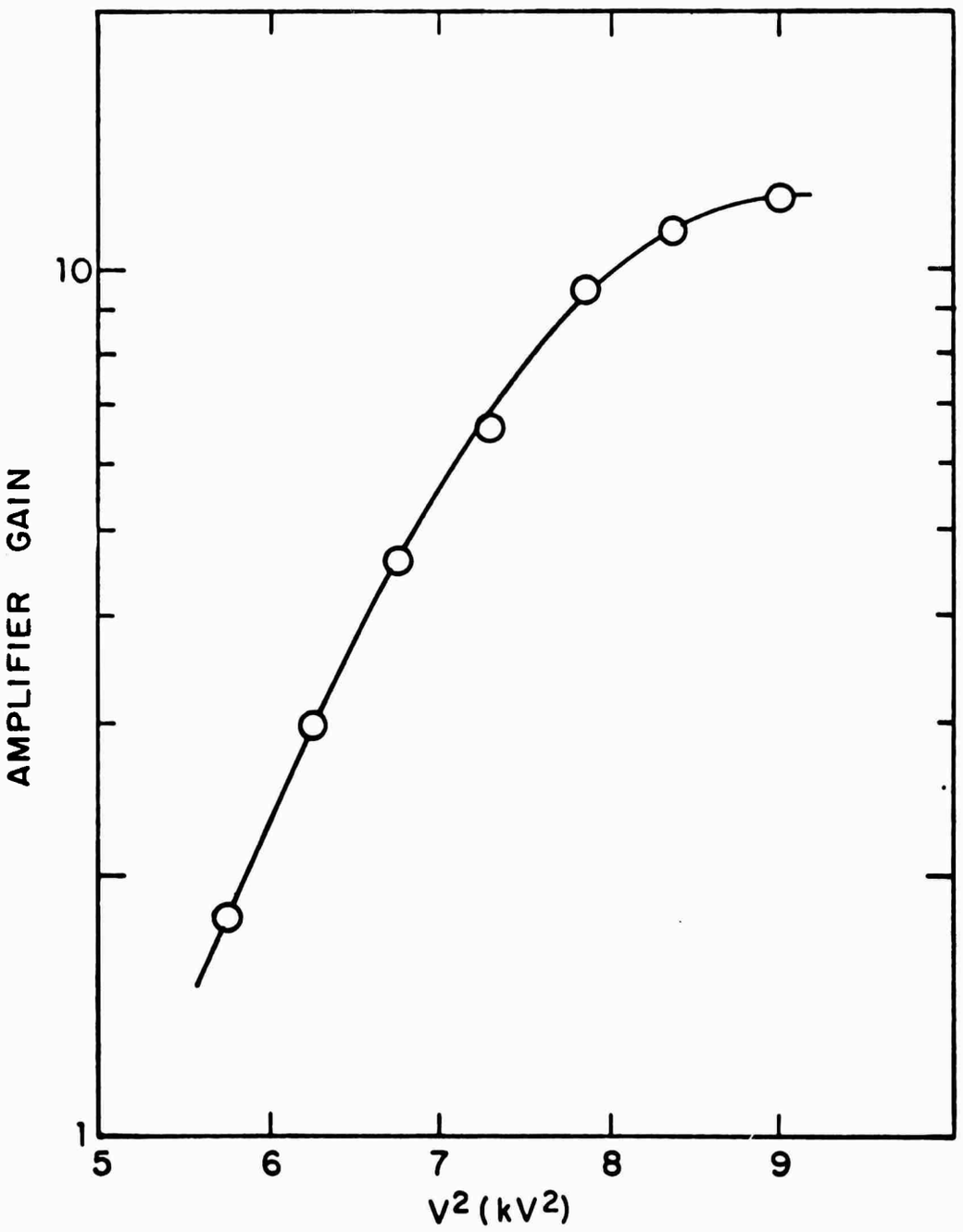

Fig. 3.10 Amplifier Gain as a Function of Pumping Voltage

the amplifier rod. The combination of these additions were successful as no further damage to the amplifier rod occurred.

Whenever a laser beam is directed into a material which scatters light coherently in the backward direction (stimulated Brillouin scattering is an excellent example) there is some danger that the backscattered light will re-enter the laser and cause damage. With an amplifier this danger is increased. The intensity of the backward stimulated Brillouin scattered light may be ~10-20% of the intensity of the laser beam. When this field passes back through the amplifier its intensity is increased by a factor of 10. Consequently the field intensity of the backscattered light when it arrives at the oscillator may be as high as the original output from the amplifier and can cause damage in the oscillator rod. Even if no damage should occur, there is still another problem caused by the feedback. After the backscattered light has passed back through the amplifier and oscillator it will come out again as a new laser pulse, pass back through the amplifier and if sufficiently intense, will stimulate for example, the second Stokes Brillouin line. This behavior was observed when the laser beam was focused into SF_6 gas at 10 atmospheres pressure. The field oscillated back and forth between the gas cell and laser, stimulating a higher order Brillouin Stokes line with each pass. As many as the first 10 Brillouin Stokes lines of SF_6 were observed by use of a Fabry Perot interferometer in this manner. The oscillation continues until the amplifier gain has decreased to the point that the laser intensity is insufficient to stimulate the next Stokes line.

Ideally the laser should be isolated from the scattering material by a Kerr cell or a Faraday rotator. Lacking this equipment, another method was used. A dye cell was placed immediately after the amplifier and a 50 nanosecond optical delay between the laser and experimental area was introduced. The final arrangement for the oscillator-amplifier system is shown in Figure (3.11). After passing through the amplifier and dye cell, the beam is turned by 90 degrees by an arrangement of two prisms shown in Figure (3.12). This arrangement also rotates the beam polarization from horizontal to vertical (this is true because the beam polarization remains perpendicular or parallel to the plane of incidence upon total internal reflection). The polarization is rotated because vertical polarization is desired for the experiment. The beam then travels a distance of 6.78 m to the spherical mirror. This distance is equal to the mirror radius of curvature so the mirror reimages the beam with 1:1 magnification at a position just to the right of the double prism as indicated in Figure (3.11). The laser output is then directed into the cell containing the gas mixtures under investigation. The total time then required for light to make a round trip from the amplifier to the gas cell and back to the amplifier is $\sim$100 ns which is approximately the duration of the laser pulse as shown in Figure (3.2b). Thus the end of the laser pulse has left the amplifier before the front of the backscattered pulse has reached the amplifier. The dye concentration in the amplifier dye cell is adjusted so that it bleaches when the laser pulse passes through but not when the back-

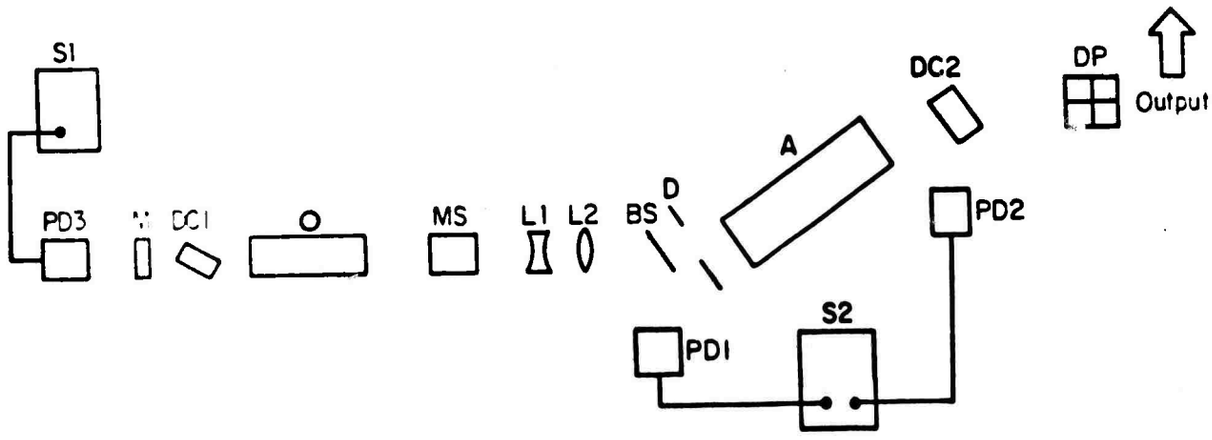

A Amplifier
BS Beamsplitter
D Diaphragm
DC1 Oscillator Q switch dye cell
DC2 Dye cell
L1 Lens, -10 cm focal length
L2 Lens, +20 cm " "
M Oscillator rear mirror
MS Mode selector
O Oscillator
PD1 RCA 917 photodiode
PD2 ITT photodiode
PD3 TRG 105B photodiode
S1 Tektronix 519 oscilloscope
S2 " 555 "
SM Spherical mirror 6.78m radius

SM

Fig. 3.11 Oscillator - Amplifier System

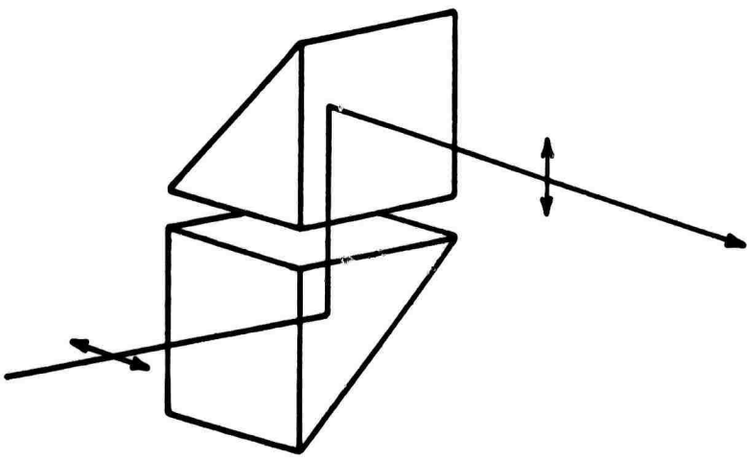

Fig. 3.12 Double Prism Arrangement for Turning Laser Beam and Changing Polarization from Horizontal to Vertical

scattered pulse passes through. This introduces enough loss in the backscattered beam that it will not be amplified to sufficient intensity to stimulate any further scattering.

C. Fabry Perot Interferometer

In this experiment the occurrence of stimulated Brillouin or concentration scattering is detected by observing the frequency shift from the laser frequency of the backscattered light from the gas mixture. The range in frequency shift which must be observable is 0.005 cm^{-1} (150 MHz) to 0.03 cm^{-1} (900 MHz). Detection of a frequency shift in this range can be accomplished by a plane parallel Fabry Perot interferometer (FPP) with spacing between the plates on the order of 4-8 cm.

The general theory of the FPP is well known[8], so this section is confined to the consideration of factors which were important in the design and operation of the FPP used in this experiment.

The optical arrangement for use of the FPP is shown in Figure (3.13). The incident collimated beam of light is diverged by lens L1. For light traveling in certain directions, the phase shift for one round trip of the FPP is an integral multiple of 2π. In those directions the interference is constructive, and the interference pattern in the focal plane of the lens L2 is then a series of concentric rings. The diameter of p^{th} bright fringe is given by

$$D_p^2 = \frac{4n'\lambda f^2}{n^2 h} (p - 1 + e) \qquad (3.8)$$

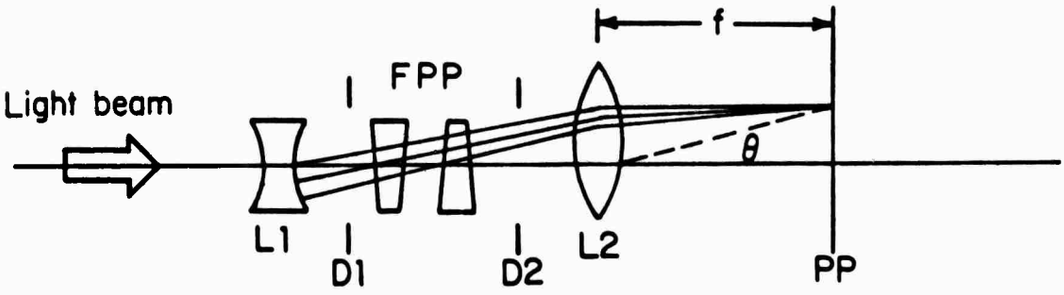

Fig. 3.13 Experimental Arrangement for Use of Fabry-Perot Etalon

where n', n are the index of refraction of the air between the plates, and outside of the plates respectively, λ is the wavelength of the light in vacuum, h is the plate separation and e the fractional order at the center of the ring pattern.

The resolving power of the FPP, i.e. the minimum frequency difference of two monochromatic components which can be resolved, is given by

$$\Delta\kappa = \frac{1}{2n'hF} \tag{3.9}$$

where F is the instrument finesse which is defined as the ratio of the fringe separation to the halfwidth of the fringe due to a monochromatic line. The fringe separation (free spectral range) is given by

$$(\Delta\kappa)_{FSR} = \frac{1}{2n'h} \tag{3.10}$$

Each loss mechanism present in the FPP cavity contributes to the cavity lifetime and therefore also contributes to the finesse. The finesse F_i associated with the i^{th} loss mechanism is related to the corresponding contribution to the cavity lifetime τ_i by

$$F_i = \frac{\pi c \tau_i}{2n'h} \tag{3.11}$$

The net instrumental finesse is given by

$$F^{-1} = \sum_i F_i^{-1} \tag{3.12}$$

The major contributions to the finesse are mirror flatness and reflectivity. For mirrors with $\frac{\lambda}{m}$ surface figure and reflectivity R, the associated values of finesse are given by

$$F_F \approx \frac{m}{2}$$

$$F_R \approx \frac{\pi\sqrt{R}}{1-R} \tag{3.13}$$

Diffraction losses usually play no significant role in determining overall finesse. The diffraction limited finesse is given by

$$F_D \simeq \frac{a^2}{2n'\lambda h} \tag{3.14}$$

where a is the aperture diameter.

The Fabry Perot interferometer used in this experiment had quartz plates with $\frac{\lambda}{200}$ surface figure, reflectivity 98% and plate separation of 6 cm. The relevant parameters for this case are

$$\begin{aligned} (\Delta K)_{FSR} &= .083 \text{ cm}^{-1} \\ F_F &\sim 100 \\ F_R &\sim 150 \\ F_D &\sim 1000 \end{aligned} \tag{3.15}$$

The actual instrumental finesse which depends, in addition to the factors already mentioned, on mirror alignment and mechanical stability of the FPP mounting, was about 25. This gave a resolving power

$$\Delta K \simeq .003 \text{ cm}^{-1} \text{ (90 MHz)} \qquad (3.16)$$

The Fabry Perot mounting is shown in Figure (3.14). The main housing and end plate were aluminum. The spacer was made of Invar. One of the quartz plates was held against the spacer by three steel ball bearings. The other plate was held by three phosphor-bronze springs. This plate was aligned to be parallel to the other plate by the fine adjustment screws on the phosphor-bronze springs.

Alignment of the FPP was done by observing the ring pattern resulting from illumination by a He-Ne laser. It is important to make the alignment with as little pressure as possible on the quartz plates to avoid any deformation which would lead to a reduction in finesse.

D. Experimental Arrangement

The first experimental arrangement which was used to detect the frequency shift between the laser and the stimulated emission from the gas mixture is shown in Figure (3.15). The collimated beam from the laser entered from the direction indicated by the arrow. Approximately 8% of the beam was split off by the glass beam splitter BS1. The polarization of this light was rotated from vertical to horizontal by the z-cut quartz 1/2-wave plate. It then reflected through the prism and passed through a calcite polarizer which was set to transmit horizontally polarized light. The remainder of the beam was focused by lens L3 (focal length 15-40 cm) into the gas mixture. If the beam intensity at the focus of lens L3

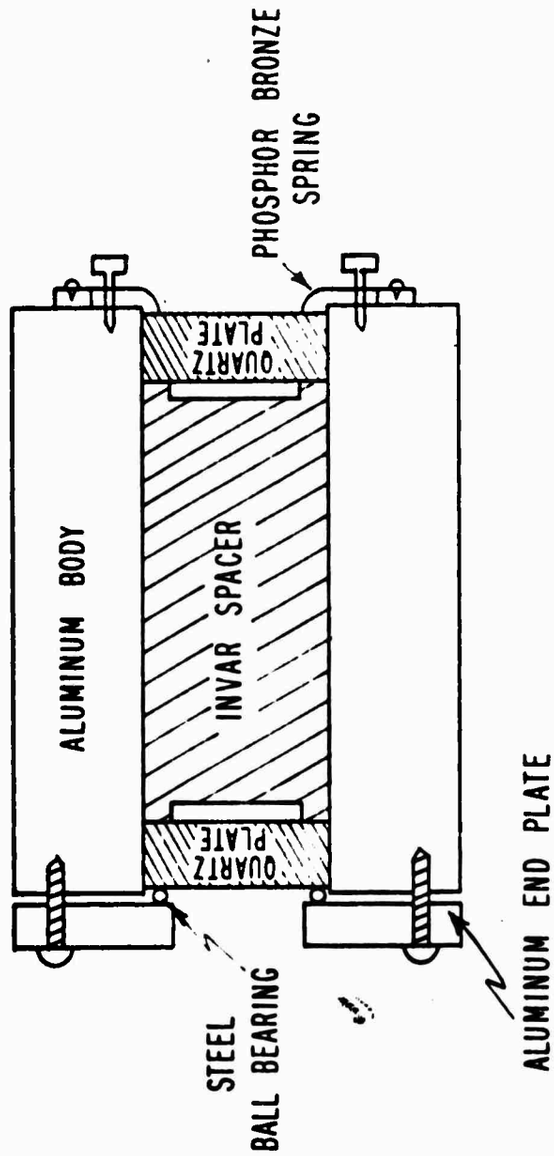

Fig. 3.14 Fabry-Perot Etalon Mounting

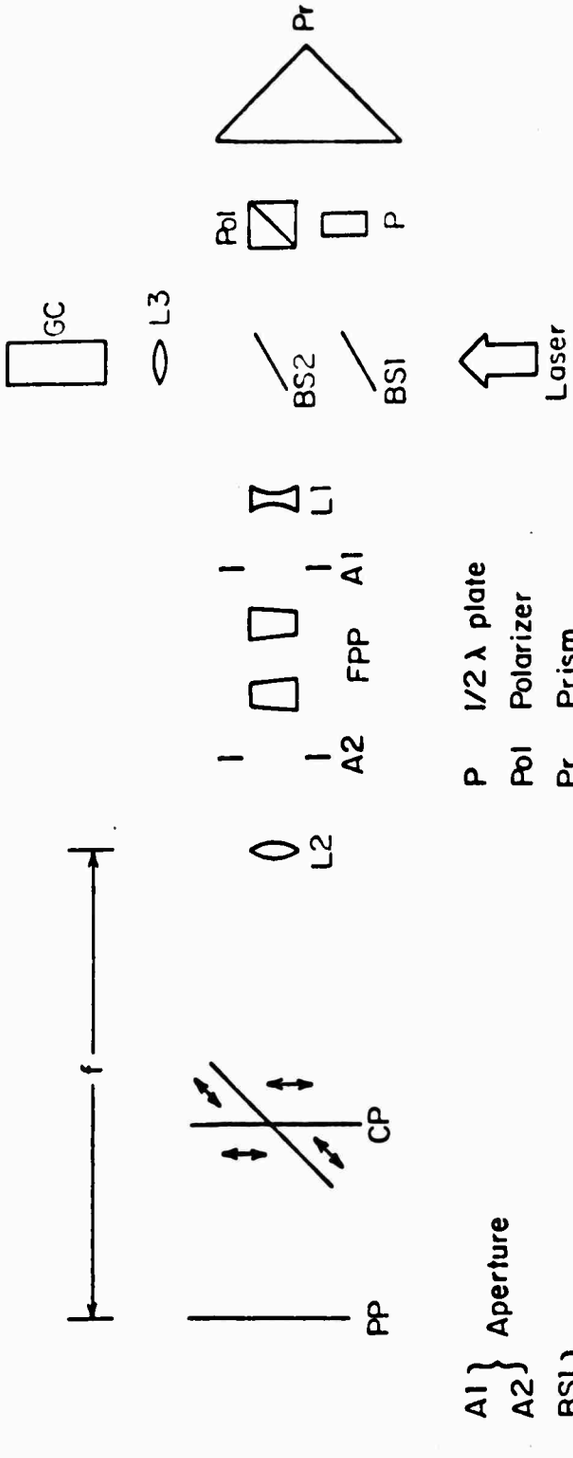

Fig. 3.15 First Experimental Arrangement

was sufficiently high to reach threshold for the stimulated scattering process, the intensity of the backscattered light was on the order of 10% of the incident laser intensity. About 8% of the backscattered beam was split off by beamsplitter BS2 and recombined with the laser light which passed through the polarizer. The total beam was then diverged by lens L2 and passed through the FPP. The interference pattern from the FPP was focused by lens L2 through the crossed polarizers onto the Polaroid film. A typical example of the results obtained is shown in Figure (3.16). The interference fringes from the laser light appear in quadrants 1 and 3 of the crossed polarizers and the fringes from the backscattered light appear in quadrants 2 and 4. The crossed polarizer plate was made from squares of Polaroid NH32 sheet polarizer. This material is a neutral color linear dichroic polarizer. The transmission for an unpolarized beam is 32% and the extinction transmittance is 0.005%. The Polaroid film used was type 413.

The frequency shift was determined from the difference in diameter of the interference fringes which were due to the laser and the stimulated backscattered light. This measurement will be discussed later.

An estimate of the laser intensity which is required to produce stimulated scattering on the gas mixtures can be made as follows. In order to reach the threshold for stimulated oscillation in the gas mixture the Stokes wave gain coefficient must be on the order of ten^{12} i.e.

$$E(\omega_S) = E_{noise}(\omega_S)\, e^{10} \qquad (3.17)$$

NOT REPRODUCIBLE

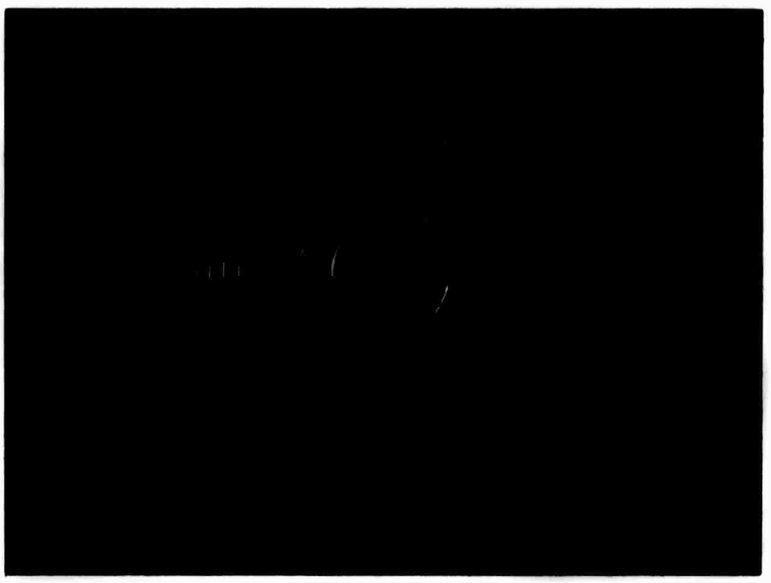

Fig. 3.16 Interference Fringes from 4 cm Fabry Perot Etalon

where $E_{noise}(\omega_S)$ is the amplitude of the noise field at the Stokes frequency ω_S. The noise field arises from spontaneous scattering from zero point or thermal fluctuations in material mode. This observation can be used to make an estimate of the laser intensity required to produce stimulated scattering. Thus

$$g I_L z = 10 \qquad (3.18)$$

where g is the Stokes field gain coefficient, I_L is the laser field intensity and z is the path length over which gain occurs. The maximum gain for the concentration mode as shown in Figure (4.3) is 10^{-10} cm/W. Thus for $z \sim 1$ cm, one must have $I_L \sim 10^{11}$ W/cm^2. For a laser output of 100 MW/cm^2 with a beam cross-sectional area of 1 cm^2, the laser power is 10^8 W. With a beam divergence of 2 mr, the beam area at the focus of a lens with 20 cm focal length is $\sim 10^{-3}$ cm^2. Therefore the laser intensity at the laser focus is $I_L \sim 10^{11}$ W/cm^2 which is the proper magnitude to produce stimulated Stokes wave oscillation.

Using the experimental arrangement shown in Figure (3.15), stimulated scattering was successfully observed in gas mixtures with Helium concentrations up to 60%. However the laser intensity required to produce stimulated scattering in the gas mixtures with higher Helium concentrations was approximately 200 MW/cm^2 in the collimated beam. As discussed earlier, this intensity produced damage in the ruby amplifier rod. Consequently it was necessary to find a way to produce stimulated scattering with a reduced laser

power. Certainly if a field with frequency ω_S could be introduced into the gas cell traveling in the backward direction, the gain required to amplify this Stokes field to the oscillation threshold would be less than the gain required to build up to oscillation from the noise field. Of course an essentially monochromatic field with frequency ω_S is not available, but it is easy to produce a field with a broad frequency spectrum beginning at the laser frequency and extending on the Stokes side. When such a broad spectrum field traveling in the backward direction is present in the gas mixture simultaneously with the laser field, the gain of the medium will amplify the portion of the broad spectrum which is at the frequency ω_S. The broad source effectively increases the amplitude of $E_{noise}(\omega_S)$. A broad spectrum of the nature described can be produced by stimulated Rayleigh wing scattering in liquids containing molecules with a large anisotropy in the polarizibility (large quadratic D.C. Kerr effect). Examples of such liquids are CS_2, benzene and many of its derivatives. A simple description of Rayleigh wing scattering can be given as follows. Consider a fluid composed of cigar-shaped molecules which have a different value for the polarizibility parallel and perpendicular to the axis. Now suppose there are two light fields present: an incident field with frequency ω_L and a scattered field with frequency ω_S close to ω_L. The two field will interfere and the resultant field is modulated at the difference frequency $\omega_L - \omega_S$. If the characteristic molecular orientation time τ is not too long, the molecular orientation and therefore the polarizibility can follow the modulation

at $\omega_L - \omega_S$. This process results in a large material polarization at the frequency ω_S which leads to enhancement of the scattered wave intensity. The frequency dependence of the Rayleigh wing gain is given by

$$\frac{G(\omega_S)}{2\,G_{max}} = \frac{(\omega_L - \omega_S)\tau}{1 + (\omega_L - \omega_S)^2\tau^2}$$

where G_{max} is the gain at $(\omega_L - \omega_S)\,\tau = 1$. The value of G_{max} depends upon the ellipticity of the incident light and upon the scattering angle. This gain produces a Stokes shifted Rayleigh line which has been observed by several authors[13] and a theory which describes most of the experimental results has been given by Chaio and Godine[14]. Foltz et. al.[13] have also observed that excitation with linearily polarized light produces in the forward direction a diffuse Stokes wing of the same polarization with the maximum intensity at ω_L. This case has been treated by Chaio, Kelly and Garmire[15]. As a result of Stokes-anti Stokes coupling, scattering in the near forward direction was shown to be dominated by the degenerate light by light scattering with no shift in the scattered light frequency.

Several liquids were investigated for use in this experiment (CS_2, nitrobenzene, acetone, aniline, and quinoline). Nitrobenzene produced the most satisfactory results. For nitrobenzene $\tau = 4.78 \times 10^{-11}$ sec. The frequency dependence of the Rayleigh wing gain for nitrobenzene is shown in Figure (3.17).

The experimental arrangement which was used is shown in

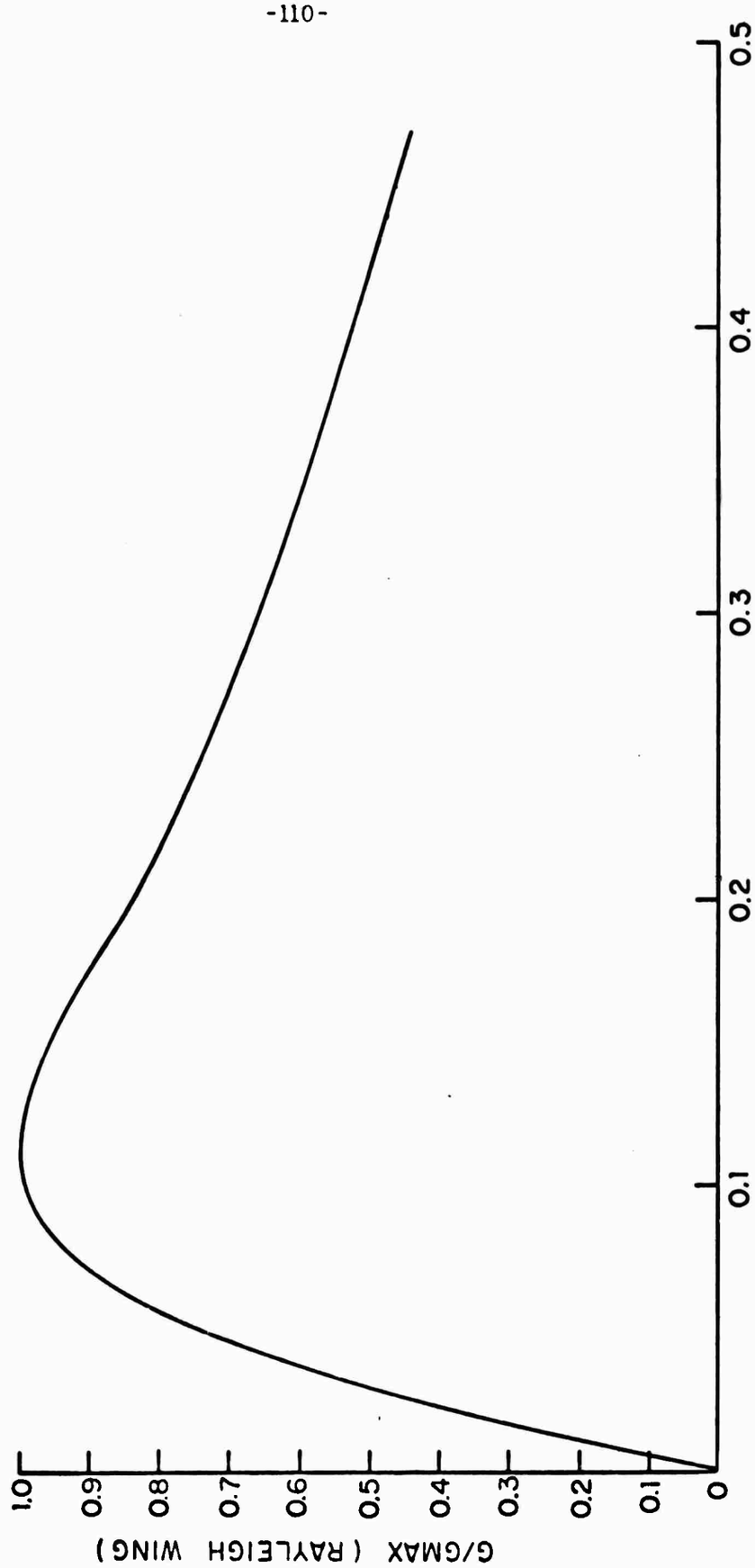

Fig. 3.17 Frequency Dependence of Stimulated Rayleigh-Wing Gain in Nitrobenzene

Figure (3.18). The collimated linearily polarized beam from the laser entered as indicated by the arrow. It passed through the glass beam splitter BS1 and was focused by lens L3 (focal length 15-40 cm) into the gas cell GC. After passing through the gas cell the beam was recollimated by lens L4 (focal length 20 cm) and then focused by lens L5 into the liquid cell LC which contained nitrobenzene. The laser beam self-focused in the nitrobenzene and produced strong stimulated Brillouin scattering with a frequency shift of 0.26 cm^{-1} in addition to the stimulated Rayleigh wing scattering. Denariez and Bret[13] have investigated the stimulated scattering in nitrobenzene. They found that the Brillouin gain is $\sim 10^{-5}$ cm/W while the maximum of the Rayleigh wing gain is $\sim 5 \times 10^{-6}$ cm/W. However the Brillouin time constant is $\sim 10^{-9}$ sec compared to $\sim 10^{-12}$ sec for the Rayleigh wing. Thus the Rayleigh wing reaches steady state conditions before the Brillouin mode so that both stimulated processes are observed. The backscattered light from the nitrobenzene was recollimated by lens L5. Approximately 8% of this beam was reflected by the glass beam splitter BS2. This portion of the beam was directed around the gas cell by the prisms Pr1, Pr2. Its polarization was rotated from vertical to horizontal by the half wave plate P. The remainder of the backscattered light from nitrobenzene passed back into the gas cell where it interacted with the gas mixture and the laser beam in the focal volume of lens L3. Approximately 8% of the beam traveling in the backward direction out of the gas cell was reflected by the beam splitter BS1 and recombined with the portion of the light from the

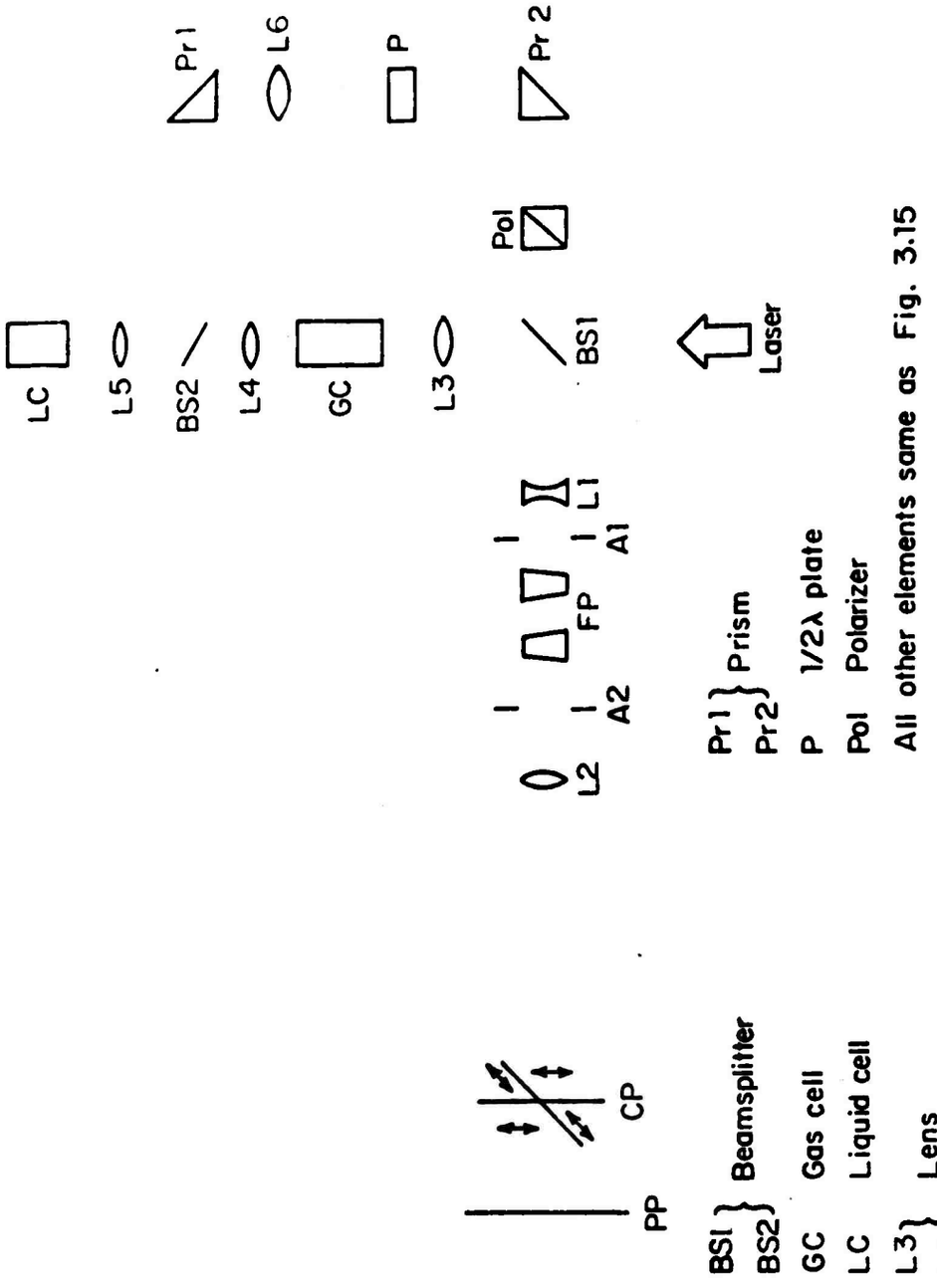

Fig. 3.18 Final Experimental Arrangement

liquid which had traveled around the gas cell. The combined beam was then analyzed by the FPP in the manner described earlier. A typical example of the FPP fringes photographed with this arrangement are shown in Figure (3.19). The fringes which appear in quadrants 1 and 3 are due to the light from the nitrobenzene which has traveled around the gas cell. This is then the input spectrum in the backward direction into the gas cell consisting of the nitrobenzene Brillouin line as indicated in Figure (3.19) and the Rayleigh wing. The Rayleigh wing intensity is too low to appear on the film, in addition to which it is much broader than the free spectral range of the FPP and so would appear only as a general fogging of the photograph. The FPP fringes which appear in quadrants 2 and 4 give the output spectrum from the gas cell. This consists of the nitrobenzene Brillouin wave which has simply passed through the gas cell, a portion of the incident laser beam which has been reflected from the gas cell window and the stimulated line from the gas mixture. By monitoring the spectrum input to the gas cell one can be certain that the line, which is attributed to the gas mixture, was not by some process coming from the nitrobenzene.

This technique of using a broad spectrum to assist the oscillation of a low gain process has to the author's knowledge never been used before. Its effectiveness is illustrated by the result that the laser intensity required to produce stimulated Brillouin scattering (SBS) in SF_6 gas at a pressure of 5 atm dropped from 60 MW/cm^2 in the collimated beam when the beam was simply focused into the gas to 20 MW/cm^2 when this amplifier technique was used. The reduction in the laser

Fig. 3.19 Interference Fringes from 6 cm Fabry Perot Etalon Used in Final Experimental Arrangement

power required to reach stimulated oscillation utilizing this technique was the singular factor which allowed completion of the experiment with the existing laser system. It was then possible to produce stimulated scattering in gas mixtures with Helium concentration as high as 90%.

Since the peak intensity of the Rayleigh wing spectrum occurs at a shift of 0.111 cm^{-1} it was necessary to investigate whether using the amplifier technique introduced any pulling of the frequency of the stimulated scattering in the gas mixture. This was done by studying the frequency shift of the stimulated line in gas mixtures with low Helium concentrations. In these mixtures the laser intensity was great enough to produce oscillation by simpling focusing into the gas mixture as well as with the amplifier technique. The shift in frequency was the same in both cases within the accuracy of the measurement.

E. Gas Handling Equipment

The system diagrammed in Figure (3.20) was constructed to fill the gas cell and measure the pressure of the gases contained in the cell. All of the tubing used was 1/4 inch outer diameter copper tubing. Tubing connections were made with Gyrolok fittings. These fittings proved leak free at pressures as high as 1200 psig. Before filling, the entire system was evacuated by a Precision Scientific Model 25 vacuum pump. System vacuum was monitored by an NRC Model 501 thermocouple gauge. After evacuation, the SF_6 or Xenon gas was slowly leaked into the system until the desired pressure was

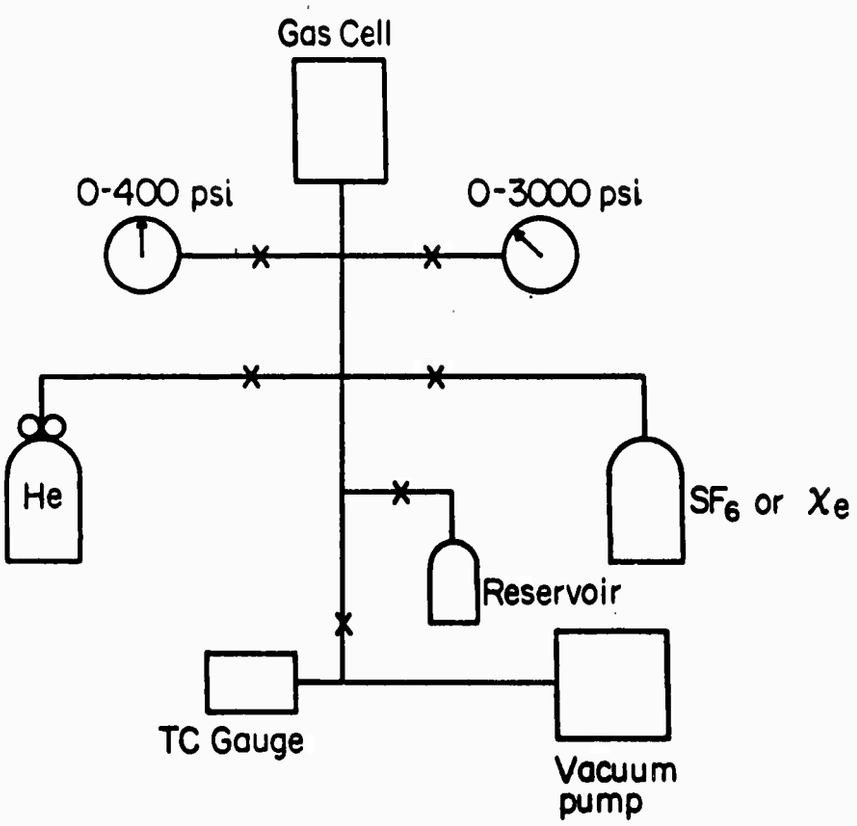

Fig. 3.20 Gas Handling System

reached. System pressure was measured by the two pressure gauges indicated in Figure (3.20). Both gauges were made by U. S. Gauge and were purchased from Matheson Gas Products. The low pressure gauge was a high accuracy gauge, accurate to 1/2% over the entire scale. The gas mixture was made by slowly leaking Helium gas into the system until the required total pressure was reached. At least one hour was allowed for complete mixing to take place before any measurements were made. There was no observable change in the scattered light spectrum when longer mixing times were allowed.

The Helium gas used in this experiment was supplied by the U. S. Navy. The Xenon and SF_6 were purchased from Matheson Gas Products. The SF_6 is inexpensive and so was simply discarded whenever necessary to change concentration. However Xenon gas is quite expensive and so it was desirable to trap and recycle the gas. This can easily be done since Xenon freezes at 161 degrees Kelvin. The reservoir shown in Figure (3.20) was immersed in liquid nitrogen (77 degrees Kelvin) and time was allowed for the system pressure to come to equilibrium. At this time all of the Xenon was frozen in the reservoir. The vapor pressure of Xenon at 77 degrees Kelvin is less than 1 Torr. The Helium gas could then be pumped out of the system leaving only Xenon. When the reservoir returned to room temperature the pure Xenon could be reused.

F. Data Analysis

The frequency shift of the stimulated scattering in the gas mixture from the laser frequency can be determined from the Fabry

Perot fringes. The method of that analysis is given in this section following the discussion given in Born and Wolf[8].

The condition for constructive interference which gives the bright fringe is that the phase shift δ of the light in making a round trip of the FPP cavity is an integral multiple of 2π. This condition is expressed by

$$m = \frac{\delta}{2\pi} = \frac{2n'h\cos\theta'}{\lambda} + \frac{\phi}{\pi} \qquad (3.19)$$

where n' is the index of refraction of the medium between the plates, h is the plate separation, θ' is the angle of reflection, and ϕ is the phase change on internal reflection; m is the integer order of the interference. For $\theta = 0$, the expression on the right is not in general an integer. So one may write

$$m' + e = \frac{2n'h}{\lambda} + \frac{\phi}{\pi} \qquad (3.20)$$

where m' is the integer order of the innermost ring and $e < 1$. The integer order of the p^{th} ring out from the center of the interference pattern is $m' - (p-1)$ and the diameter of this ring is given by

$$D_p^2 = \frac{4n'\lambda f^2}{n^2 h}(p - 1 + e) \quad . \qquad (3.21)$$

Suppose now that the light field incident upon the FPP consists of two essentially monochromatic components with wavelengths $\lambda_{1,2}$ which are not too far apart. Then equation (3.20) may be written for each component. In terms of spectroscopic wave number $\kappa = \frac{1}{\lambda}$

$$m'_{1,2} + e_{1,2} = 2n'K_{1,2} + \frac{\phi}{\pi} \quad . \tag{3.22}$$

Subtraction gives the result

$$\Delta K = K_1 - K_2 = \frac{1}{2n'h}(m'_1 - m'_2 + e_1 - e_2) \quad . \tag{3.23}$$

The value of $m'_1 - m'_2$, which is the number of orders overlap between the two patterns, can be determined by changing the plate separation. In this experiment, the frequency shift is less than the free spectral range of the FPP so $m'_1 - m'_2 = 0$. The difference in the fractional orders $e_1 - e_2$ is obtained from measurements of the ring diameters. If $\lambda_1 \sim \lambda_2$, the ring diameters for each component are given by

$$D^2_{1,2p} = A(p - 1 + e_{1,2}) \tag{3.24}$$

where

$$A = \frac{4n'\lambda f^2}{n^2 h} \quad .$$

Subtracting the square of the diameter of successive rings for each component gives

$$D^2_{1,2\,p+1} - D^2_{1,2p} = A \quad . \tag{3.25}$$

Subtracting the square of the diameter of the rings due to each component for the same order of interference gives

$$D^2_{1p} - D^2_{2p} = A(e_1 - e_2) \tag{3.26}$$

Note that the right hand side of both equations (3.25) and (3.26) does not depend upon p so both of these subtractions can be carried out for

many orders of interference. This will give good average values for A and $D_{1p}^2 - D_{2p}^2$. Denoting the average value by a —, the difference in fractional orders is given by

$$\overline{e_1 - e_2} = \frac{\overline{D_{1p}^2 - D_{2p}^2}}{A} \qquad (3.27)$$

The frequency shift is then given by equation (3.23).

The FPP ring diameters were measured from the Polaroid photographs taken in this experiment to the nearest 0.0001 inch using a traveling microscope. Usually 4 or 5 rings were clearly visible so the averaging described above was done over this number of fringes.

References: Chapter III

1. R. H. Dicke, U. S. Patent Number 2, 851, 652, September 9, 1958.

2. A. L. Schawlow and C. H. Townes, Phys. Rev. 112, 1940 (1958).

3. A. G. Fox and T. Li, B.S.T.J. 40, 453 (1961).

4. G. D. Boyd and J. P. Gordon, B.S.T.J. 40, 489 (1961).

5. G. D. Boyd and H. Kogelnik, B.S.T.J. 41, 1347 (1962).

6. D. A. Kleinman and P. P. Kisliuk, B.S.T.J. 41, 453 (1962).

7. D. Fradin, private communication.

8. M. Born and E. Wolf, Principles of Optics (Pergamon Press New York, third edition, 1965).

9. D. Pohl, Physics Lett. 26A, 357 (1968).

10. G. L. McAllister, M. M. Mann and L. G. DeShazer, J.Q.E. 6, 44, (1970).

11. The author wishes to thank J. F. Reintjes for assistance in this project.

12. N. Bloembergen, Am. J. of Phys. 35, 989 (1967).

13. Many authors have studied stimulated Rayleigh wing scattering. The references which were most useful for this investigation were: N. D. Foltz, C. W. Cho, D. H. Rank and T. A. Wiggins, Phys. Rev. 165, 396 (1968). M. Denariez and G. Bret, Phys. Rev. 171, 160 (1968). Other references are given in these papers.

14. R. Y. Chaio and J. Godine, Phys. Rev. 185, 430 (1969).

15. R. Y. Chaio, P. L. Kelly and E. Garmire, I.R.L. 17, 281, (1966).

CHAPTER IV

NUMERICAL CALCULATIONS. EXPERIMENTAL RESULTS AND DISCUSSION

A. Introduction

In this chapter, the gas transport coefficients are discussed. The primary interest in studying the transport coefficients is to provide a means by which accurate calculations of them may be made for the gas mixtures under investigation. It is necessary to understand these calculations in order to know their limitations in describing the physical system. The various transport phenomena and the relations between the coefficients can be obtained from the simple kinetic theory. However to obtain accurate values one must resort to the rigorous kinetic theory of gases in which the solution of the Boltzmann equation is given by the Chapman-Enskog perturbation procedure.

Since the gas mixtures under investigation are at moderate pressures ($\sim$ 5-100 atm), corrections to the ideal gas equation of state must be included in the calculations.

The experimental results are presented and compared with the predictions of the theory which was developed in Chapter II.

B. Calculation of Gas Transport Coefficients

1. Simple Kinetic Theory

The phenomena of diffusion, viscosity and thermal conductivity are all physically similar in that they involve the transport of some physical property through the fluid. Diffusion is the transfer of mass due to a concentration gradient, viscosity is the transfer of momentum

due to a velocity gradient, and thermal conductivity is the transport of thermal energy resulting from a temperature gradient. The basic relations between these coefficients and their dependence on temperature, pressure, mass and size of the gas molecules can be easily determined from a simplified kinetic theory. In this simple kinetic theory, all the gas molecules are assumed to be rigid, non-attracting spheres, all traveling at the same speed V with an equal number traveling parallel to each coordinate axis. In this simple approach, the transport coefficients can be expressed in terms of the mean free path $\bar{l} = \frac{V}{R}$ where R is the collision rate. Following this approach, we find the results for the diffusion coefficient, viscosity and thermal conductivity respectively,

$$D = \frac{1}{3} V \bar{l} = \frac{\lambda m}{\rho c_v} = A \frac{\sqrt{T^3/m}}{P\sigma^2}$$

$$\eta = \frac{1}{3} N m V \bar{l} = \rho D = B \frac{\sqrt{T\,m}}{\sigma^2} \qquad (4.1)$$

$$\lambda = \frac{1}{3} N c_v V \bar{l} = \frac{c_v \eta}{m} = C \frac{\sqrt{T/m}}{\sigma^2}$$

where $\rho = Nm = \frac{P_m}{k_T}$ is the density and σ is the molecular diameter. The constants A, B, C depend upon units and are of no interest here.

2. Rigorous Kinetic Theory

a. Chapman-Enskog Solution of Boltzmann Equation

The rigorous development of the kinetic theory of gases is based on knowledge of the molecular distribution function $f(\vec{r}, \vec{v}, t)$ which represents the number of molecules at time t in a volume of phase space at $(\vec{r}, \vec{v})$. When the system is in equilibrium, f reduces to the Maxwellian distribution. When the system is not at equilibrium, the distribution function satisfies the Boltzmann equation. Under the conditions that the deviation from equilibrium is small, f is nearly Maxwellian and the Boltzmann equation can be solved by a perturbation method developed by Chapman and Enskog. The resulting solutions are then used to obtain expressions for the transport coefficients. With this approach, all of the transport coefficients are expressed in terms of a set of integrals $\Omega_{ij}^{(\ell, s)}$, which explicitly involve the dynamics of the molecular encounter and thus the intermolecular force law. For collisions between molecules of type i and j, these integrals are defined by[1]

$$\Omega_{ij}^{(\ell, s)} = \sqrt{\frac{2\pi k_B T}{\mu_{ij}}} \int_0^\infty \int_0^\infty e^{-\gamma_{ij}^2} \gamma_{ij}^{2s+3} (1 - \cos \ell \theta)\, b\,db\,d\gamma_{ij}$$

In these integrals, μ_{ij} is the reduced mass of the colliding molecules i and j, θ is the angle by which the molecules are deflected in the center of gravity coordinate system, b is the impact parameter, and γ_{ij} is the reduced initial relative speed of the colliding molecules given by

$$\gamma_{ij} = \sqrt{\frac{\mu_{ij}}{2k_B T}}\, g_{ij}$$

where g_{ij} is the initial relative velocity of the two molecules. The most satisfactory calculations of $\Omega_{ij}^{(\ell, s)}$ are those made on the basis of the Lennard-Jones (6-12) potential which describes reasonably well the interaction between spherical, non-polar molecules.

The Chapman-Enskog theory considers only binary collisions so the results are not applicable at densities sufficiently high that three body collisions become important. The theory also assumes that the molecular mean free path is small compared to the dimensions of the container, so that surface effects are not important. The Chapman-Enskog theory is therefore most useful for describing the properties of a dense gas.

Strictly speaking, the Chapman-Enskog theory applies only to monatomic gases. Since inelastic collisions occur between molecules with internal degrees of freedom, the kinetic energy is not conserved upon collision, although clearly mass and momentum are conserved. Consequently, the viscosity and diffusion are not appreciably affected by the presence of internal degrees of freedom, and the theory of monatomic gases may be applied to polyatomic molecules with success, provided the molecules are approximately spherical. However, the thermal conductivity is significantly affected by internal degrees of freedom. For a monatomic gas, the thermal conductivity is related to the viscosity by

$$\lambda = \frac{15}{4} \frac{R}{M} \eta$$

where M is the molecular weight of the gas and R is the gas constant. This relation has been confirmed experimentally.

The specific heat and bulk viscosity of the gas are also affected by the transfer of energy to internal degrees of freedom of the molecules. The magnitude of contribution of the internal degrees of freedom depends of course on the frequency at which the measurement is made. This point is discussed in greater detail in connection with the calculation of the specific heat. The contribution of the internal degrees of freedom to the thermal conductivity can then be given by a correction term which depends upon the specific heat.

$$\lambda = \frac{15}{4} \frac{R}{M} \eta \left[\frac{4}{15} \frac{\tilde{c}_v}{R} + \frac{3}{5}\right] \qquad (4.2)$$

This formula was first proposed by Eucken and gives good agreement with experimental results. For a monatomic gas $\tilde{c}_v = \frac{3}{2} R$ and the Eucken formula reduces to the thermal conductivity for monatomic gas.

b. Transport Coefficients in Chapman-Cowling Integral Form

In this section, the transport coefficients are presented in terms of the Chapman-Cowling integrals $\Omega_{ij}^{(\ell, s)}$. These results may be derived following the work of Chapman and Cowling[2], and also Hirschfelder, Curtiss and Bird[1]. This calculation is quite involved and will not be discussed here. We present only the results which are

necessary for the calculation of numerical values for the transport coefficients of the gas mixtures under consideration. All of the results presented here are those which arise from the first order approximation of the Chapman-Enskog solution of the Boltzmann Equation. The values of the Chapman Cowling integrals (CCI) which are used are those calculated for the Lennard-Jones (6-12) potential. The parameters which describe this potential are indicated in Fig. 4.1. The values of the potential parameter ϵ and collision diameter σ are given in Table 4-1. For a gas mixture, the collision diameter is given by

$$\sigma_{12} = \frac{1}{2}(\sigma_1 + \sigma_2)$$

and the potential parameter is

$$\epsilon_{12} = \sqrt{\epsilon_1 \epsilon_2}$$

The CCI are calculated as functions of the reduced temperature $T^* = \frac{Tk_B}{\epsilon}$, where k_B is the Boltzmann constant. The transport coefficients are given in terms reduced integrals $\Omega^* = \frac{\Omega}{\Omega}_{\text{rigid sphere}}$. The values of T^* and the CCI of interest $\left(\Omega_{(11)}^{(2,2)*}(T_1^*),\ \Omega_{(22)}^{(2,2)*}(T_2^*),\ \Omega_{12}^{(2,2)*}(T_{12}^*),\ \Omega_{12}^{(1,1)*}(T_{12}^*) \right)$ are also given in Table 3-1. Certain ratios of the CCI appear frequently. They are

$$A^* = \Omega^{(2,2)*}/\Omega^{(1,1)*}$$

$$B^* = [5\Omega^{(1,2)*} - 4\Omega^{(1,3)*}]/\Omega^{(1,1)*}$$

$$C^* = \Omega^{(1,2)*}/\Omega^{(1,1)*}$$

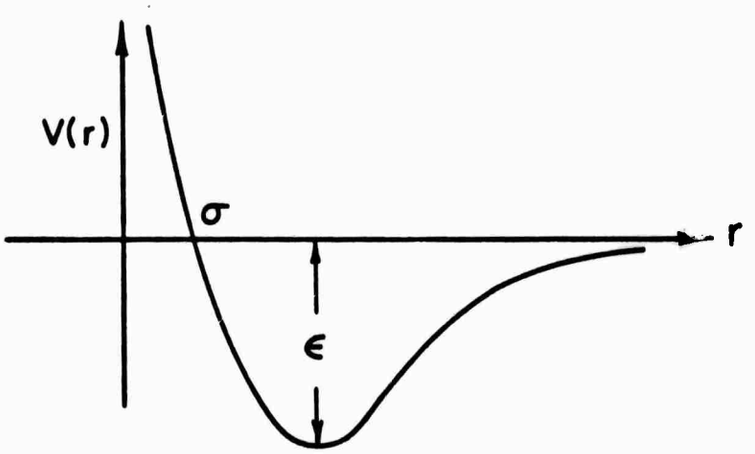

LENNARD – JONES (6-12) POTENTIAL

Fig. 4.1 Lennard-Jones (6-12) Potential Versus Distance Between Molecules

	σ^{+} (ANGSTROMS)	$\epsilon/k_B{}^{+}$ (^{o}k)	M (gm)	T^{*}	$\Omega^{22*}(T^{*})^{+}$	$\alpha \times 10^{24}$ (cm^3)	$\eta \times 10^{4}$ (gm/cm sec)	$\lambda \times 10^{-3}$ (erg/gm sec k)
Helium	2.576	10.22	4.003	28.767	0.706	0.2051	1.955	15.24
SF_6	5.51	200.9	146.07	1.463	1.328	4.537	1.549*	0.4102
Xenon	4.055	229.	131.1	1.284	1.407	4.146	2.267	0.5382

	$\sigma_{12}{}^{+}$ (ANGSTROMS)	$\epsilon_{12}/k_B{}^{+}$ (^{o}k)	M_{12} (GM.)	T^{*}_{12}	$\Omega^{22*}_{12}(T^{*})^{+}$	$\Omega^{11*}_{12}(T^{*})^{+}$	$\eta_{12} \times 10^{4}$ (gm/cm sec)	$\lambda_{12} \times 10^{-3}$
SF_6-He	4.043	45.31	3.896	6.488	0.885	0.8013	0.8832	3.536
Xe-He	3.3155	48.38	3.884	6.077	0.894	0.8106	1.297	5.207

*Experimental value
+These values from Hirschfelder, Curtis and Bird[2]

Table 4-1 Transport Coefficients and Other Characteristic Parameters for the Pure Gases He, SF_6, Xe

	$\ell \times 10^4$ (cm)	y
Helium	$\frac{0.1770}{P}$	0.3520 P
SF_6	$\frac{0.0209}{P}$	2.978 P
Xenon	$\frac{0.0346}{P}$	1.800 P

	D (cm^2/sec)	A_{12}^{*+}	B_{12}^{*+}	C^{*+}
SF_6-He	$\frac{0.3623}{P}$	1.104	1.091	0.9387
Xe-He	$\frac{0.5316}{P}$	1.103	1.096	0.9377

P - Pressure in Atmospheres

These values are also given in Table 4-1. For calculations pertaining to the mixtures, it is convenient to introduce a parameter M_{12} given by

$$M_{12} = \frac{2M_1M_2}{M_1+M_2}$$

where M_1, M_2 are the molecular weights of the component species.

(1) Viscosity

To a first approximation, the viscosity of a pure gas is given by

$$\eta_i = 2.6693 \times 10^{-5} \frac{\sqrt{M_i T}}{\sigma_i^2 \Omega_i^{(2,2)*}} \quad \frac{gm}{cm, sec} \qquad (4.3)$$

This result may be used to obtain the viscosities of both pure gases η_1, η_2. To obtain viscosity of the mixture, it is convenient to introduce a viscosity η_{12} which is given by Equation (4.3) with i replaced by 12. The viscosity of a binary mixture is then given by

$$\frac{1}{\eta_{mix}} = X_\eta \left[\frac{1+Y_\eta/X_\eta}{1+Z_\eta}\right] \qquad (4.4)$$

where

$$X_\eta = \frac{(1-c')^2}{\eta_1} + \frac{2c'(1-c')}{\eta_{12}} + \frac{c'^2}{\eta_2}$$

$$Y_\eta = \frac{3}{5} A_{12}^* \left\{ \frac{(1-c')^2}{\eta_1} \left(\frac{M_1}{M_2}\right) + \frac{2(1-c')c'}{\eta_{12}} \left(\frac{(M_1+M_2)^2}{4M_1M_2}\right) \left(\frac{\eta_{12}^2}{\eta_1\eta_2}\right) + \frac{c_1'^2}{\eta_2} \left(\frac{M_2}{M_1}\right) \right\}$$

$$Z_\eta = \frac{3}{5} A_{12}^* \left\{ (1-c')^2 \left(\frac{M_1}{M_2}\right) + 2c'(1-c') \left[\frac{(M_1+M_2)^2}{4M_1M_2} \left(\frac{\eta_{12}}{\eta_1} + \frac{\eta_{12}}{\eta_2}\right) - 1 \right] + c'^2 \left(\frac{M_2}{M_1}\right) \right\}$$

(2) Thermal Conductivity

For a pure gas the thermal conductivity is given by

$$\lambda_i = 8292.5 \frac{\sqrt{T/M_i}}{\sigma_i^2 \Omega_i^{(2,2)*}} \quad \frac{\text{erg}}{\text{cm sec } ^\circ\text{k}} \tag{4.5}$$

For the polyatomic SF_6 molecules, $\tilde{c}_v = 3R$ so this result must be multiplied by $\frac{7}{5}$ (Eucken correction). The parameter λ_{12} is again given by the expression for λ_i with $i = 12$. The thermal conductivity for a gas mixture is given by

$$\frac{1}{\lambda_{mix}} = X_\lambda \left[\frac{1+Y_\lambda/X_\lambda}{1+Z_\lambda}\right] \tag{4.6}$$

where

$$X_\lambda = \frac{(1-c')^2}{\lambda_1} + \frac{2c'(1-c')}{\lambda_{12}} + \frac{c'^2}{\lambda_2}$$

$$Y_\lambda = \frac{(1-c')^2}{\lambda_1} U^{(1)} + \frac{2c'(1-c')}{\lambda_{12}} U^{(Y)} + \frac{c'^2}{\lambda_2} U^{(2)}$$

$$Z_\lambda = (1-c')^2 U^{(1)} + 2c'(1-c') U^{(Z)} + c'^2 U^{(2)}$$

$$U^{(1)} = \frac{4}{15} A_{12}^{*} - \frac{1}{2} \left(\frac{12}{5} B_{12}^{*} + 1\right) \frac{M_1}{M_2} + \frac{1}{2} \frac{(M_1 - M_2)^2}{M_1 M_2}$$

$$U^{(2)} = \frac{4}{15} A_{12}^{*} - \frac{1}{12} \left(\frac{12}{5} B_{12}^{*} + 1\right) \frac{M_2}{M_1} + \frac{1}{2} \frac{(M_2 - M_1)^2}{M_1 M_2}$$

$$U^{(Y)} = \frac{4}{15} A_{12}^{*} \left(\frac{(M_1 + M_2)^2}{4 M_1 M_2}\right) \frac{\lambda_{12}^2}{\lambda_1 \lambda_2} - \frac{1}{12} \left(\frac{12}{5} B_{12}^{*} + 1\right)$$

$$- \frac{5}{32 A_{12}^{*}} \left(\frac{12}{5} B_{12}^{*} - 5\right) \frac{(M_1 - M_2)^2}{M_1 M_2}$$

$$U^{(Z)} = \frac{4}{15} A_{12}^{*} \left[\frac{(M_1 + M_2)^2}{4 M_1 M_2} \left(\frac{\lambda_{12}}{\lambda_1} + \frac{\lambda_{12}}{\lambda_2}\right) - 1\right] - \frac{1}{12} \left(\frac{12}{5} B_{12}^{*} + 1\right)$$

(3) Coefficient of Diffusion

The coefficient of diffusion for a binary mixture is given by

$$D = \frac{2.628 \times 10^{-3} \sqrt{T^3 / M_{12}}}{P \sigma_{12}^2 \Omega_{12}^{(1,1)*}(T_{12}^{*})} \frac{cm^2}{sec} \qquad (4.7)$$

where P is the pressure in atmospheres.

(4) Thermal Diffusion Ratio

The thermal diffusion ratio for a binary gas mixture is given in first approximation to be

$$k_T = \frac{c'(1 - c')}{6 \lambda_{12}} \frac{s^{(1)}(1 - c') - s^{(2)} c'}{X_\lambda + Y_\lambda} (6 c_{12}^{*} - 5) \qquad (4.8)$$

where

$$s^{(1)} = \frac{M_1 + M_2}{2M_2}\,\frac{\lambda_{12}}{\lambda_1} - \frac{15}{4A^*_{12}}\left(\frac{M_2 - M_1}{2M_1}\right) - 1$$

$$s^{(2)} = \frac{M_2 + M_1}{2M_1}\,\frac{\lambda_{12}}{\lambda_2} - \frac{15}{4A^*_{12}}\left(\frac{M_1 - M_2}{2M_2}\right) - 1$$

Choice of the correct sign for k_T requires some attention. When a mixture of gases with large, heavy molecules and small light molecules is placed in a thermal gradient, the lighter molecules diffuse toward the warmer regions[2]. The concentration gradient, which is established by thermal diffusion, is opposed by ordinary mass diffusion which tends to equalize the composition, and, in time, a steady state is reached in which the opposing influences of thermal and ordinary diffusion balance. Then, ignoring pressure gradients, the concentration diffusion equation (2.29) becomes

$$\frac{\partial c}{\partial t} = D\left[\nabla^2 c + \frac{k_T}{T}\nabla^2 T\right] = 0$$

where c is the mass concentration of the light gas (Helium). Integration over an arbitrary volume of the mixture and use of Green's Theorem to convert to a surface integral gives

$$\oint_S \left(\nabla c + \frac{k_T}{T}\nabla T\right) \cdot d\vec{s} = 0 \quad .$$

which implies

$$\nabla c = -\frac{k_T}{T}\nabla T \quad .$$

Thus the thermal diffusion ratio k_T must be negative so that the concentration of the light molecules increases as the temperature increases.

The values of the various transport coefficients for the pure gases are given in Table 4-1, for the He-SF_6 mixtures in Table 4-3 and for the He-Xe mixtures in Table 4-3.

3. Polarizibility and Specific Heat of the Gas Mixture

The value of the molecular polarizibility for Helium was obtained from Dalgano and Kingston[3] and the values for Xenon and SF_6 were obtained from Landolt-Borstein[4]. The values of the polarizibility are given in Table 4-1. The average molecular polarizibility of the mixture is given by

$$\alpha = (1+c')\alpha_1 + c'\alpha_2$$

It is a well known result from kinetic theory that the heat capacity at constant volume c_v for a monatomic ideal gas is $\frac{3}{2}\frac{Nk_B}{\rho}$, which is due to the contribution of $\frac{1}{2}\frac{Nk_B}{\rho}$ from each of the three translational degrees of freedom. For a polyatomic molecule the specific heat depends on the frequency at which the measurement is made. For frequencies less than $\frac{1}{\tau_R}$, where τ_R is the rotational relaxation time (the time which is required for a molecule to change its rotational energy) the three rotational degrees of free will each contribute $\frac{1}{2}\frac{Nk_B}{\rho}$ to the specific heat. Similarly, for frequencies less than $\frac{1}{\tau_v}$, where τ_v is the vibrational relaxation time, the

vibrational modes (fifteen for SF_6) can each take up energy and thus contribute to the specific heat.

The time between collisions τ_c can be calculated from kinetic energy considerations with a knowledge of the gas viscosity η.[5]

$$\tau_c = \frac{\eta \times 10^{-5} \text{ sec}}{12.66\ P(\text{atm})}$$

For SF_6 at 5 atm, $\tau_c \simeq 10^{-11}$ sec. A value for the rotational relaxation time $\tau_R = 2.5\ \tau_c$ estimated from the theory of Sather and Dahler[6] has given good agreement with measurements of sound attenuation in SF_6 by Holmes and Stott[7]. Thus for frequencies less than 5000 MHz the rotational degrees of freedom contribute to the specific heat.

O'Connor[8] and Holmes and Stott[7] have shown however that the vibrational relaxation time $\tau_v \sim 10^3\ \tau_c$ and the experimental results show that for frequencies above 30 MHz the vibrational degrees of freedom do not contribute to the specific heat.

The frequencies of the material excitation in this experiment are ~ 100-500 MHz as will be shown later. In this region the specific heat at constant volume for the SF_6 is $3\frac{Nk_B}{\rho}$ from the 3 translational and 3 rotational degrees of freedom. The specific heats for the $He\text{-}SF_6$ mixture are

$$c_{v\,mix} = (3\,N_{SF_6} + \tfrac{3}{2}\,N_{He})\,\frac{k_B}{\rho}$$

$$c_{P\,mix} = c_{v\,mix} + \frac{Nk_B}{\rho}$$

For the monatomic Xenon gas of course these considerations do not

apply and $c_v = \frac{3}{2} \frac{Nk_B}{\rho}$.

The bulk viscosity ζ of the polyatomic molecule is also related to the transfer of energy to internal degrees of freedom. The bulk viscosity is related to relaxation times by[1]

$$\zeta = \frac{Nk_B^2 T}{c_v^2} \sum_{\ell} c_v^{(\ell)} \tau_{\ell}$$

where $c_v^{(\ell)}$ is the contribution of the particular degree of freedom to the specific heat per molecule c_v. For SF_6 at 5 atm pressure $\zeta = .34\,\eta$. For Xenon, the bulk viscosity is zero since there are no internal degrees of freedom.

One might reasonably be concerned that the addition of Helium to the SF_6 would substantially decrease the relaxation times and allow vibrational contributions to enter the specific heats, thermal conductivity and bulk viscosity. However the recent investigation of spontaneous scattering from the He-SF_6 mixtures made by Gornall[9] et. al. indicate that the vibrational degrees of freedom are not in fact excited.

4. Derivatives of Thermodynamic Parameters

The expressions which were used to calculate the derivatives of the thermodynamic parameters which appear in the various gain expressions are presented in this section. These results were calculated using the ideal gas law $P = Nk_B T$. Extensions of these forms to include corrections due to the non-ideality of the gas are given in Section (C2). We need to know the variation of mass density with temperature and pressure, the variation of the chemical potential

with concentration and the variation of the dielectric constants with T, P, and c. These results are given as follows

$$\left(\frac{\partial \rho}{\partial P}\right)_{T,c} = \frac{\rho}{Nk_B T} = \frac{1}{v_T^2} = \gamma \left(\frac{\partial \rho}{\partial P}\right)_{s,c} = \frac{\gamma}{v_s^2}$$

$$\left(\frac{\partial \rho}{\partial T}\right)_{P,c} = -a_T \rho = -\frac{\rho}{T}$$

$$\left(\frac{\partial \rho}{\partial c}\right)_{P,T} = \frac{\rho^2 (m_2 - m_1)}{N m_1 m_2}$$

$$\left(\frac{\partial \mu}{\partial c}\right)_{P,T} = \frac{k_B T \rho}{c(1-c) N m_1 m_2}$$

where v_T, v_s are the isothermal and adiabatic sound velocities respectively and

$$\gamma = \frac{c_P}{c_v}$$

$$\left(\frac{\partial \epsilon}{\partial P}\right)_{T,c} = \frac{4\pi (N_1 a_1 + N_2 a_2)}{Nk_B T}$$

$$\left(\frac{\partial \epsilon}{\partial c}\right)_{P,T} = \frac{4\pi \rho^2 (a_2 - a_1)}{N m_1 m_2}$$

$$\left(\frac{\partial \epsilon}{\partial T}\right)_{P,c} = -\frac{4\pi (N_1 a_1 + N_2 a_2)}{T}$$

C. The Equation of State

1. Virial Expansion

The well known equation of state for the ideal gas

$$P = Nk_BT \quad ,$$

needs some correction even at atmospheric pressure. The virial equation of state describes these corrections as a power series expansion in the number density

$$\frac{P}{Nk_BT} = 1 + B(T)\left(\frac{N}{N_a}\right) + c(T)\left(\frac{N}{N_a}\right)^2 + \ldots \qquad (4.9)$$

where N_a is Avagadro's number and B(T), c(T) are the second and third virial coefficients.

From the statistical mechanical expressions for the virial coefficients, it becomes evident that the second and third coefficients represent deviations from ideal behavior when collisions between two and three molecules become important. As the pressure increases, more virial coefficients must be included. As an indication of the contribution of the second and third virial coefficients for the gases of interest, the following results are found at 0°c

$$SF_6 \text{ at } 10 \text{ atm}, \quad \frac{P}{Nk_BT} = 1 - 0.12 + .005$$

$$Xe \text{ at } 10 \text{ atm}, \quad \frac{P}{Nk_BT} = 1 - 0.06 + .0008$$

$$He \text{ at } 100 \text{ atm}, \quad \frac{P}{Nk_BT} = 1 + .05 + .002$$

The third virial coefficients are not significant in this work and this is consistent with the calculations of the transport coefficients which considered only binary collisions. It is perhaps interesting to note that the sign of the second virial coefficient correction is different for the heavy gases and for Helium. This result is due to the fact that the interaction between the heavy molecules is dominated by the strong attractive part of the potential. The attractive potential for the Helium atoms is weak and thus the atomic interactions are dominated by the excluded volume effect due to the short range repulsive part of the potential. In mixtures with a 10:1 ratio of Helium to heavy gas number density, at pressures low enough that the third virial coefficients do not contribute significantly, the ideal gas law is not a bad approximation.

For the gas mixture, the second virial coefficient is given by[1]

$$B(T)_{mixture} = (1-c')^2 B_1(T) + c'^2 B_2(T) + 2c'(1-c') B_{12}(T) \tag{4.10}$$

where B_1, B_2 are the virial coefficients calculated from the potential functions for molecules of type 1 and 2 and B_{12} is calculated from the potential function which characterizes the interaction between the two molecules.

The virial coefficients are calculated from the intermolecular potential $\phi(r)$ where r is the molecular separation. The second virial coefficient is given by

$$B(T) = -2\pi N_a \int_0^\infty [e^{-\phi(r)/kT} - 1] r^2 dr$$

Numerical values for the reduced second virial coefficients B^* given by

$$B^* = \frac{B}{b_0}$$

$$B_k^* = T^{*k} \left(\frac{d^k B^*}{dT^{*k}}\right)$$

$$b_0 = \frac{2}{3}\pi \, Na \, \sigma^3 \quad \text{(second virial coefficient for hard sphere molecules)}$$

for the Lennard-Jones (6-12) potential.

$$\phi(r) = 4\epsilon\left[\left(\frac{\sigma}{r}\right)^{12} - \left(\frac{\sigma}{r}\right)^{6}\right]$$

have been given by Hirschfelder Curtiss and Bird[1]. The relevant values for the gain calculations are given in Table 4-2.

2. Non-Ideal Gas Corrections

The non-ideal gas corrections are included in the calculations by observing that there are a set of gas parameters which are more or less fundamental. These parameters are fundamental in the sense that all of the other gas parameters, thermodynamic derivatives and transport coefficients depend upon the values of these fundamental parameters. Thus if these fundamental parameters are corrected for the non-ideal behavior of the gas mixtures, the corrections to all the remaining parameters and transport coefficients will be made automatically.

These fundamental parameters are the pressure (or number density), isothermal coefficient of expansion α_T, specific heats at

	T^*	b_o	$B^*(T^*)^+$	$B_1^*(T^*)^+$	$B_2^*(T^*)^+$
Helium	28.767	21.56	.52673	-.01180	- .08414
SF_6	1.4634	211.0	-1.2622	2.5009	-6.0434
Xenon	1.2838	81.04	-1.6229	3.0213	-7.4610
SF_6-He	6.4883	83.36	.34887	.35756	- .84055
Xe-He	6.0772	45.97	.3270	.3781	- .9069

+These values from Hirschfelder, Curtiss and Bird[2]

Table 4-2 Second Virial Coefficient and its Derivatives for the Pure Gases and Mixtures

constant volume and a constant pressure and the isothermal sound velocity. The non-ideal gas corrections for these parameters can be derived from the virial expansion Equation (4.9) using the thermodynamic expressions for the various parameters. The derivation is straightforward and will be omitted and the results for the gas mixture given as follows

$$P_1 = N_1 k_B T \left[1 + \frac{B_1}{\tilde{v}}\right]; \quad N_1 = \frac{P_1}{k_B T}\left[1 - \frac{B_1}{\tilde{v}}\right]$$

$$P = N k_B T \left[1 + \frac{B_{mix}}{\tilde{v}}\right]; \quad N = \frac{P}{k_B T}\left[1 - \frac{B_{mix}}{\tilde{v}}\right]$$

$$\alpha_T = \frac{1}{\tilde{v}}\left(\frac{\partial \tilde{v}}{\partial T}\right)_P = \frac{1}{T}\left[1 + \frac{B_{1mix}/\tilde{v}}{1 + B_{mix}/\tilde{v}}\right]$$

$$c_v = c_v^o - \left(\frac{2B_{mix}}{\tilde{v}} + \frac{B_{2mix}}{\tilde{v}}\right)\frac{Nk}{\rho}$$

$$c_P = c_P^o - \frac{B_{2mix}}{\tilde{v}}\,\frac{Nk}{\rho}$$

$$v_T^2 = \frac{Nk_B T}{\rho}\left[1 + \frac{2B_{mix}}{\tilde{v}}\right]$$

where $\tilde{v} = \frac{Na}{N}$, P_1 is the partial pressure of the heavy gas and c_v^o, c_P^o are the ideal gas values of specific heat. Since the value of N appears in $\tilde{v}$, the expressions for the number density must be evaluated in an iterative fashion.

D. Numerical Calculations and Experimental Results

1. Introduction

The values of the gas transport coefficients and other relevant parameters for the gas mixtures have been calculated by use of a computer from the expressions presented in the preceding sections. The calculations were made for the mixtures which were investigated experimentally. For the He-SF_6 mixtures, the partial pressure of SF_6 was 5 atm and the Helium concentration was increased by adding Helium. For the He-Xe mixture, the Xe partial pressure was 8 atm. The values for the He-SF_6 and He-Xe mixtures are presented in Tables (4-3) and (4-4) respectively.

These values of the transport coefficients and gas parameters were then used to calculate the values of g_B, g_c, g_T given by Equations (2.62), (2.65) and (2.69) respectively. The value of $g_{BcT}(\omega)$ was calculated for frequency shifts from 0 to 1200 MHz in increments of 5 MHz.

The values of the gas parameters and transport coefficients which are calculated in this fashion are identical to the values used by Gornall et. al. Since these values gave an excellent theoretical fit to the experimental spontaneous light scattering spectra for the same gas mixtures as investigated in this experiment, we may assume that the values are quite accurate, particularly for the mixtures with low He concentration. For the mixtures with Helium concentrations above 50%, the accuracy of the calculated values may be somewhat diminished due to the fact that the non-ideal gas corrections and the

He c'	He P (PSIA)	$\rho \times 10^2$ (gm/cm^3)	$\eta \times 10^4$ (gm/cm sec)	$\lambda \times 10^{-2}$ (erg/gm sec°k)	$D \times 10^2$ (cm^2/sec)	$c_p \times 10^{-6}$ (erg/gm°k)	γ	$v_T \times 10^{-4}$ cm/sec	Γ MHz
0	0	3.27	1.55	4.10	6.71	2.44	1.41	1.21	26.1
0.1	9.	3.28	1.58	6.70	5.99	2.59	1.42	1.29	47.0
0.2	20.	3.29	1.61	9.84	5.29	2.78	1.44	1.38	68.6
0.3	34.	3.31	1.65	13.7	4.59	3.02	1.45	1.48	91.2
0.4	53.	3.33	1.69	18.6	3.91	3.34	1.47	1.60	114.
0.5	80.	3.36	1.74	24.8	3.23	3.78	1.50	1.76	138.
0.6	121.	3.40	1.80	33.3	2.57	4.42	1.52	1.98	162.
0.7	189.	3.48	1.88	45.2	1.91	5.45	1.55	2.28	183.
0.8	325.	3.63	1.96	63.1	1.26	7.40	1.59	2.76	199.
0.9	741.	4.08	2.04	93.2	0.622	12.4	1.63	3.76	186.

Table 4-3 Transport Coefficients for the He-SF_6(5 atm) Mixture

He c'	He P (PSIA)	$\rho \times 10^2$ gm/cm^3	$\eta \times 10^4$ gm/cm sec	$\lambda \times 10^{-2}$ erg/gm sec°k	$D \times 10^2$ cm^2/sec	$c_P \times 10^{-6}$ erg/gm°k	γ	$v_T \times 10^{-4}$ cm/sec	Γ MHz
0	0	4.65	2.27	5.38	6.53	1.72	1.76	1.30	30.4
0.1	14.	4.66	2.31	9.02	5.84	1.89	1.76	1.38	57.6
0.2	32.	4.68	2.35	13.4	5.61	2.10	1.75	1.47	84.5
0.3	54.	4.71	2.40	18.6	4.48	2.38	1.74	1.57	111.
0.4	85.	4.74	2.45	25.1	3.82	2.73	1.73	1.70	136.
0.5	127.	4.79	2.50	33.3	3.16	3.22	1.72	1.87	159.
0.6	191.	4.86	2.55	44.0	2.51	3.94	1.71	2.09	180.
0.7	299.	4.98	2.59	58.2	1.87	5.10	1.71	2.41	196.
0.8	516.	5.21	2.60	78.0	1.23	7.25	1.70	2.91	202.
0.9	1183.	5.92	2.49	107.	.600	12.7	1.69	3.96	175.

Table 4-4 Transport Coefficients for He-Xe (8 atm) Mixture

effects of He-heavy gas interactions are becoming more important. Both of these effects are included in the calculations in an empirical fashion as discussed in the preceding sections.

2. <u>He-SF_6 Mixture</u>

Before beginning work on the He-SF_6 mixtures, measurements were made of the Brillouin threshold for pure SF_6 as a function of gas pressure. The reasons for doing this were to determine the minimum pressure of SF_6 in which stimulated Brillouin scattering could be observed and, as a by-product, to test that the Brillouin threshold was inversely proportional to the square of the gas density as predicted by Equation (2.62). It was important to know the minimum SF_6 pressure at which the available laser power could produce stimulated scattering because, as we have seen, the possibility of observing concentration scattering is greatest at low pressure. The results of this measurement are shown in Fig. (4.2). The minimum SF_6 pressure in which stimulated Brillouin scattering (SBS) was observed was 4 atm. In the range of pressure from 4 atm. to 14 atm. the experimental value of the SBS threshold power agrees very well with the theoretical prediction.

It was decided on the basis of these results and from gain calculations, that a partial pressure of 5 atm of SF_6 would be appropriate for the investigation of stimulated scattering from He-SF_6 mixtures. The He concentration of the mixture was increased by adding He. Thus, as the He concentration increased, the total

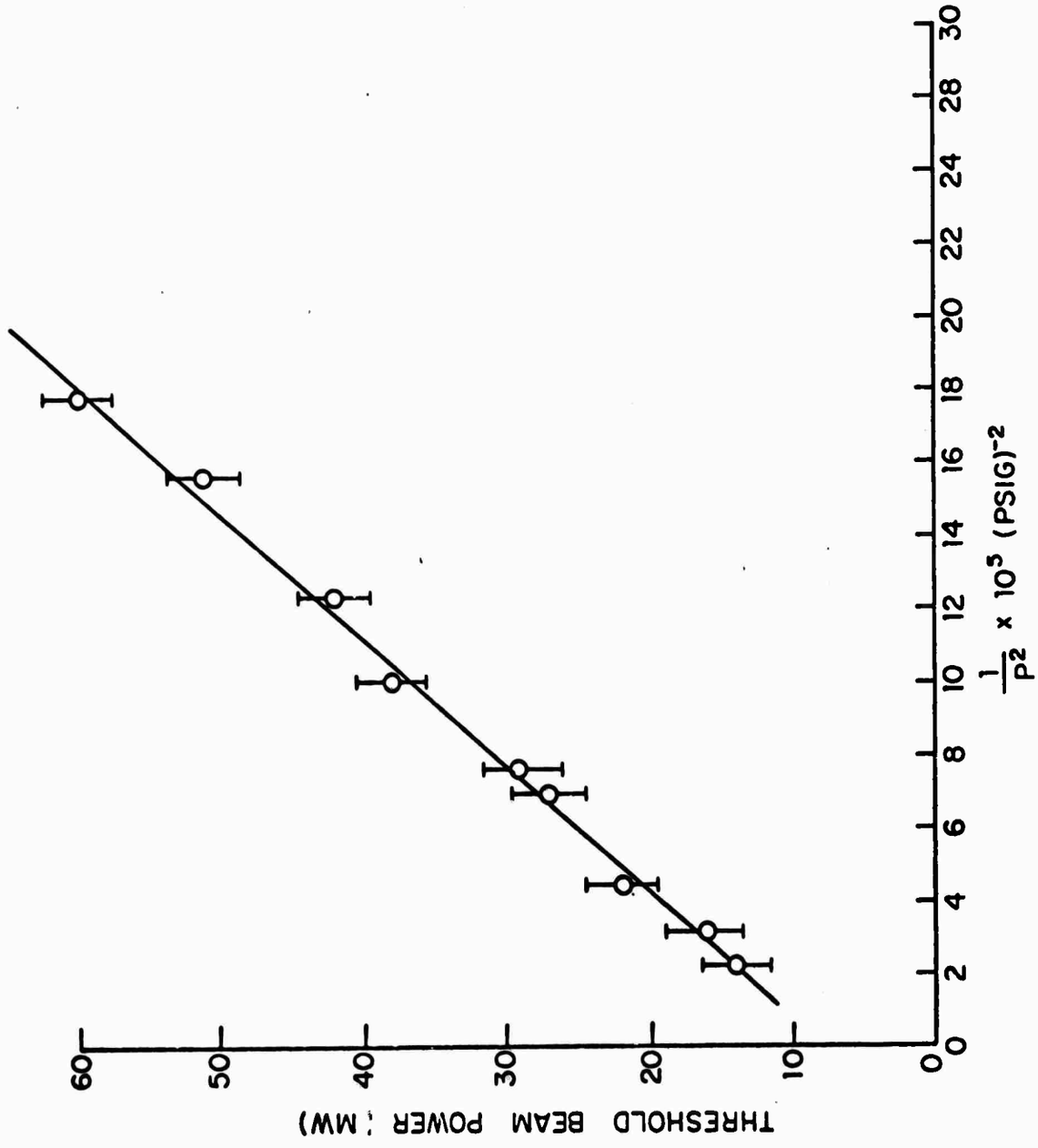

Fig. 4.2 Threshcld Intensity for Stimulated Brillouin Scattering in SF_6 Gas as a Function oi Pressure

pressure also increased. The gain coefficients in the decoupled mode approximation g_B, g_c, g_T were calculated as functions of He concentration. The results of this calculation are shown in Fig. (4.3). The main features shown in this figure are the following: the Brillouin gain decreases steadily with increasing He concentration up to about 85% He concentration (total pressure $\simeq$ 33 atm) and rises sharply for higher concentrations (higher total pressure). The reason for this behavior is that, as the He is added, the sound wave damping constant Γ given by Equation (2.78) increases so the Brillouin gain Equation (2.62) decreases. However g_B also has a ρ^2 dependence which at high pressures eventually dominates the increase in Γ and so the value of g_B increases. The thermal Rayleigh gain g_T decreases steadily as c' increases. The concentration gain g_c increases and, for the pressures which were chosen for the experiment, g_c becomes larger than g_B at a concentration of about 90%. Thus, considering the decoupled gain coefficients as a first approximation to the problem, one expects to see a transition from Brillouin scattering to concentration scattering at about 90% concentration.

The gain constant $g_{BcT}(\omega)$ for the complete coupled mode solution given by Equation (2.73) was calculated for frequency shifts from 0 to 1200 Mhz in intervals of 5 MHz. The result of this calculation is presented in Fig. (4.4) which shows $g_{BcT}(\omega)$ as a function of the frequency shift ω. The gain for pure SF_6 (c' = 0) has its maximum at the Brillouin shift

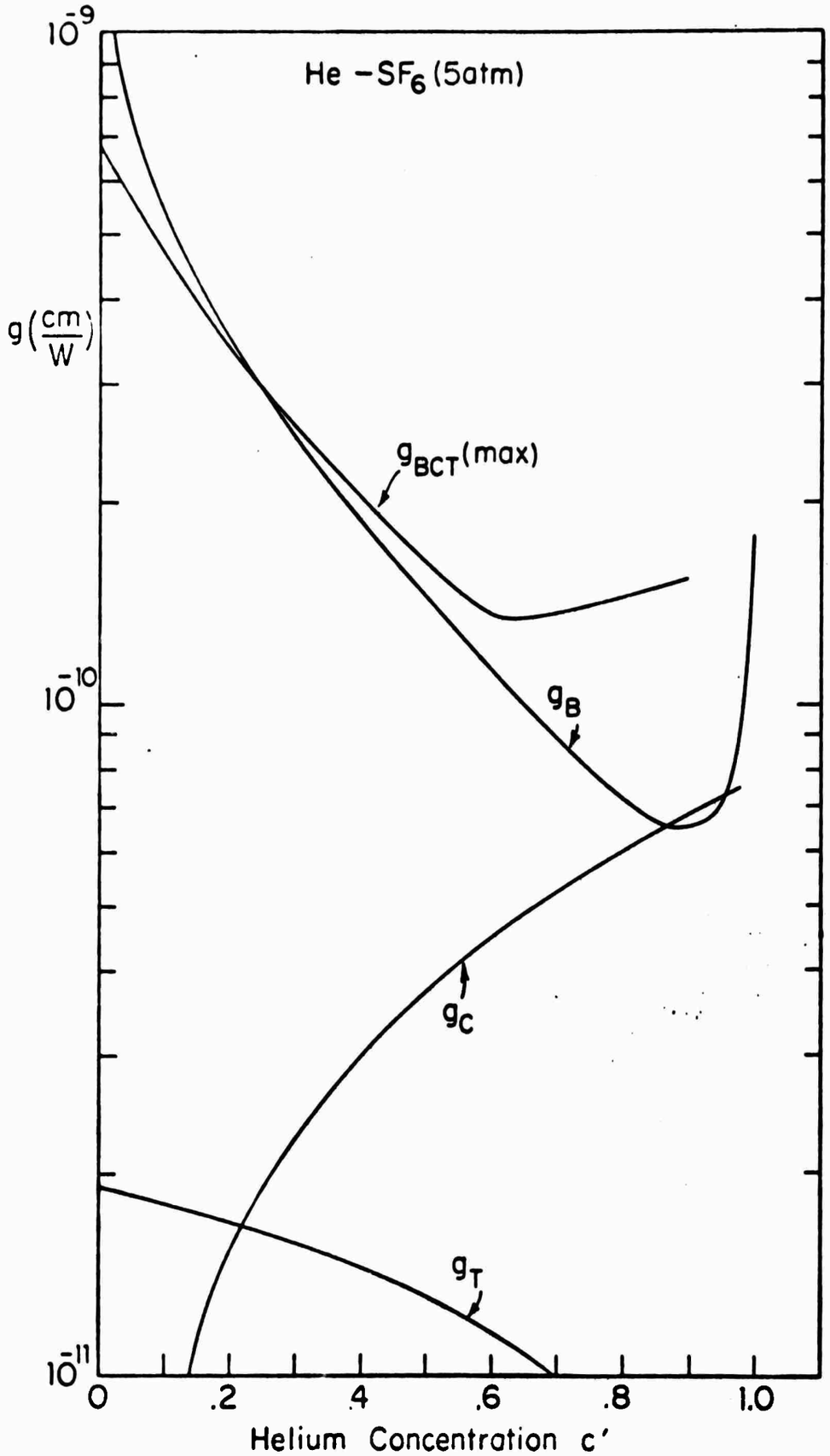

Fig. 4.3 Gain Coefficients Versus Helium Concentration for He-SF_6 (5 atm) Mixture

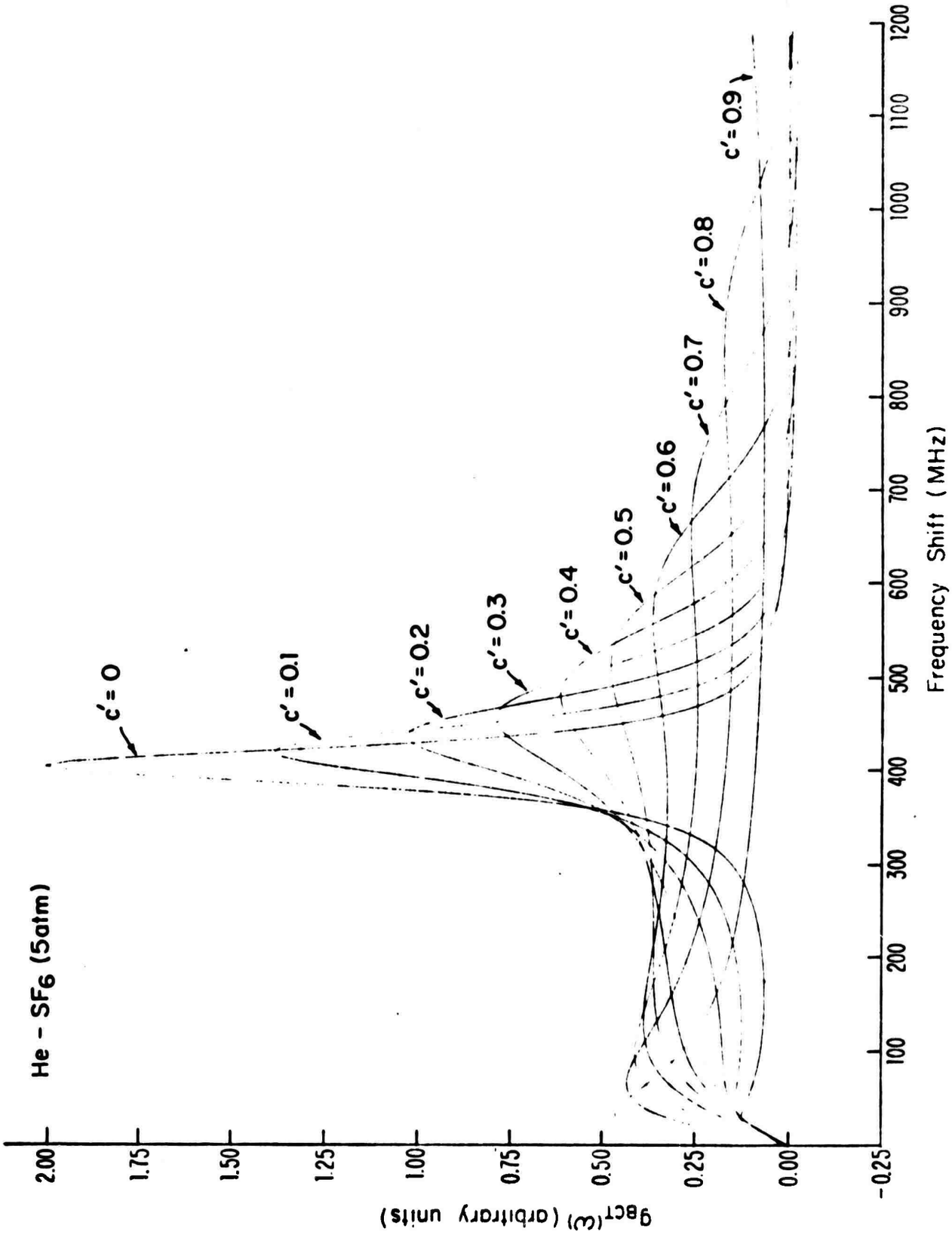

Fig. 4.4 Gain Coefficient g_{BcT} Versus Frequency Shift for He-SF_6 (5atm) Mixture

$$\omega_B = k v_s \simeq 400 \text{ MHz}$$

As the concentration c' increases, the gain at the Brillouin shift decreases and the frequency shift at which the peak of g_{BcT} occurs increases as predicted by the theory. Also as the concentration increases, the height of the local maximum in $g_{BcT}(\omega)$ at the frequency shift characteristic of stimulated scattering from the concentration mode

$$\omega_c \simeq Dk^2 \simeq 100 \text{ MHz}$$

increases. At a concentration of about 60%, the gain at ω_c becomes larger than the gain at ω_B. Thus for concentrations greater than 60% the observed stimulated scattering is from the concentration mode.

The frequency shifts for the various modes as functions of the He concentration are presented graphically in Fig. (4.5). The frequency shift for the decoupled Brillouin mode is kv_s as indicated by Equation (2.61). This result is due to the fact, discussed earlier, that, for the gases under consideration, the low frequency, long wavelength approximation to the sound wave dispersion relation is valid. In this approximation, sound propagates at the adiabatic velocity. The frequency shift which would be predicted if the sound velocity were the isothermal velocity v_T is also shown in Fig. (4.5). The frequency shift predicted from the coupled mode solution is shown in Fig. (4.5). This shift indicates that as the He concentration is increased, the sound velocity tends toward the isothermal value.

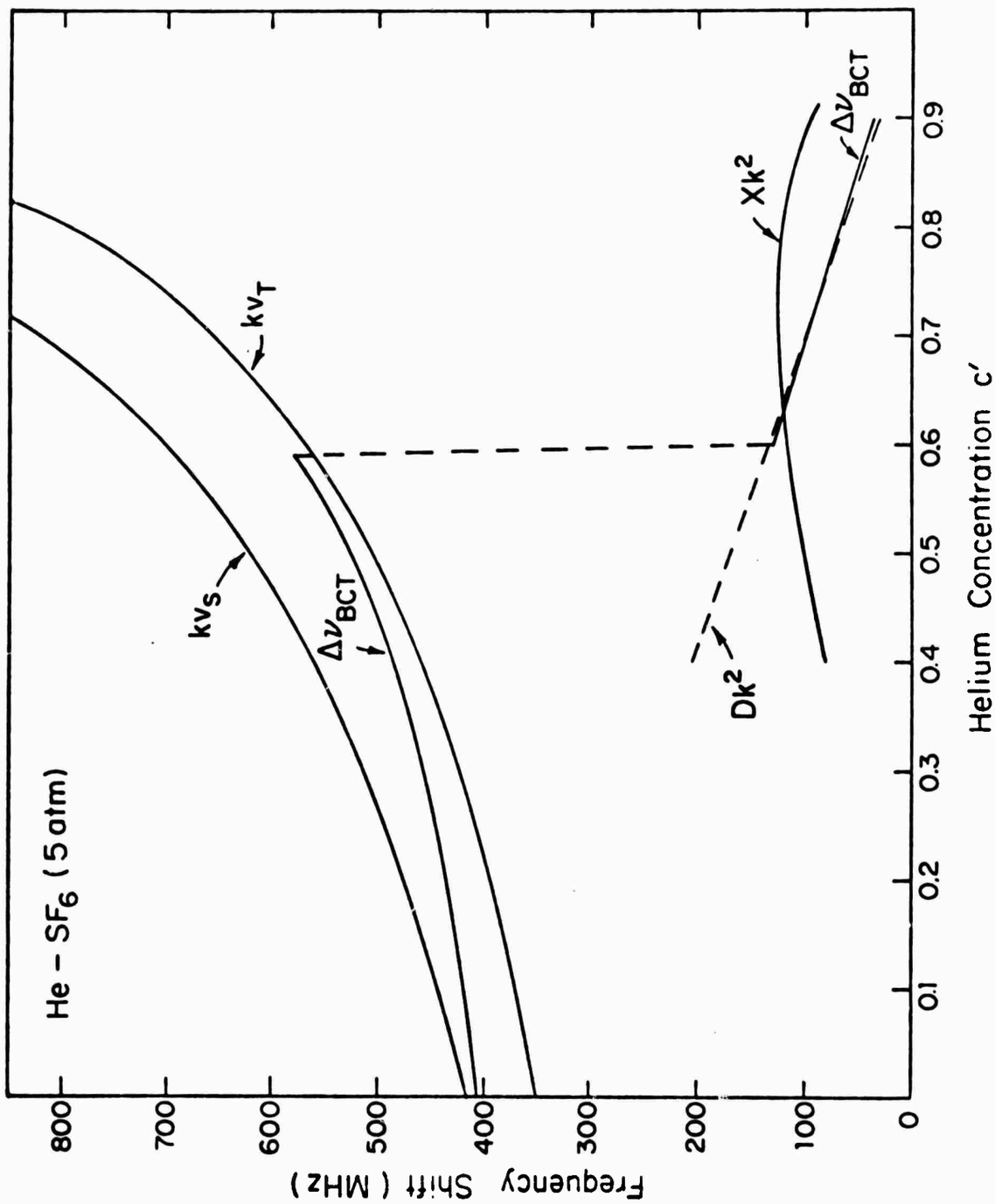

Fig. 4.5 Frequency Shift Versus Helium Concentration for Stimulated Scattering from the Various Modes of the He-SF_6 (5 atm) Mixture

The reason for this behavior is that the light He gas diffuses so fast that it established isothermal conditions during the period of the sound wave which is determined by the heavy component and comparatively low. The frequent collisions of the He atoms transports sufficient energy to establish thermal equilibrium during the period of the fluctuations. The sound wave is heavily damped as discussed earlier, because the heavy and light atoms relax toward thermal equilibrium with different rates. There is therefore more dissipation of energy during a cycle of the pressure oscillations. This has also been observed by Gornall et. al.[9].

The frequency shift associated with the uncoupled thermal diffusion mode ($\omega = \chi k^2$) and with the uncoupled concentration mode ($\omega = Dk^2$) are also shown in Fig. (4.5). The solution of the coupled mode equations predicts an abrupt change at a concentration of 60% in the value of the frequency shift at which the absolute maximum of the gain g_{BcT} occurs. This change from large to small shift indicates the transition from Brillouin to concentration scattering.

The experimental results for the He-SF_6 mixture[10] are presented in Fig. (4.6). The decrease in the gain as the He concentration increased was experimentally observed as an increase in the threshold for stimulated oscillation. For He concentration below 60%, the observed frequency shift is in very good agreement with the theoretical value. The theoretical value shown in this figure is the frequency shift at which g_{BcT} is maximum. For Helium partial pressure above 8 atm the value of the observed frequency shift

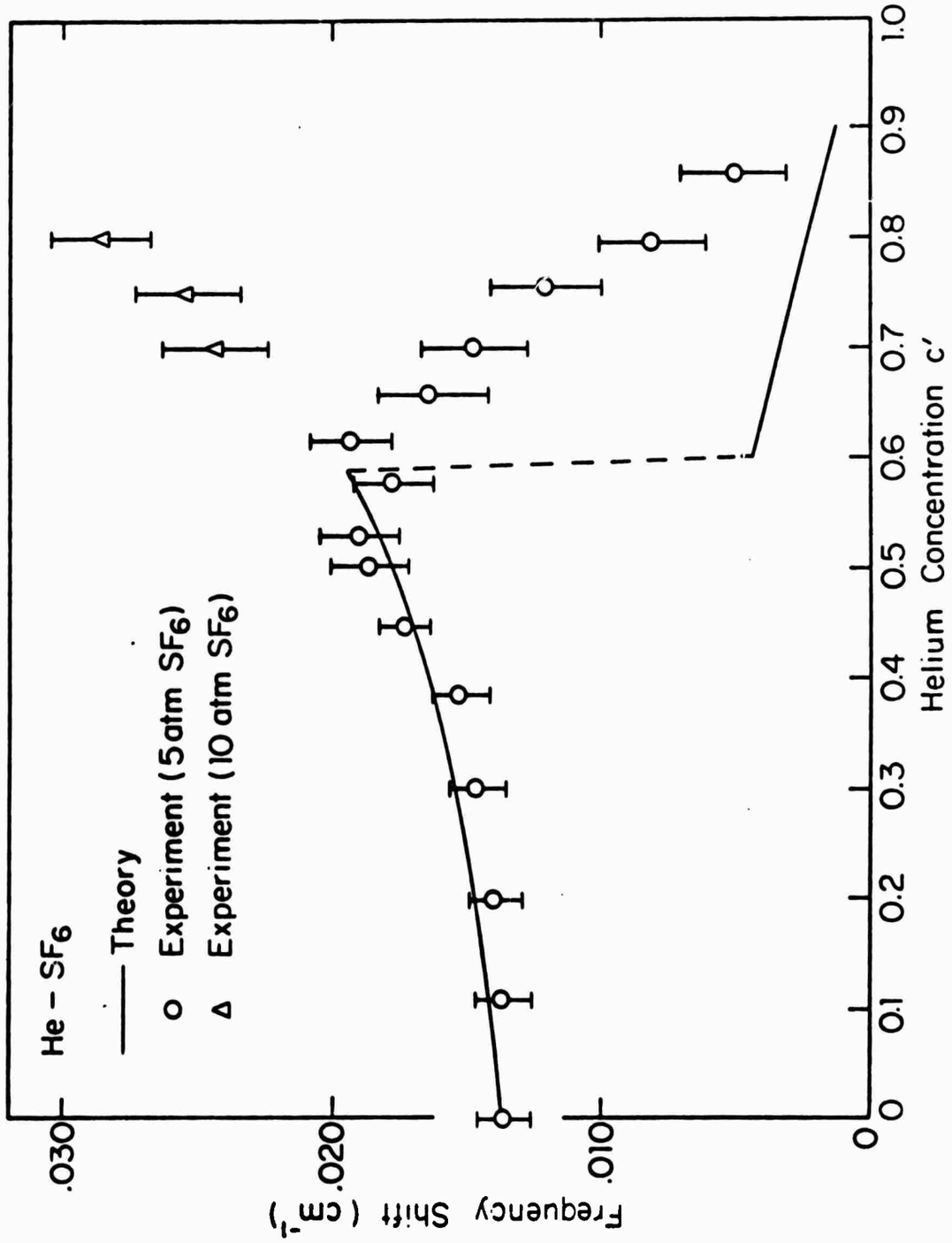

Fig. 4.6 Experimental Results for the He-SF_6 (5 atm) Mixture

decreases rapidly toward the small values which are characteristic of the concentration mode. The observed frequency shift makes a smooth transition from large to small values rather than the abrupt change predicted by the theoretical calculations. The probable explanation for this discrepancy is that the scattering from the concentration diffusion mode becomes transient as the pressure increases. The steady state solution Equation (2.53) are valid only if the laser pulse duration t_p is long compared to the product of the steady state gain and the material relaxation time. The condition then which must be satisfied for the steady state concentration scattering is

$$t_p > \frac{4g|E_L|^2 z}{Dk^2} \simeq \frac{40}{Dk^2}$$

When this condition is not satisfied, the Stokes wave amplification is given by a complete transient solution of the coupled Equations (2.49-2.52) and depends on the laser pulse duration as well as on the distance z. The transient solution of the coupled equations is quite difficult and has not been performed. In general, however, the transient gain is less than the steady state value. Since $D \sim \frac{1}{P}$, $\frac{1}{Dk^2}$ increases as the pressure and He concentration increases. The laser pulse duration indicated by Fig. (3.2b) is $t_p \simeq 5 \times 10^{-8}$ sec., assuming that the pulse envelope is smooth. Then, for pressure about 10 atm, $\frac{1}{Dk^2} \simeq 5 \times 10^{-10}$ sec which clearly allows the validity of the steady state solution. However, for P ~ 50 atm, $\frac{1}{Dk^2} \simeq 2.5 \times 10^{-9}$ sec. Thus we are approaching the region in which the

steady state solution may not be accurate. If we consider the gain versus frequency shift results shown in Fig. (4.4) we see that qualitatively this explanation predicts the observed behavior. A transient response in the concentration mode reduces the gain at $\omega = Dk^2$. Since the gain at $\omega \simeq kv_s$ continues to decrease as the He concentration increases, the $g_{BcT}(\omega)$ should pass through a transition region where g_{BcT} is maximum for ω decreasing smoothly from the value kv_s to the value Dk^2. This is exactly the behavior which is observed experimentally.

When a partial pressure of 10 atm SF_6 is used, the observed frequency continues to increase as the He concentration increases in agreement with theoretical predictions. The observed shift remains characteristic of the Brillouin scattering for the mixture up to a Helium concentration of 80% as shown in Fig. (4.6).

3. <u>He-Xe Mixture</u>

In order to further verify the stimulated scattering from the concentration mode, it was desirable to observe the effect in a mixture of monatomic gases. This removed some of the uncertainties in the calculations of the transport properties which occur with a polyatomic molecule.

The Brillouin gain in Xe is about half the gain for SF_6 at the same pressure. Consequently a higher partial pressure of Xe was required to observe stimulated Brillouin scattering. On the basis of preliminary calculations, a Xe partial pressure of 8 atm was chosen.

The main features of the He-Xe scattering were identical to those of He-SF_6 scattering. However, additional experimental difficulties were encountered.

It was observed that the electrical breakdown threshold in Xe was approximately equal to the Brillouin threshold. The breakdown threshold was measured to be $\sim 10^{11} \frac{W}{cm^2}$. The actual value of this number is of little significance unless the transverse mode structure, and thus the focusing characteristics of the beam, are specified. However, this observed threshold is in agreement with the results of an earlier study of optically induced gas breakdown in the Noble gases[11].

In order to make accurate measurements, it was necessary to avoid gas breakdown since the breakdown may cause thermal Brillouin or Rayleigh scattering to occur[12] which would confuse the observations. It was discovered that by focusing the laser into the gas mixture with a lens of 40 cm focal length, the gas breakdown did not occur.

The values of the decoupled gain coefficients g_B, g_c, g_T are shown in Fig. (4.7). The solutions for the coupled gain coefficient g_{BcT} as a function of frequency are presented in Fig. (4.8) and the frequency shifts for the various modes are shown in Fig. (4.9). Finally, the experimental values for the frequency shift as a function of He concentration are shown in Fig. (4.10) along with the theoretical prediction. As was the case for the He-SF_6 mixture, the theory predicts an abrupt change from large to small shift at 60% concentration. This is the point at which the observed shift begins to decrease rapidly.

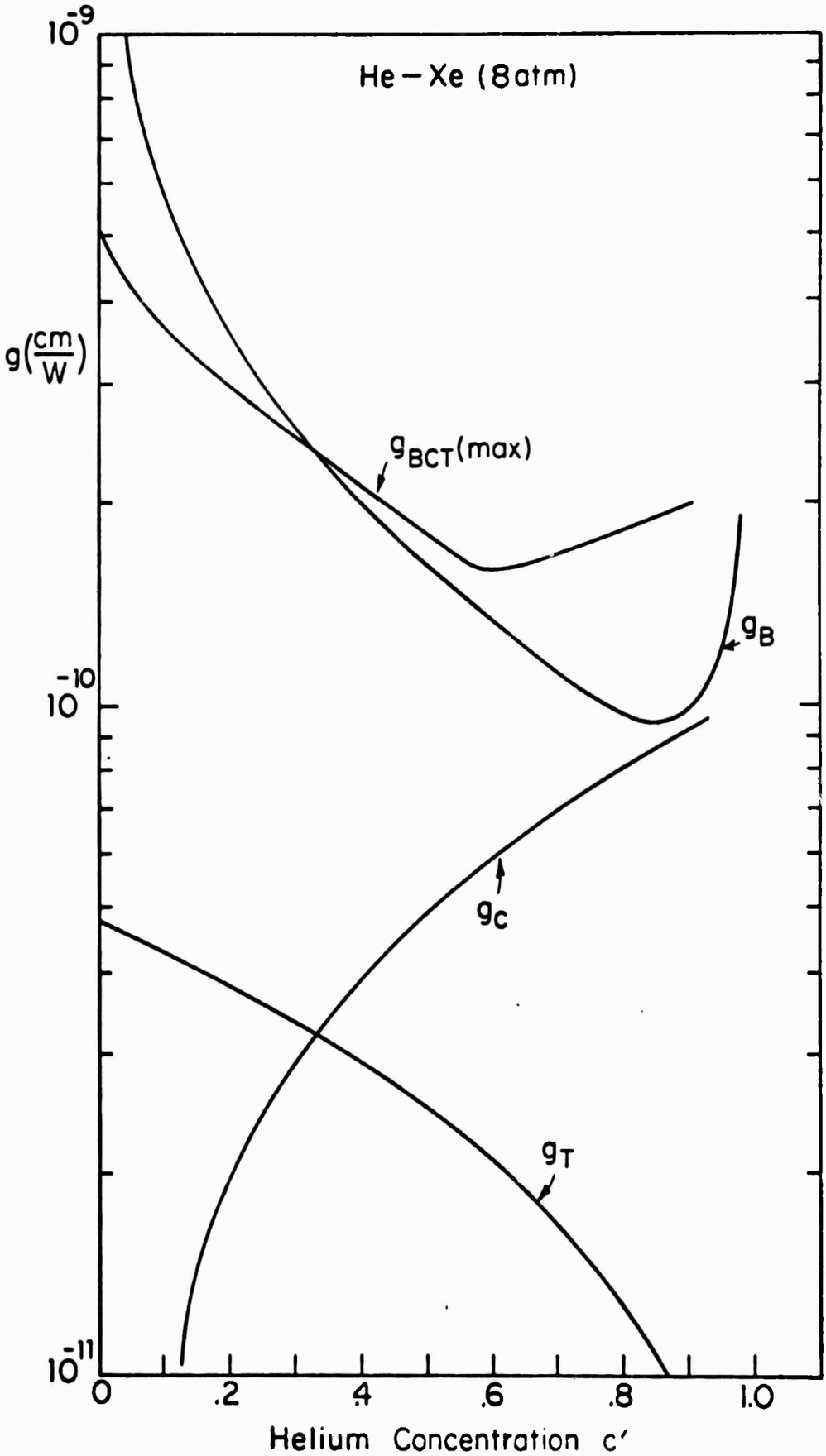

Fig. 4.7 Gain Coefficients Versus Helium Concentration for He-Xe (8 atm) Mixture

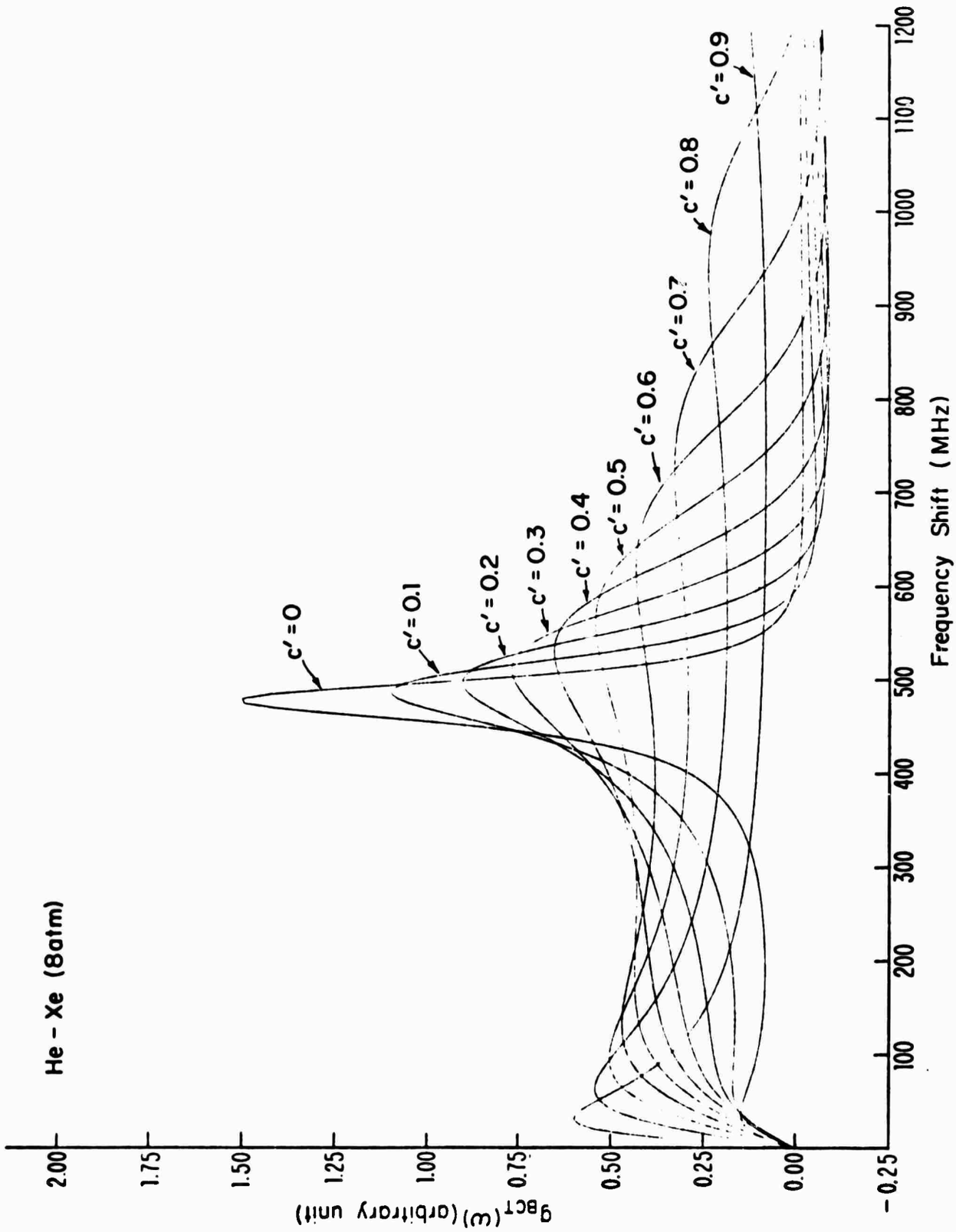

Fig. 4.8 Gain Coefficient g_{BcT} Versus Frequency Shift for He-Xe (8 atm) Mixture

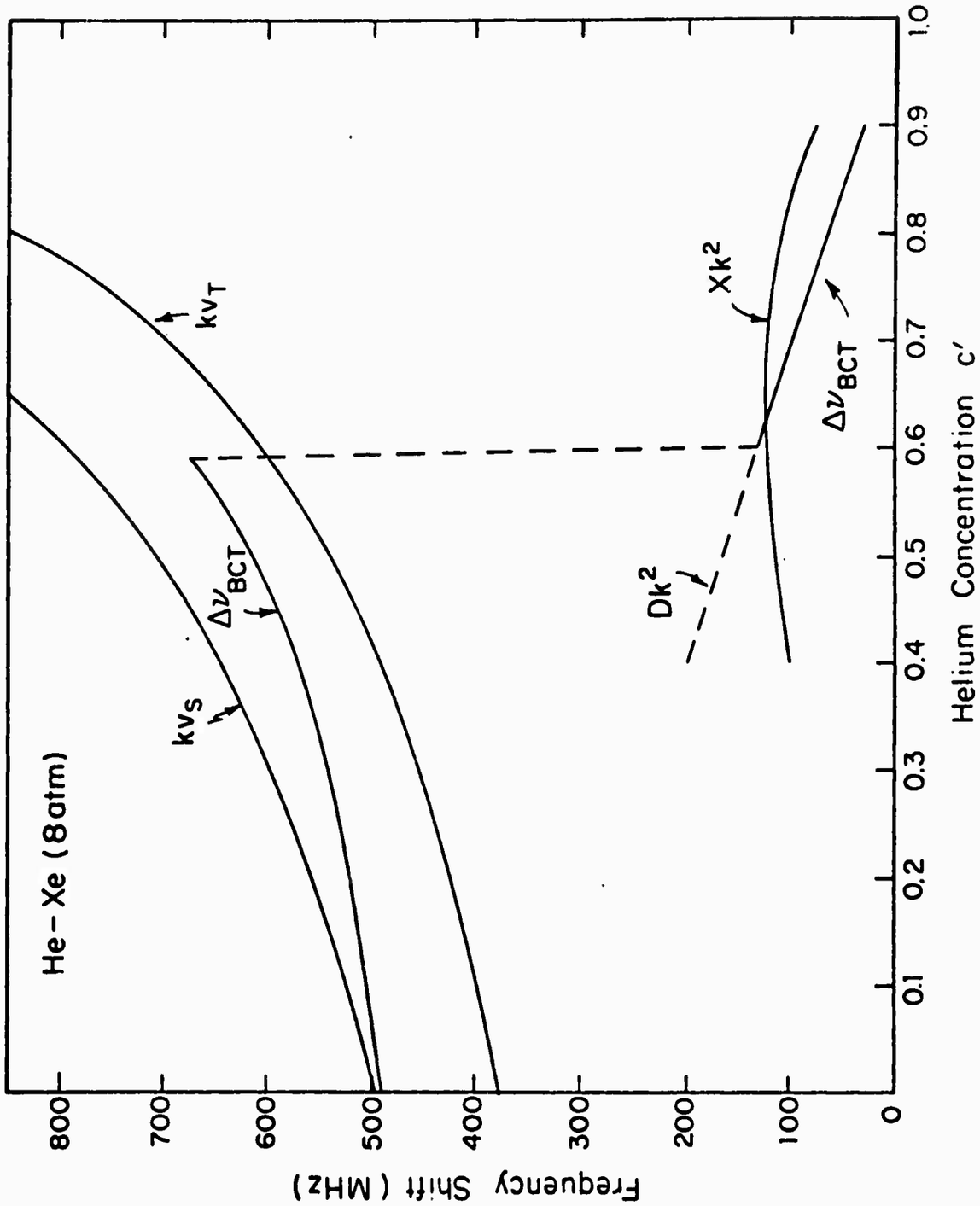

Fig. 4.9 Frequency Shift Versus Helium Concentration for Stimulated Scattering from the Various Modes of the He-Xe (8 atm) Mixture

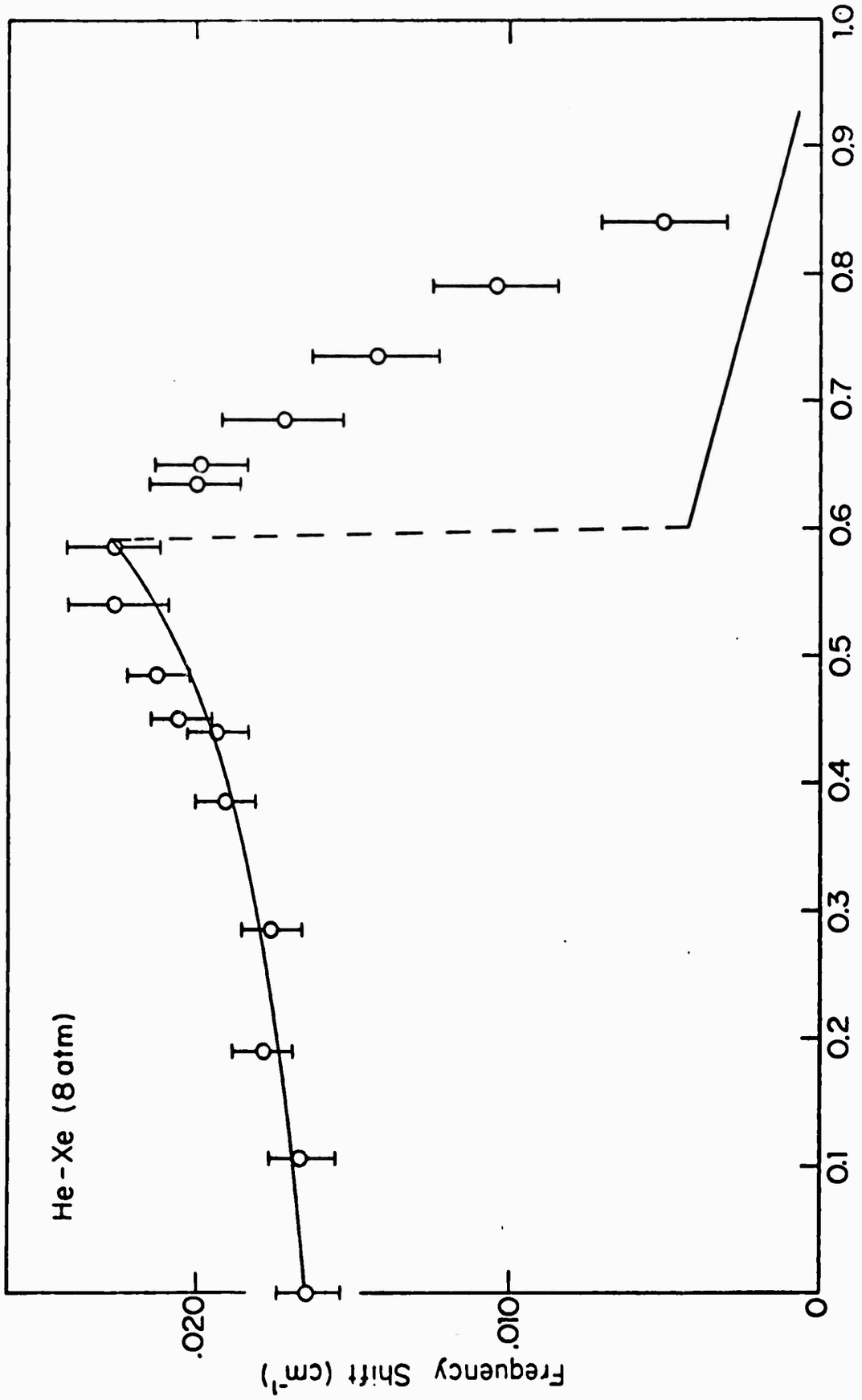

Fig. 4.10 Experimental Results for the He-Xe (8 atm) Mixture

The statements made about the transient response of the concentration scattering for the He-SF_6 mixture apply equally for the He-Xe mixture.

E. Summary and Conclusions

In this work, it has been shown that the dynamical equations of the binary mixture predict the existence of three normal modes of the system. These modes are the sound wave and thermal and concentration diffusion. In mixtures composed of roughly equal amounts of both gases, these normal modes are strongly coupled and the effect of this coupling is to increase the damping constants and decrease the sound velocity of the mixture. These normal modes are each coupled to applied electromagnetic fields through the dependence of the dielectric constant on the thermodynamic parameters which characterize the mixture. This coupling allows the electromagnetic fields to drive coherent fluctuations in these thermodynamic parameters which in turn react on the electromagnetic fields through the modulation of the index of refraction and can lead to stimulated scattering. The resultant gain for the scattered wave has been calculated and it shows that in mixtures at relatively low pressure in which the different molecules have a large difference in polarizibility and in mass, it is possible to observe stimulated scattering from the concentration fluctuations. The stimulated scattering has been observed in two mixtures and the results are in good agreement with the theory. Concentration scattering should be observable in certain other gas

mixtures, for example He-CF_4, He C_2F_6 and possibly He-Ar, however it is doubtful that any additional information would be obtained. In less select gas mixtures and all liquid mixtures the concentration gain will be less than the Brillouin gain, and thus stimulated concentration scattering cannot be observed.

In this experiment, a new technique was introduced which resulted in substantial reduction of the threshold for stimulated scattering. This technique should be applicable in the observation of low gain scattering processes when only limited laser power is available. We believe that this is the first unambiguous demonstration of stimulated concentration scattering, in which the frequency of the scattered light is systematically investigated as a function of concentration.

Earlier investigations of stimulated light scattering from binary mixtures have been made and provided the impetus for the present investigation. The first experiment which claimed to have observed stimulated concentration scattering[13] was performed in a liquid mixture of n-hexane (58% weight concentration) and nitrobenzene (42%). However, the ratio of the gain constants in the decoupled mode approximation is $\frac{g_C}{g_B} \simeq 1.25 \times 10^{-5}$ which throws considerable doubt on the interpretation of this experiment. Near the critical point in a binary mixture where $\frac{\partial \mu}{\partial c} \rightarrow 0$, the concentration gain could become large. However, the diffusion constant D approaches zero at the same time. Thus the correlation time for concentration fluctuations becomes large $\sim 10^{-3}$ sec. The steady state analysis

breaks down for solid state laser pulses, and even with gas laser beams it would be difficult to maintain the required coherence for such long times. A transient analysis must be made and the experimental difficulties would be further enhanced by the large spontaneous critical opalescence, although amplification of this spontaneous emission at high intensities may well be detectable.

The second experiment[14] was done with a Xe and He mixture with He concentration $c' = 0.9$. At this concentration, the Brillouin shift should be $0.0479\ cm^{-1}$ rather than $0.055\ cm^{-1}$ as reported. The gain ratio should be $\frac{g_c}{g_B} = 21$ in contrast to the estimate of $\frac{g_c}{g_B} = 0.1$ as estimated in Ref. 14. The observed concentration shift $0.033\text{-}0.042\ cm^{-1}$ agrees with the value $\Delta\nu_c = \frac{Dk^2}{2\pi c} = 0.032\ cm^{-1}$. At a higher total pressure, the stimulated Brillouin scattering should dominate the concentration scattering as suggested in Ref. 14, however this should not occur at a total pressure as low as 4 atm. Also at such low pressure the condition for the validity of the hydrodynamic equations $y > 3$ is not satisfied and the experimental technique is subject to error, since positive effects were only observed in the presence of gas breakdown. Sparks lead to low frequency scattering even in pure noble gases, presumably caused by thermal Rayleigh scattering.

Chapter IV: References

1. J. O. Hirschfelder, C. F. Curtiss, R. B. Bird, The Molecular Theory of Gases and Liquids, (Wiley, New York, 1954).

2. S. Chapman and T. G. Cowling, Mathematical Theory of Non-uniform Gases, (Cambridge U.P. Cambridge, England 1970).

3. A Dalgarro and A. E. Kingston, Proc. Roy. Soc. A259, 424 (1960).

4. Landolt-Börstein, Zahlenwerte und Funktionen, 6. Anlage, II. Band, 8. Teil p. 6-871 (Springer-Verlag).

5. M. Kohler, Z. Physik 5, 715 (1949).

6. N. F. Sather and J. S. Dahler, J. Chem. Phys., 35, 2029 (1961).

7. R. Holmes and M. A. Stott, Brit. J. Appl. Phys. 1, 1331 (1968).

8. C. L. O'Connor, J. Acoust. Soc. Am. 26, 361 (1954).

9. W. S. Gornall, C. S. Wang, C. C. Yang, and N. Bloembergen, Phys. Rev. Letters

10. N. Bloembergen, W. H. Lowdermilk, and C. S. Wang, Phys. Rev. Letters 25, 1476 (1970).

11. H. T. Buscher, R. G. Tomlinson and E. K. Damon, Phys. Rev. Letters 15, 847 (1965).

12. D. R. Dietz, C. W. Cho, D. H. Rank, and T. A. Wiggins, Appl. Optics 8, 1248 (1969).

13. V. I. Bespalov and A. M. Kubarev, Soviet Phys. J.E.T.P. Letters 6, 31 (1967).

14. I. M. Aref'ev and V. V. Morozov, Soviet Phys. J. E. T. P. Letters 9, 296 (1969).

ACKNOWLEDGEMENT

I wish to express my appreciation to Professor Nicholaas Bloembergen who supervised this research. His instruction has greatly increased my understanding of the basic principles of nonlinear optics.

I have profited from my friendship and discussions with all members of the solid state research group at Gordon McKay Laboratory. In particular, I would like to thank Dr. Chen-Show Wang for his research on the theoretical aspects of this work. His patient explanations have contributed greatly to its completion. The substantial contribution of Dr. Masahiro Matsuoka in the early phases of the experiment are gratefully acknowledged.

The advice and excellent shop work of Mr. Alfred Franzosa and Mr. John Keith were heavily relied upon and are greatly appreciated. I would like also to thank Mrs. Renate D'Arcangelo for skillfully typing the thesis.

The financial assistance of the National Science Foundation is gratefully acknowledged.

The patience and love of my wife, Elaine, through these years of long hours in the laboratory and my frequent preoccupation with the work will always be remembered with great appreciation.